Myosin VIII and XI isoforms interact with *Agrobacterium* VirE2 protein and help direct transport from the plasma membrane to the perinuclear region during plant transformation

Nana Liu, Lan-Ying Lee, Fang-Yu Hsu, Yanjun Yu, Praveen Rao, and Stanton B. Gelvin*

Department of Biological Sciences, Purdue University, West Lafayette, IN 47907

*Corresponding author: Stanton B. Gelvin (gelvin@purdue.edu)

Short title: Myosins mediate plant transformation

NL, L-YL, and SBG designed the experiments; NL, L-YL, F-YH, YY, and PR carried out the experiments; NL and SBG wrote the manuscript with the help of L-YL; SBG envisaged the project and obtained funding support.

The author responsible for distribution of materials integral to the findings presented in this article in accordance with the policy described in the Instructions for Authors (https://academic.oup.com/plcell/pages/General-Instructions) is: Stanton B. Gelvin (gelvin@purdue.edu)

Authors e-mail addresses:
NL: liu2333@purdue.edu
L-YL: lee34@purdue.edu
F-YH: hsuf@purdue.edu; g9680517@oz.nthu.edu.tw
YY: yyj74@163.com
PR: Praveen_Rao@URMC.Rochester.edu
SBG: gelvin@purdue.edu

ABSTRACT

Virulent *Agrobacterium* strains transfer single-strand T-DNA (T-strands) and virulence effector proteins into plant cells. VirE2, one of these virulence effectors, enters the plant cell and is thought to bind T-strands, protecting them from nuclease degradation and helping guide them to the nucleus. How VirE2 is trafficked inside the plant cell is not fully understood. Using bimolecular fluorescence complementation, *in vitro* pull-down, yeast two-hybrid, and *in vivo* co-immunoprecipitation assays, we found that VirE2 binds directly to the cargo binding domains of several myosin VIII family members, and to myosin XI-K. We observed reduced susceptibility of several *Arabidopsis* actin mutants and a myosin *VIII-1/2/a/b* quadruple mutant to *Agrobacterium*-mediated transformation. Expression of cargo binding domains of myosin VIII-1, VIII-2, VIII-A, or VIII-B in transgenic plants inhibits *Arabidopsis* root transformation. However, none of the myosin VIII proteins contribute to the intracellular trafficking of VirE2. Expression of myosin *VIII-2*, *-A*, *-B*, but not *VIII-1*, cDNAs in the myosin *VIII-1/2/a/b* mutant partially restored transformation. Furthermore, functional fluorescently-tagged VirE2, synthesized in plant cells, relocalized from the cellular periphery into the cytoplasm after delivery of T-strands from *Agrobacterium*. Surprisingly, mutation of myosin *XI-k* and expression of the myosin XI-K cargo binding domain had no effect on transformation, although it blocked VirE2 movement along actin filaments. We hypothesize that myosin VIII proteins facilitate VirE2 tethering to the plasma membrane and are required for efficient localization of VirE2 to membrane sites from which they bind incoming T-strands. Myosin XI-K is important for VirE2 movement through the cytoplasm towards the nucleus.

INTRODUCTION

The soil-borne phytopathogen *Agrobacterium tumefaciens* is the causative agent of crown gall disease in plants (Gelvin, 2000; Tzfira et al., 2004). The ability of *Agrobacterium* to genetically transform plant cells has made *Agrobacterium*-mediated transformation the most widely used platform for generating transgenic plants (Gelvin, 2017). During transformation, T-DNA, a defined segment of the resident tumor inducing (Ti) plasmid, is transferred to the plant cell along with several virulence (Vir) effector proteins (Gelvin, 2003; McCullen and Binns, 2006; Lacroix and Citovsky, 2013). Virulence effector proteins VirD5, VirE2, VirE3, and VirF, along with VirD2, which covalently links to T-strands (single-strand T-DNA molecules), are transferred from *Agrobacterium* to the plant through a type IV secretion system (T4SS) (Cascales and Christie, 2004; Christie et al., 2005).

VirE2, the most abundant of the virulence effector proteins (Engstrom et al., 1987), is important for efficient plant transformation as *virE2* mutant *Agrobacterium* strains are highly attenuated in virulence (Stachel and Nester, 1986; Rossi et al., 1996). *In vitro*, VirE2 binds to single-strand (ss)DNA in a sequence-independent manner and has been proposed to interact with single-strand T-strands, linked to VirD2, in the plant cytoplasm, forming a "T-complex" and protecting T-strands from nuclease degradation (Citovsky et al., 1989; Sen et al., 1989; Howard and Citovsky, 1990; Yusibov et al., 1994; Rossi et al., 1996; Gelvin, 1998). VirE2 does not interact with T-strands in *Agrobacterium* (Cascales and Christie, 2004) and its interaction with T-strands to form a T-complex *in planta* has only been inferred. In addition to its *in vitro* DNA binding activity, VirE2 can form membrane channels which permit the transport of ssDNA through artificial membranes (Dumas et al., 2001; Duckely et al., 2005). Recent research showed that VirE2 is anchored on the host plasma membrane through interaction with VirE3 at *Agrobacterium*-host contact sites. Such membrane associations may facilitate the proposed interactions between VirE2 and T-strands as the T-strands enter the plant cell (Li et al., 2018, 2020).

Efficient plant transformation by a *virE2* mutant *Agrobacterium* strain (the "T-DNA donor") can be restored by co-inoculation with a bacterial strain lacking T-DNA but expressing VirE2 (the "VirE2 donor"; Otten et al., 1984; Simone et al., 2001), and a *virE2* mutant *Agrobacterium* strain can be complemented to full virulence by expression of a *VirE2* transgene *in planta* (Citovsky et al., 1992; Lapham et al., 2021), indicating that VirE2 is functional in plants during

transformation. However, the subcellular localization of VirE2 remains controversial. Early reports demonstrated nuclear localization of VirE2 (Citovsky et al., 1992), but other studies from several laboratories indicated that VirE2 localizes in the cytoplasm (Grange et al., 2008; Gelvin, 2010; Roushan et al., 2018). A recent report claimed that a small amount of VirE2 can enter the nucleus, but only in the presence of VirD2 and T-strands (Li et al., 2020). How VirE2, and potentially associated T-strands, are trafficked from their entry point at the cell periphery to the nucleus remains unknown.

Myosins, motor proteins that convert chemical energy into directed movement of cargo proteins along actin filaments, are key players in trafficking proteins and organelles in plants (Vale, 2003; Richards and Cavalier-Smith, 2005). Two classes of myosins, myosin VIII and XI, are encoded by plant genomes. *Arabidopsis thaliana* encodes 13 myosin XI group members and four myosin VIII group members (Bezanilla et al., 2003; Foth et al., 2006). Generally, myosin proteins contain a highly conserved N-terminal motor domain for actin binding, a neck domain with a number of IQ repeats for light-chain binding, a coiled-coil domain that is responsible for myosin protein dimerization, and a specific C-terminal tail domain that binds cargo (Trybus, 2008). Class XI myosins, known as organelle transporters, colocalize with organelles and are involved in the rapid trafficking of Golgi stacks, streaming of endoplasmic reticulum (ER), and cellular remodeling (Lee and Liu, 2004; Reisen and Hanson, 2007; Avisar et al., 2008b; Sparkes et al., 2009; Ueda et al., 2010). In addition, myosins XI-K and XI-2 play major and overlapping roles in root hair development (Peremyslov et al., 2008). In contrast to class XI myosins, considerably less is known about the intracellular functions of class VIII myosins. Class VIII myosins colocalize with plasmodesmata, the endoplasmic reticulum, and the plasma membrane (Golomb et al., 2008) and may function in intercellular protein and RNA delivery to the plasmodesmata, in endocytosis, and in anchoring actin filaments at plasmodesmata sites (Reichelt et al., 1999; Wojtaszek et al., 2005; Avisar et al., 2008a; Golomb et al., 2008; Sattarzadeh et al., 2008). Moreover, myosin VIII is important for the cell-to-cell movement of virus proteins, and is required for viral movement protein targeting to and virus trafficking through plasmodesmata (Amari et al., 2014).

The actin cytoskeleton functions to organize the endomembrane system and trafficking patterns within the cell (Smith and Oppenheimer, 2005; Hussey et al., 2006). Cargo-binding and intracellular transport by myosin is proposed to exert force on the actin filaments (Staiger et al.,

2009). Yang et al. (2017) reported that trafficking of VirE2 inside plant cells is powered by myosin XI-K via the endoplasmic reticulum and F-actin filaments. However, our knowledge of the roles of plant myosins in specific steps of VirE2 trafficking and transformation remains sparse. In the present study, we investigated the roles of myosin VIII family members and myosin XI-K in *Agrobacterium*-mediated transformation and in VirE2 intracellular movement. Using a dominant-negative approach by overexpressing individual myosin cargo-binding domains, and by overexpressing various individual full-length myosin cDNAs, we show that *Arabidopsis* myosins VIII-2, VIII-A, and VIII-B, but not XI-K, are important for transformation. These three myosin VIII isoforms interact with VirE2 and retain it at the periphery of root cells. When T-DNA enters the plant cell, a portion of peripherally localized VirE2 relocalizes into the cytosol, especially the perinuclear region. However, class VIII myosins do not affect the movement of VirE2 along actin filaments within the cytoplasm. In contrast, myosin XI-K supports the intracellular movement of VirE2. We propose that myosins VIII-2, VIII-A, and VIII-B tether VirE2 to the plasma membrane. Entry of VirD2/T-strands into the plant cell releases VirE2 from the membrane, following which VirE2 translocates to the perinuclear region along actin filaments, powered by myosin XI-K.

RESULTS

The actin cytoskeleton is important for *Agrobacterium*-mediated transformation

The actin cytoskeleton is conserved in diverse eukaryotic organisms and is important for a variety of plant developmental and other processes, including cell growth, division, and expansion; organelle motility; organization of the cellular interior; endomembrane trafficking; and host defense responses (Smith and Oppenheimer, 2005; Embley and Martin, 2006; Hussey et al., 2006; Szymanski and Cosgrove, 2009; Peremyslov et al., 2010). To test whether the actin cytoskeleton plays a role in *Agrobacterium*-mediated transformation, we conducted transient and stable *Arabidopsis* root transformation assays using wild-type plants and plants individually mutant in two root-expressed actin genes, *actin2* (*act2*) and *actin7* (*act7*). These actin mutant plants showed substantial reductions (three- to five-fold) in transformation. Introduction of a wild-type *Act7* cDNA into the *act7-4* mutant restored both transient and stable transformation (Figure 1A). These results show that root-expressed actin genes are important for transformation

149 of *Arabidopsis* roots. We also conducted root transformation assays using a mutant of the
150 pollen-expressed *actin12* gene (*act12*) and the *botero* (*bot1*) mutant that shows disorganization
151 of the root cortical microtubule network (Bichet et al., 2001). These mutants showed wild-type
152 levels of transformation (Figure 1A), indicating that neither a pollen-expressed actin gene nor the
153 correct organization of root microtubules is essential for *Agrobacterium*-mediated root
154 transformation.

155 Yang et al. (2017) showed that the *Agrobacterium* virulence effector protein VirE2 uses
156 myosin XI-K to traffic through the plant cytoplasm. Given the importance of VirE2 for
157 transformation, we individually tested *Arabidopsis* mutants in each of the 13 myosin XI and four
158 myosin VIII gene family members for their susceptibility to transient and stable *Agrobacterium*-
159 mediated transformation. Figures 1B and C, and Supplemental Figure S1 show that, apart from
160 the *myosin XI-h* mutant, mutation of no other single myosin gene affected transformation. In
161 particular, mutation of the *myosin XI-k* gene did not decrease transformation. Because of
162 potential functional redundancy among the plant myosin VIII and XI family members
163 (Prokhnevsky et al., 2008), we also tested several higher order myosin VIII and myosin XI
164 mutants. Higher order *myosin XI-k* mutants (*XI-k/i*, *XI-k/1/2*, and *XI-k/1/2/i*) showed decreased
165 transformation susceptibility (Figures 1B and 1C). Similarly, the higher order myosin VIII
166 mutants *1/a*, *2/b*, *1/2/a*, and *1/2/a/b* showed reduced transformation susceptibility compared to
167 wild-type Col-0 plants (Figures 1B and 1C).

168 We compared root and above-ground plant growth of each of the higher order myosin XI and
169 myosin VIII mutants. Similar to what was previously observed (Ojangu et al., 2007; Peremyslov
170 et al., 2008), the myosin *XI-k/1/2/i* quadruple mutant displayed a strong growth and
171 developmental phenotype compared with Col-0 plants: the main roots had fewer lateral branches
172 and shorter root hairs, and the plants were dwarf. However, the myosin *VIII 1/2/a/b* quadruple
173 mutant appeared similar to Col-0 plants in growth, root development, and the ability to form calli
174 from cut root segments (Supplemental Figures S2A and S2B). Roots and the crown of the plant
175 are the natural target tissues for *Agrobacterium*-mediated transformation. Because we were
176 conducting quantitative root transformation assays (Gelvin, 2006), we did not continue to
177 investigate transformation susceptibility of the abnormal roots of the myosin *XI-k/1/2/i* quadruple
178 mutant. We therefore turned our attention to investigating the importance of the various myosin
179 VIII isoforms for transformation, and to the myosin XI-K protein.

180

181 **Expression of full- length myosin *VIII-2*, *VIII-A*, and *VIII-B* cDNAs, but not a myosin *VIII-***
182 ***1* cDNA, increases susceptibility of the myosin *VIII-1/2/a/b* quadruple mutant to**
183 ***Agrobacterium*-mediated transformation**

184 To determine the importance of each *myosin VIII* gene for *Agrobacterium*-mediated root
185 transformation, we individually expressed cDNAs for each *myosin VIII* gene in the *myosin VIII-*
186 *1/2/a/b* quadruple mutant. We placed each *myosin VIII* cDNA under the control of a strong
187 Cauliflower Mosaic Virus (CaMV) double 35S promoter (hereafter reported in Supplemental
188 Table 1 as the *Agrobacterium* strains used to make the transgenic lines; At2361-At2164; At2360
189 was used as an empty vector control) or a β-estradiol-inducible promoter (Zuo et al., 2000;
190 At2389-2392) and generated multiple transgenic lines. Because of the importance of myosins in
191 trafficking molecules and organelles through the plant cytoplasm (Avisar et al., 2008b), we
192 hereafter limited our transformation assays to transient transformation which measures T-DNA
193 and virulence effector protein movement through the cytoplasm, entry into the nucleus, and
194 expression of non-integrated transgenes. Thus, these assays predominantly measure non-
195 integrated transgenes.

196 Transient root transformation assays of five independent transgenic lines of each *myosin VIII*
197 cDNA indicated that individual expression of the *myosin VIII-2*, *VIII-A*, and *VIII-B* cDNAs
198 increased the transformation susceptibility of the *myosin VIII-1/2/a/b* quadruple mutant (Figure
199 2A and Supplemental Figures S3B-D), indicating a role for these myosins in *Agrobacterium-*
200 mediated transformation. However, expression of the *myosin VIII-1* cDNA in the quadruple
201 mutant background did not increase transformation susceptibility (Figure 2A and Supplemental
202 Figure S3A). This latter result suggests either that myosin VIII-1 does not contribute to
203 transformation or that expression of myosin VIII-1 is not sufficient to increase transformation in
204 the absence of the other three myosin VIII isoforms. To distinguish between these two
205 possibilities, we individually overexpressed each *myosin VIII* cDNA in wild-type Col-0 plants.
206 Interestingly, overexpression of the *myosin VIII-1* cDNA, but not the *myosin VIII-2*, *VIII-A*, or
207 *VIII-B* cDNAs, increased susceptibility of Col-0 plants to *Agrobacterium*-mediated
208 transformation (Figure 1E and Supplemental Figures S3A-D). These results indicate that myosin
209 VIII-1 can contribute to transformation, but that expression of myosin VIII-1 is not sufficient to
210 do so in the absence of the other myosin VIII isoforms. Transgenic plants harboring inducible

211 *myosin VIII* cDNAs yielded results similar to that of plants constitutively expressing these
212 cDNAs (Supplemental Figures S4A-D).
213 Finally, we generated transgenic lines that expressed two *myosin VIII* cDNAs (*VIII-A* and
214 *VIII-B* [At2375], or *VIII-2* and *VIII-B* [At2376]) in both the *myosin VIII-1/2/a/b* quadruple
215 mutant (Figure 2C) and in wild-type Col-0 plants (Figure 2D). Overexpression of these two sets
216 of myosin cDNAs did not increase transformation of otherwise wild-type plants. However,
217 expression of these pairs of myosin cDNAs in the *myosin VIII-1/2/a//b* quadruple mutant
218 enhanced transformation to a greater extent than did expression of these cDNAs individually
219 (Figures 2C and Supplemental Figures S5A-D). These results indicate that *myosin VIII-A*, *VIII-B*,
220 and *VIII-2* genes contribute synergistically to transformation. These results further suggest that
221 the level of expression of the *myosin VIII-2*, *VIII-A*, and *VIII-B* genes in wild-type roots is
222 sufficient for maximal transformation, and that increasing expression of these genes cannot
223 further increase transformation.

224 **Inducible expression of *myosin VIII*, but not *myosin XI-K*, cargo binding domain transgenes**
225 **affects *Agrobacterium*-mediated transient root transformation**

226 Yang et al. (2017) demonstrated that expression of a myosin XI-K cargo binding (globular tail)
227 domain inhibited VirE2 movement in tobacco leaf cells. To determine whether specific myosin
228 VIII members are important for *Agrobacterium*-mediated transformation using a similar
229 dominant-negative approach, we generated transgenic *Arabidopsis* lines individually expressing
230 cDNAs encoding each of the four myosin VIII cargo binding domains (CBD; At2315-2318), or
231 the myosin XI-K CBD (At2319), under the control of a β-estradiol inducible promoter. Because
232 these CBD constructs lack the myosin motor domain, they are not able to transport their cargoes
233 along actin filaments. We tested the susceptibility of 3-4 independent transgenic lines for each
234 CBD construct to *Agrobacterium*-mediated transient transformation, either after 24 hr transgene
235 induction or without induction. Induction of each of the four *myosin VIII* CBD transgenes
236 decreased transformation two- to three-fold, whereas induction of the *myosin XI-K* CBD
237 transgene had no significant effect on transformation (Figure 3 and Supplemental Figures S6A-
238 E). These data further suggest that the four myosin VIII proteins contribute to *Agrobacterium*-

239 mediated transformation, whereas myosin XI-K is not required for transformation. However,
240 below we show that myosin XI-K is important for VirE2 movement through the cytoplasm.

241 **Myosin VIII proteins are required for *Arabidopsis* roots expressing VirE2 to complement**
242 **the virulence of a *virE2* mutant *Agrobacterium* strain, and to mitigate VirE2 aggregation**

243 *Agrobacterium virE2* mutants are severely debilitated in virulence (Rossi et al., 1996). However,
244 expression of VirE2 or VirE2-Venus transgenes in plants restores virulence, indicating that the
245 major role of VirE2 in transformation occurs in the plant (Citovsky et al., 1992; Bhattacharjee et
246 al., 2008; Lapham et al., 2021). To determine the importance of myosin VIII proteins for such
247 "*in planta*" complementation, we generated numerous *Arabidopsis* transgenic lines expressing a
248 *VirE2-Venus* transgene, under the control of a β-estradiol-inducible promoter, in both wild-type
249 and in *myosin VIII* quadruple mutant plants. Twenty four hr after incubation of roots of these
250 lines in medium with or without inducer, we cut the roots into small segments and infected them
251 with *A. tumefaciens* At1879 containing the T-DNA binary vector pBISN2 with a *gusA*-intron
252 gene in the T-DNA (Narasimhulu et al., 1996). Six days later we assessed transient
253 transformation efficiency by conducting β-glucuronidase (GUS) activity assays using the
254 chromogenic substrate 5-bromo-4-chloro-3-indolyl-β-D-glucuronide (X-gluc). As previously
255 reported (Lapham et al., 2021), induction of the *VirE2-Venus* transgene in wild-type Col-0 plants
256 complemented the loss of VirE2 function when a *virE2 Agrobacterium* mutant was used.
257 However, induction of the *VirE2-Venus* transgene in *myosin VIII* quadruple mutant plants could
258 not compensate the loss of VirE2 function when a *virE2 Agrobacterium* mutant was used
259 (Figures 4A and 4B). Thus, *Myosin VIII* expression is required for *in planta* complementation of
260 an *Agrobacterium virE2* mutant.
261 VirE2 usually localizes in the plant cytoplasm, although in the presence of the virulence
262 effector protein VirD2 and T-strands a small amount may enter the nucleus (Gelvin, 2010; Li et
263 al., 2020). To determine whether myosin VIII affects the subcellular distribution of VirE2, we
264 used confocal microscopy to visualize β-estradiol induced VirE2-Venus in both the Col-0 and
265 *myosin VIII* quadruple mutant backgrounds containing an inducible *VirE2-Venus* transgene.
266 VirE2 is known to aggregate both *in vitro* and in plants (Bhattacharjee et al., 2008; Dym et al.,
267 2008). Under our induction conditions VirE2-Venus showed a pattern of aggregation in the

268 *myosin VIII* quadruple mutant distinct from that seen in the Col-0 background. In roots of the
269 quadruple mutant, VirE2-Venus aggregated to a greater extent than it did in wild-type roots
270 (Figure 4C). The sizes of VirE2 aggregates from two random areas of each of six images were
271 measured and the average sizes were calculated. The average VirE2 aggregate size in root cells
272 of the *myosin VIII* quadruple mutant was 6.2±0.6 μm^2, compared to an average aggregate size of
273 2.0±0.3 μm^2 in wild-type roots (Figure 4D). Furthermore, the total cellular area occupied by
274 these VirE2 aggregates was greater in root cells of the *myosin VIII* mutant (17.0±1.1%) than in
275 similar wild-type cells (4.7±0.9%) (Figure 4D). To determine whether this extensive VirE2
276 aggregation in myosin *VIII* mutant cells resulted from higher levels of VirE2-Venus expression
277 in roots, we extracted total proteins from β-estradiol-induced roots of these plants and
278 determined the relative amounts of VirE2-Venus expressed in roots using anti-GFP antibodies.
279 As a loading control for the protein blots, we used an antibody targeting the house-keeping
280 protein phosphoenolpyruvate carboxylase (PEPC). Strikingly, myosin *VIII* quadruple mutant
281 roots express, on average, less VirE2-Venus than do wild-type roots (Figure 4E). Therefore, the
282 more extensive aggregation of VirE2-Venus in *myosin VIII* mutant roots is unique and cannot be
283 explained by greater accumulation of this protein.
284 To determine which myosin protein influences VirE2-Venus aggregation, we generated
285 numerous transgenic *Arabidopsis* lines (using *Agrobacterium* strains At2315-At2319), in the
286 *myosin VIII* quadruple mutant background, expressing both VirE2-Venus and individual
287 *mCherry-myosin VIII CBD* cDNAs under the control of a β-estradiol-inducible promoter.
288 Following induction, we measured the size of the VirE2-Venus aggregates in root cells and the
289 percentage of root cell volume taken up by these aggregates. Figures 5A and 5B show that,
290 compared to expression of VirE2-Venus in the absence of expression of a myosin CBD
291 transgene, expression of myosin VIII-A, VIII-B, and VIII-2 CBDs reduced both the size of
292 VirE2-Venus aggregates (from 7.5±1.9 μm^2 down to 2.4±0.3 μm^2, 3.7±0.5 μm^2, and 3.1±0.3
293 μm^2, respectively) and the percentage of the cell volume (from 17.7±2.0% down to 3.6±0.6%,
294 6.3±0.4%, and 6.1±0.5%, respectively) occupied by these aggregates, due to their dominant
295 negative effects. However, the CBD of myosin VIII-1 did not substantially reduce aggregate
296 size or the percentage of the cell volume occupied by the aggregates (Figure 5A): the average
297 aggregates size was 6.7±0.7 μm^2, and the percentage of the cell volume was 11.8±1.1%. These

results suggest that myosin VIII-A, VIII-B, and VIII-2 CBDs interact with VirE2 in plant cells and that the myosin VIII-1 CBD may fundamentally differ from the CBDs of the other three myosin VIII members.

VirE2 interacts directly with some, but not all, myosin VIII cargo binding domains and with the CBD of myosin XI-K

Because myosin VIII proteins are required for VirE2 to function in virulence, and because myosin VIII CBD expression affects the degree to which VirE2 aggregates *in planta*, we investigated whether myosin protein cargo binding domains interact with VirE2. We first tested the direct interaction of VirE2 with each of the myosin VIII and the myosin XI-K protein CBDs using an *in vitro* pull-down assay. We individually incubated recombinant VirE2-Venus with recombinant myc-tagged myosin CBDs. As a control, we substituted recombinant Venus protein for VirE2-Venus. As further controls, we incubated VirE2-Venus with myc-tagged VIP1, a protein known to interact with VirE2 (Tzfira et al., 2001; Djamei et al., 2007), or myc-tagged Lamin C, a protein known not to interact with VirE2 (Ueki and Citovsky, 2005). We captured VirE2-Venus, or Venus, and any interacting proteins on anti-GFP antibody beads, subjected the bound proteins to SDS gel electrophoresis, then conducted Western blot analysis using anti-myc antibodies. Figures 6A-F show that the CBDs of myosins VIII-A, VIII-B, VIII-2, and XI-K directly interacted with VirE2-Venus, but not with Venus. However, we were not able to detect interaction of VirE2-Venus with the CBD of myosin VIII-1. As expected, VirE2-Venus interacted with myc-tagged VIP1 but not with myc-tagged Lamin C (Figure 6). These data were confirmed using a yeast two-hybrid system. VirE2 interacted in yeast with the CBDs of myosins VIII-A, VIII-B, VIII-2, and XI-K, as well as with VIP1. However, VirE2 did not interact in yeast with the CBD of myosin VIII-1 or with the negative control Lamin C (Figures 7A and 7B).

To assess the interactions of VirE2 with myosin VIII or XI-K CBD proteins *in vivo*, we conducted co-immunoprecipitation experiments using transgenic *Arabidopsis* roots expressing VirE2-Venus and, individually, each of the myc-tagged myosin VIII or the myosin XI-K CBDs. Using anti-GFP antibody beads to capture VirE2-Venus and associated proteins followed by immunoblotting using anti-myc tag antibody to detect CBDs, we observed robust co-immunoprecipitation between VirE2-Venus and the myosin VIII-2, VIII-A, VIII-B, and XI-K

CBDs (~4% of the input myc-myosin VIII-2, VIII-A, VIII-B, and XI-K CBDs were co-immunoprecipitated with anti-GFP antibody). However, we also observed some co-immunoprecipitation between VirE2 and the myc-tagged myosin VIII-1 CBD (~1.6-2% of the input myosin VIII-1 CBD; Figures 8A and 8B). As expected, VirE2-Venus interacted with VIP1 (Figure 8A), and the myosin VIII-2 CBD did not interact with the control Venus protein (Figure 8B). The *in vivo* co-immunoprecipitation of VirE2-Venus with the myosin VIII-2, VIII-A, VIII-B, and XI-K CBDs recapitulated the *in vitro* interaction and yeast two-hybrid results. However, *in vivo* co-immunoprecipitation of the myosin VIII-1 CBD with VirE2-Venus, in the absence of interaction *in vitro* and in yeast, suggests that this *in vivo* interaction may be indirect and mediated by other factors within *Arabidopsis* roots.

VirE2 and Myosin VIII cargo binding domains co-localize at the cell periphery

The vast majority of VirE2 protein localizes within the cellular cytoplasm, and in wild-type *Arabidopsis* roots is often found in the peripheral regions of the cell (Shi et al., 2014). VirE2 has been proposed to form membrane channels through which VirD2/T-strands translocate from *Agrobacterium* into the plant cell (Dumas et al., 2001; Duckely et al., 2005). Myosin VIII proteins also localize to the plasma membrane (Golomb et al., 2008). To determine whether VirE2 and myosin cargo binding domains co-localize at the cell periphery, we generated transgenic *Arabidopsis* plants expressing VirE2-Venus and various mCherry-tagged myosin CBD cDNAs under the control of a β-estradiol inducible promoter (using *Agrobacterium* strains At2315-At2319). After β-estradiol induction, we imaged roots using confocal microscopy (Figures 9A and 9B). The CBDs of myosins VIII-A and VIII-2 localized almost exclusively to the cellular periphery, whereas the CBD of myosin VIII-B localized both to the cellular periphery and to the nucleus (Figure 9A). The myosin VIII-1 and XI-K CBDs localized not only at the cellular periphery but also throughout the cytoplasm (Figure 9A).

When co-expressed in the Col-0 background, VirE2 and the myosin VIII-2, VIII-A, VIII-B, and XI-K CBDs partially co-localized at the cell periphery (Pearson's correlation coefficient = 0.56±0.04, 0.68±0.05, 0.63±0.04, and 0.69±0.03, respectively; overlap coefficient = 0.65±0.03, 0.72±0.06, 0.70±0.03, and 0.77±0.04, respectively; Figure 9B). However, co-localization of VirE2 with the myosin VIII-1 CBD at the cell periphery was less extensive (Pearson's

356 correlation coefficient = 0.44±0.03; overlap coefficient = 0.48±0.01; Figure 9B). Staining
357 VirE2-Venus expressing *Arabidopsis* roots with the plasma membrane dye FM4-64 revealed that
358 VirE2 localized near to but not in the plasma membrane (Pearson's correlation coefficient =
359 0.42±0.07; overlap coefficient = 0.45±0.03; Supplemental Figures S7A and B). However, in the
360 myosin VIII quadruple mutant background, VirE2 localized less extensively at the cellular
361 periphery and more within the general cytoplasm (Supplemental Figures S8A and B). Co-
362 expression of mCherry-myosin VIII-1, VIII-A, or VIII-2 CBDs with the plasma membrane
363 marker PIP2A-Venus (using *Agrobacterium* strains At2370, At2371, and At2374, respectively)
364 revealed that these myosin VIII CBDs co-localize with PIP2A (Supplemental Figures S9A-C),
365 similar to what has previously been reported (Golomb et al., 2008). Taken together, these results
366 suggest that the myosin VIII-2, VIII-A, and VIII-B CBDs localize to the plasma membrane
367 where they may temporarily tether VirE2.

368 **VirE2 and several myosin VIII cargo binding domains interact at the cell periphery**

369 In order to test whether VirE2 may be a cargo of myosin VIII proteins, we conducted
370 bimolecular fluorescence complementation (BiFC) assays to visualize *in planta* protein-protein
371 interactions. We generated transgenic *Arabidopsis* plants expressing VirE2-cYFP and nVenus-
372 tagged myosin CBD cDNAs under the control of a β-estradiol inducible promoter (using
373 *Agrobacterium* strains At2320-At2324). The plants also constitutively expressed mCherry-actin
374 binding domain 2 (ABD2) as an actin marker. After inducing the plants with β-estradiol, we
375 detected YFP fluorescence mainly at the cellular periphery of root cells when VirE2-cYFP was
376 co-expressed with the nVenus-tagged CBDs of myosins VIII-A, VIII-B, VIII-2, or myosin XI-K,
377 but no fluorescence with the myosin VIII-1 CBD (Figures 10A-F), indicating a lack of direct
378 interaction. VirE2-cYFP additionally interacted with the CBD of myosin XI-K in the cytoplasm.
379 VirE2-cYFP did not interact with the negative control protein Lamin C. These results again
380 suggest that the CBDs of myosin VIII-2, VIII-A, VIII-B, and XI-K may temporarily tether VirE2
381 to the plasma membrane, but that only myosin XI-K may transport VirE2 along actin filaments
382 through the cytoplasm.
383

384 **Some VirE2 molecules re-localize to the perinuclear region during infection by a virulent**
385 ***Agrobacterium* strain**
386 Some VirE2-Venus fluorescence, when constitutively expressed in *Arabidopsis* roots, localizes
387 at the cellular periphery, especially at the cell poles (Shi et al., 2014). Li et al. (2020) showed
388 that during agroinfiltraion, a small amount of VirE2 can enter the nucleus of tobacco leaf cells,
389 and this entry requires the presence of VirD2 and T-strands. To determine whether
390 transgenically-expressed VirE2 also relocalizes to the nucleus in the presence of VirD2 and T-
391 strands, we incubated *Arabidopsis* roots containing an inducible *VirE2-Venus* transgene with β-
392 estradiol. After 24 hr, we infected root segments with a *virE2*-deletion *Agrobacterium* strain
393 either lacking T-DNA (At2403; no binary vector) or containing T-DNA on a binary vector
394 (At2404). Twenty-four hours after inoculation, we observed VirE2-Venus subcellular
395 localization by confocal microscopy. Root segments infected by *A. tumefaciens* At2403 did not
396 show altered VirE2-Venus subcellular localization: fluorescence was distributed throughout the
397 cytoplasm, including at the cellular periphery (Supplemental Figure S10A). However, infection
398 by *A. tumefaciens* At2404 resulted in a partial redistribution of VirE2-Venus within the
399 cytoplasm: fluorescence increased in the perinuclear area (Supplemental Figure S10B).
400 Quantitative analysis of fluorescence intensity showed that perinuclear VirE2 increased ~5-fold
401 in the presence of T-DNA (Figure 11A). However, we were unable to detect VirE2-Venus
402 within the nucleus. These data suggest that the transfer of T-DNA to plant cells results in a
403 partial redistribution of VirE2 to the area surrounding the nucleus.

404 **T-strands delivered by *Agrobacterium* can relocalize VirE2 from the cellular periphery into**
405 **the cytosol**

406 Because much VirE2 produced *in planta* is already in the general cell cytosol, the data presented
407 in Figure 11A and the movies in Supplemental Figure S11 were not able to show redistribution
408 of VirE2-Venus specifically from the cell periphery into the perinuclear area. We therefore
409 conducted the VirE2-Venus re-localization experiments, following *Agrobacterium* infection, on
410 root segments overexpressing the various myosin VIII or myosin XI-K CBDs. We reasoned that
411 when most VirE2-Venus is tethered to the plasma membrane by myosin VIII-A, VIII-B, VIII-2,

412 and (to a lesser extent) XI-K, as seen in Figure 9A, we may be able to detect re-distribution to
413 VirE2-Venus more easily when T-strands are introduced into the cells by *Agrobacterium*.
414 We generated transgenic plants expressing VirE2-Venus and individual myc-tagged myosin
415 CBD cDNAs (using *Agrobacterium* strains At2423-At2427), both under the control of a β-
416 estradiol-inducible promoter. After inducing the transgenes for 24 hr, we infected root segments
417 with *virE2* mutant *Agrobacterium* strains lacking or containing a T-DNA binary vector. The
418 bacteria (At2403 and At2404, respectively) additionally contained a plasmid expressing mCherry
419 to mark the location of the bacteria during infection. We observed fluorescence by confocal
420 microscopy eight hours after infection and calculated the percentage of fluorescence shift
421 between the cell periphery and the cytosol. When At2404, capable of transferring T-DNA, was
422 used, some of the VirE2-Venus fluorescence signal re-localized from the cell periphery into the
423 cytoplasm when plants expressed the myosin VIII-A, VIII-B, or VIII-2 CBDs (Figures 11C,
424 11D, and 11E, respectively, and movies in Supplemental Figures S13-15). No such
425 redistribution of the VirE2-Venus signal was observed when we infected roots with a strain,
426 At2403, lacking T-DNA. The distribution of VirE2-Venus signal was not altered in roots
427 infected with *A. tumefaciens* At2404 and expressing the CBDs of myosins VIII-1 or XI-K
428 (Figures 11 B and F; movies in Supplemental Figures S12 and S16). These results further
429 suggest that myosins VIII-A, VIII-B, and VIII-2 may temporarily tether VirE2 at the cell
430 periphery. However, upon transfer of T-DNA into the cell, VirE2 is released into the cellular
431 interior.
432
433 **Following T-DNA transfer, VirE2 moves from the cellular periphery to the interior along**
434 **actin filaments**
435 To address whether VirE2-Venus moves along actin filaments, we used *Arabidopsis* transgenic
436 lines expressing inducible VirE2-Venus and myc-tagged myosin VIII CBD cDNAs, and
437 expressing mCherry-ABD2 to mark actin filaments (using *Agrobacterium* strains At2365-
438 At2369). Time-lapse imaging of control plants, which expressed VirE2-Venus and mCherry-
439 ABD2 but without any myosin CBD, indicated that some VirE2-Venus moves along actin
440 filaments at a velocity of 0.353±0.06 μm/sec (Figure 12). In the presence of either one of the
441 four myosin VIII CBDs, the velocity of VirE2-Venus along actin filaments in leaf or root cells
442 remained unchanged (Table 1). Additionally, the velocity of VirE2-Venus movement along

actin filaments was not altered in the *myosin VIII-1/2/a/b* quadruple mutant (Figure 12, Table 1). However, when the myosin XI-K CBD was expressed in the plant, no VirE2 movement was detected in either leaf or root cells. These results indicate that only myosin XI-K, but not myosin VIII proteins, are important for VirE2 trafficking through leaf and root cells.

To test if the blockage of VirE2-Venus movement along actin filaments by the myosin XI-K CBD could be reversed by the presence of VirD2/T-strands, we infected roots with a *virE2* mutant *Agrobacterium* strain harboring a T-DNA with a mCherry-intron-NLS expression cassette (At2405). Time-lapse confocal microscopy still indicated no movement of VirE2-Venus in the mCherry expressing cells. (Table 1 and Supplemental Figure S17).

Taken together, our results indicate that myosin XI-K but not myosin VIII proteins are important for VirE2 intracellular trafficking. We suggest that myosin VIII proteins help tether VirE2 to the plasma membrane/peripheral regions of the cell. Upon introduction of VirD2/T-strands, VirE2 is released and is trafficked through the cell by myosin XI-K.

DISCUSSION

Importance of VirE2 in *Agrobacterium*-mediated plant transformation

Agrobacterium tumefaciens can transfer virulence (Vir) proteins and T-DNA into plant, fungal, and yeast cells (Chilton et al., 1977; Bundock et al., 1995; Piers et al., 1996; de Groot et al., 1998). During the transfer process, VirE2, the most abundant virulence protein (Engstrom et al., 1987), and four other Vir proteins exit the bacterium via a VirB/VirD4 type IV secretion system (T4SS) and facilitate transformation (Schrammeijer et al., 2003; Cascales and Christie, 2004; Vergunst et al., 2005). VirE2 is a single-strand (ss) DNA binding protein that binds ssDNA *in vitro* (Zupan et al., 1996). A popular theory proposes that VirE2 binds T-strands that enter the plant cell following infection by *Agrobacterium*, and that the resulting hypothetical T-complexes, composed of VirD2 covalently linked to T-strands and coated by VirE2 molecules, are the form of T-DNA that traffics within the cell (Li et al., 2020). However, T-complexes have not yet been identified in *Agrobacterium*-infected plants.

virE2 mutant *Agrobacterium* strains are highly attenuated in virulence (Stachel and Nester, 1986). Fewer T-strands can be isolated from plant cells infected by an *Agrobacterium virE2* mutant than from cells infected by a wild-type *Agrobacterium* strain (Yusibov et al., 1994), and the few transformants produced by a *virE2* mutant *Agrobacterium* strain generally harbor large T-DNA deletions, suggesting a protective function of VirE2 on T-strands (Rossi et al., 1996). However, a *virE2* mutant *Agrobacterium* strain can efficiently transform plants expressing VirE2 (*in planta* complementation), indicating both the importance of VirE2 in transformation and that the function of VirE2 in transformation occurs within the plant (Citovsky et al., 1992; Lapham et al., 2021). The efficient rescue of an *Agrobacterium virE2* mutant by *in planta* complementation indicates that VirE2 trafficking within a plant cell can be studied using plant lines that produce VirE2, rather than studying VirE2 trafficking after delivery from *Agrobacterium*. However, our *in planta* system is not appropriate for investigating initial VirE2 delivery into the plant.

As well as its proposed protective function, VirE2 may facilitate T-DNA entry into the plant by forming single-strand DNA-specific pores in the plant plasma membrane, as it can in artificial membranes (Dumas et al., 2001). Following transfer to the plant, VirE2 initially accumulates on the cytoplasmic side of host plasma membranes at points where bacteria contact the plant cell (Li and Pan, 2017). Accumulation of VirE2 on the membrane is facilitated by its interaction with

the *Agrobacterium* effector protein VirE3, which also accumulates in the host plasma membrane at contact sites with the bacteria (Lacroix et al., 2005; Li et al., 2018; Li et al., 2020). Interaction of VirE2 with importin alpha may help guide VirE2 towards the nucleus (Bhattacharjee et al., 2008), although this interaction is weak (Chang et al., 2014). Therefore, VirE2 may be involved in the trafficking of the T-complex inside the plant cell. However, our knowledge of the precise trafficking process of VirE2 inside the host cells, and the proteins that coordinate this trafficking to facilitate transformation, remains sparse.

Importance of the actin cytoskeleton for transformation and intracellular VirE2 movement

The actin cytoskeleton is essential for numerous biological processes in plants, including cell morphogenesis, tip growth, organelle movement, vesicle trafficking, and maintenance of cell polarity (Hussey et al., 2006; Staiger et al., 2009; Duan and Tominaga, 2018). Actin genes are categorized according to their expression patterns. In *Arabidopsis*, the vegetative actins (*ACT2*, *ACT7*, and *ACT8*) are mainly expressed in roots (Meagher et al., 1999), whereas *ACT4* and *ACT12* are primarily expressed during pollen development (Huang et al., 1996). We conducted transient and stable root transformation assays of *act2* and *act7* mutants (Figure 1A). These assays indicated that mutation of these genes greatly inhibited transformation. Restoration of transformation-susceptibility by introducing an *ACT7* cDNA into *act7* mutant plants confirmed that the transformation deficiency of the *act7* mutant was caused by mutation of this gene. Mutation of the pollen-expressed *ACT12* gene had no effect on root transformation, as expected. In addition, we measured the velocity of VirE2-Venus movement along actin filaments, which were marked with mCherry-ABD2, in *Arabidopsis* leaf cells. VirE2 aggregates moved with an average velocity of 0.353 $\pm$ 0.06 μm/sec in leaf cells and 0.312 ± 0.07 μm/sec in root cells (Table 1), similar to the velocity (0.434 μm/sec) recorded by Yang et al. (2017) within tobacco leaf cells.

Salman et al. (2005) showed that VirE2 binds to microtubules *in vitro*, and Sakalis et al. (2014) showed colocalization of YFP-VirE2 with fluorescently tagged microtubules in yeast and plant cells. However, they did not assay transformation in the presence of microtubule disrupting agents. We observed no difference in transformation between wild-type and *bot-1* mutant *Arabidopsis* roots, which have a disorganized cortical microtubule network, indicating that correctly organized microtubules are not required for efficient transformation of plants.

520 **Importance of *Arabidopsis* myosin isoforms for transformation**

521 The movement of molecules, vesicles, and organelles along actin filaments relies on the highly
522 conserved myosin motors (Avisar et al., 2008b; Madison and Nebenfuhr, 2013; Ueda et al., 2015;
523 Citovsky and Liu, 2017). Myosins have actin-binding, ATPase, and cargo binding domains, and
524 these activities contribute to a wide range of physiological processes, including root hair growth,
525 organelle motility, tip growth of pollen tubes, and gamete nuclear migration (Prokhnevsky et al.,
526 2008; Peremyslov et al., 2010; Madison et al., 2015; Geeves, 2016). Plants contain two classes
527 of myosins, the plant-specific myosin VIII class comprising four members (myosins VIII-1, 2, A,
528 and B) and the myosin XI class comprising 13 members (myosins XI-A through K, and myosins
529 XI-1 and XI-2). Most of the myosin XI proteins are localized in the cytosol and are responsible
530 for intracellular movement of their cargos, including vesicles and organelles (Peremyslov et al.,
531 2008; Peremyslov et al., 2010). Myosin XI-K in particular is important for vesicular trafficking
532 (Yang et al., 2014). Myosin VIII proteins localize predominantly to the cellular periphery,
533 including the plasma membrane, plasmodesmata, and cortical microtubules (Golomb et al., 2008;
534 Haraguchi et al., 2014; Bar-Sinai et al., 2022) although we have found that myosin VIII-B also
535 localizes to the nucleus (Figure 9A). Myosin VIII proteins may be important for intercellular
536 movement of viral proteins and for helping guide plant cell division (Avisar et al., 2008a; Amari
537 et al., 2014; Wu and Bezanilla, 2014).

538 Upon entry into a plant cell, VirE2 may interact with VirE3 and associate with the plasma
539 membrane where myosin VIII proteins localize, then move towards the nucleus after associating
540 with T-DNA (Li et al., 2018; Tu et al., 2018). We therefore tested the importance of each
541 myosin XI and myosin VIII protein for transformation by conducting transient and stable root
542 transformation assays on individual myosin gene mutants (Figures 1B and 1C). Interestingly,
543 only disruption of the myosin *XI-h* gene substantially (greater than two-fold) inhibited
544 transformation (Supplemental Figure S1A). Myosin XI-H is moderately strongly expressed in
545 all root tissues and is phylogenetically most closely related to myosins XI-B and XI-G, that are
546 not well-expressed in roots, and to myosin XI-2 which does show root expression (Peremyslov et
547 al., 2011). No specific cellular function had previously been assigned to myosin XI-H (reviewed
548 by Duan and Tominaga, 2018). We were somewhat surprised not to see an effect of a myosin *xi-*
549 *k* mutation on transformation because Yang et al. (2017) showed that RNAi inhibition of *N.*
550 *benthamiana* myosin XI-K decreased *Agrobacterium*-mediated transformation by ~50%.

551 However, *Arabidopsis* may encode more myosin XI isoforms than does *N. benthamiana* (Avisar
552 et al., 2008b), permitting functional redundancy of the *Arabidopsis* myosin XI isoforms to
553 conceal a role for *Arabidopsis* myosin XI-K in transformation.
554 Because the vast majority of single myosin XI or myosin VIII mutants did not affect
555 transformation, we tested the effect of higher order myosin mutants on this process. Roots from
556 plants mutant in two, three, or four myosin XI genes showed increasing deficiency in
557 transformation susceptibility (Figures 1B and 1C). As previously noted, these higher order
558 myosin XI mutants showed increasing root developmental defects as more myosin XI genes
559 were mutated (Supplemental Figure S1B; Ojangu et al., 2007; Peremyslov et al., 2008). Because
560 our *Arabidopsis* transformation assays were conducted on roots, the natural target for
561 *Agrobacterium*-mediated transformation, we were concerned that these root developmental
562 problems may complicate the interpretation of our transformation data. We therefore turned our
563 attention to higher order *Arabidopsis* myosin VIII mutants whose roots appeared normal
564 (Supplemental Figure S1B). These higher order myosin VIII mutants also showed decreased
565 transformation susceptibility (Figures 1B and 1C).
566 To test the importance of each myosin *VIII* gene in transformation, we individually expressed
567 cDNAs for each of the myosin VIII proteins in the myosin *VIII-1/2/a/b* quadruple mutant. Three
568 of these genes, encoding myosins VIII-2, A, and B, could partially restore transformation
569 susceptibility to the quadruple mutant (Figure 2A), indicating that they play an important role in
570 transformation. Simultaneous expression of two of these cDNAs in the quadruple mutant further
571 increased transformation (Figure 2C), indicating that these myosin VIII proteins are not
572 completely redundant with regard to transformation. However, expression of the cDNA
573 encoding myosin VIII-1 did not affect transformation (Figure 2A), suggesting a fundamental
574 difference among these class VIII myosins for their roles in *Agrobacterium*-mediated
575 transformation. As shown in Figures 6, 7, 8, 10 and discussed below, myosins VIII-2, VIII-A,
576 and VIII-B can directly interact with *Agrobacterium* VirE2, an important effector protein for
577 transformation, whereas myosin VIII-1 does not directly interact with VirE2. However, it may
578 indirectly interact with VirE2 within a protein complex. Ectopically expressed myosin VIII-A,
579 VIII-B, and VIII-2 cargo binding domains (CBD) localize strongly to the peripheral regions of
580 root cells (myosin VIII-B also localizes in the nucleus), whereas myosin VIII-1 additionally
581 localizes substantially in the cytosol (Figure 9A). Furthermore, expression of the CBDs of

582 myosins VIII-2 and VIII-A decreased the size of VirE2 aggregates that form in the myosin *VIII-*
583 *1/2/a/b* quadruple mutant, whereas expression of the myosin VIII-1 CBD did not. These
584 observations indicate a fundamental difference among these myosin VIII isoforms in their
585 interaction with VirE2, their subcellular localization, and their effects on transformation.
586 Interestingly, overexpression of a myosin *VIII-1* cDNA in wild-type *Arabidopsis* increased
587 transformation, indicating both that myosin VIII-1 does play some role in transformation, and
588 that this protein is limiting in wild-type roots (Figure 2B). Overexpression of myosin *VIII-A*,
589 *VIII-B*, or *VIII-2* cDNAs in wild-type roots, either individually or in combination, did not alter
590 transformation susceptibility, indicating that these proteins are naturally found in amounts
591 maximal for transformation.
592
593 **Some myosin VIII isoforms may tether VirE2 to the plasma membrane until T-strands**
594 **enter the plant cell**
595 Several studies have indicated that myosin VIII proteins, or their globular tail domains, localize
596 at the plasma membrane, especially at plasmodesmata (Radford and White, 1998; Reichelt et al.,
597 1999; Avisar et al., 2008a; Golomb et al., 2008; Amari et al., 2014). Our results showed that
598 VirE2-Venus substantially co-localizes with each of the four transgenically expressed myosin
599 VIII protein CBDs at the plasma membrane of root cells, although co-localization with myosin
600 VIII-1 is less extensive (Figure 9A). When roots of these transgenic plants were incubated with
601 *Agrobacterium* lacking T-DNA, the association of VirE2 with the peripheral regions of the cell
602 remained largely unchanged. However, incubation of these roots with *Agrobacterium* containing
603 T-DNA relocalized much of the VirE2-Venus signal to the cytosol. In addition, incubation of
604 roots expressing VirE2-Venus (but not any myosin VIII CBD) with *Agrobacterium* containing T-
605 DNA relocalized a portion of the VirE2-Venus signal to the perinuclear area, but not into the
606 nucleus. These results are consistent with previous observations that VirE2 localizes mainly
607 within the cytosol and, especially, perinuclear regions upon infection of cells with an
608 *Agrobacterium* strain that can transfer VirD2/T-strands to plant cells, and that only a very small
609 quantity may enter the nucleus (Li et al., 2020).
610 To examine how various myosin isoforms may faciltate VirE2 movement from the plasma
611 membrane region to the cytosol, we measured the velocity of VirE2-Venus movement along
612 mCherry-ABD2-labeled actin filaments with and without expression of various myosin VIII or

613 myosin XI-K CBDs. For these experiments, it was assumed that the CBDs could act as domiant
614 negative molecules to bind VirE2, thereby inhibiting VirE2 movement along these actin
615 filaments. In both the absence and presence of myosin VIII CBD expression, VirE2 trafficked
616 along *Arabidopsis* actin filaments with a velocity of 0.31-0.40 µm/sec, a velocity similar (~0.502
617 µm/sec) to that calculated by Yang et al. (2017) in tobacco. These data indicate that myosin VIII
618 proteins are not important for intracellular VirE2 trafficking. However, co-expression of the
619 myosin XI-K CBD with VirE2-Venus completely blocked VirE2 movement along actin
620 filaments, suggesting that this myosin isoform is at least partially responsible for intracellular
621 VirE2 trafficking, as suggested by Yang et al. (2017).
622
623 **A model for the role of myosin proteins in VirE2 plasma membrane tethering and**
624 **movement through plant cells**
625 Research from several laboratories, and this study, has informed our revised model for how
626 *Agrobacterium* virulence effector proteins, such as VirE2, and T-DNA enter a plant cell, form
627 complexes, and traffic T-DNA to the nucleus (Figure 13). VirE2 has the ability to generate pores
628 in artificial lipid membranes through which single-strand DNA molecules, such as T-strands,
629 may penetrate (Dumas et al., 2001; Duckely et al., 2005; Grange et al., 2008). VirE2 delivered
630 from *Agrobacterium* localizes to the cytoplasmic side of the plant plasma membrane, held there
631 by interaction with another virulence effector protein, VirE3 (Li et al., 2018, 2020). Our data
632 similarly show that plant-expressed VirE2-Venus, which can effect transformation by a *virE2*
633 mutant *Agrobacterium* cell, also partially localizes to the cytoplasmic side of the plasma
634 membrane. We propose that VirE2 is tethered to the plasma membrane by various myosin VIII
635 isoforms. Upon entry of VirD2/T-strands into the plant, VirE2 is released from the plasma
636 membrane and associates with T-strands. This hypothetical T-complex is trafficked along an
637 actin/endoplasmic reticulum network (Yang et al., 2017) by myosin XI-K, or a functionally
638 similar myosin XI protein, towards the nucleus. Consistent with this mechanism of trafficking,
639 we have previously shown that a Rab GTPase, which modulates vesicle trafficking in
640 biosynthetic and endocytic pathways, is important for transformation (Hwang and Gelvin, 2004),
641 and that a VAP33-like SNARE protein, that localizes to ER-plasma membrane contact sites
642 (Wang et al., 2014; Wang et al., 2015), interacts with VirE2 (Lee et al., 2012).

We are aware that one aspect of our analysis does not easily fit this proposed model: Expression of the myosin XI-K CBD completely inhibited detectable VirE2 movement through the cytosol but had no effect on *Agrobacterium*-mediated transformation. Inhibition of VirE2 movement by the myosin XI-K CBD occurred regardless of whether *Agrobacterium* was present to transfer T-DNA into the cells. We note that the requirement for VirE2 in *Agrobacterium*-mediated transformation is not absolute: 1. *Agrobacterium*-mediated yeast transformation does not require VirE2, although mutation of *virE2* results in a ~10-fold decrease in yeast transformation (Bundock et al., 1995), and 2. Some *A. rhizogenes* strains do not encode VirE2, although they are highly virulent. These strains encode two proteins, GALLS-FL and GALLS-CT, that can functionally complement a *virE2*-mutant *A. tumefaciens* strain, although the amino acid sequence and protein domains of VirE2 and GALLS proteins are highly dissimilar (Hodges et al., 2004, 2006; Ream, 2009). With regard to the results of experiments conducted in this study, we suggest either that a small, undetectable population of VirE2 molecules associates with incoming T-strands and traffics towards the nucleus to effect transformation, or (a somewhat heretical model) that VirE2 does not interact with T-strands in plant cells and that tracking VirE2 movement through the cell does not correlate with intracellular T-DNA movement. Future experiments will attempt to solve this conundrum.

661 ## MATERIALS AND METHODS

662 **Plant and bacterial materials and growth conditions.** Seeds of wild-type (ecotype Col-0),
663 mutant, and transgenic *Arabidopsis thaliana* were surface-sterilized with 50% bleach and 0.01%
664 SDS, washed five times with sterile water, then placed on Gamborg's B5 medium (Gibco) with
665 the appropriate antibiotics (when used, hygromycin 10 µg/mL). Seedlings were grown in 16 hr
666 light/8 hr dark conditions at 25°C. *E. coli* strains were grown at 37°C in LB medium (per liter:
667 Tryptone 10 g, NaCl 10 g, Yeast extract 5 g). *A. tumefaciens* strains were grown at 28°C in YEP
668 medium (per liter: Bacto peptone 10 g, Yeast extract 10 g, NaCl 5 g). When used, antibiotic
669 concentrations were: For *E. coli*, ampicillin, 100 µg/ml; kanamycin, 50 µg/ml; spectinomycin,
670 100 µg/ml; for *A. tumefaciens*, rifampicin, 10 µg/ml; spectinomycin, 100 µg/ml. All bacterial
671 strains and plasmid constructs used in this study are listed in Supplemental Tables S1 and S2.
672
673 **Construction of plasmids and binary vectors and generation of transgenic plants.** A
674 description of all plasmids used in this study, including details of their construction, is given in
675 Supplemental Table S1. Primers used for these constructions are given in Supplemental Table
676 S3. Final *E. coli* and *A. tumefaciens* strains are given in Supplemental Table S2. Recombinant
677 constructions were transformed into *E. coli* TOP10 or DH10B before characterization and
678 transfer to the appropriate *Agrobacterium* strains by electroporation. For protein expression,
679 plasmids were transferred to *E. coli* BL21DE3. T-DNA binary vectors in *Agrobacterium* were
680 used to transform plants of the Col-0 or the *myosin VIII-1/2/a/b* quadruple mutant background
681 utilizing a floral dip transformation protocol (Clough and Bent, 1998).
682
683 ***Agrobacterium*-mediated transient and stable transformation assays.** Overnight
684 *Agrobacterium* cultures were diluted 1:10 into 20 ml of YEP medium containing the appropriate
685 antibiotics and grown at 28°C until they reached an A_{600} = 0.83 (~10^9 cells/ml). The cells were
686 collected by centrifugation, washed with sterile 0.9% NaCl, and serially diluted in 0.9% NaCl for
687 transient and stable root transformation assays. For transient transformation assays, infection of
688 *Arabidopsis* root segments was performed with *Agrobacterium* strains containing the T-DNA
689 binary vector pBISN1 (Narasimhulu et al., 1996) as previously described (Tenea et al., 2009).
690 Transformation efficiency was reported as the percentage of root segments stained blue with 5-

691 bromo-4-chloro-3-indolyl-β-D-glucuronic acid (X-gluc) after two days co-cultivation with
692 bacteria on MS medium plus an additional four days on CIM (Callus-Inducing Medium)
693 containing 100 µg/ml timentin. For stable transformation, after two days of cocultivation, root
694 segments were separated onto CIM containing 100 µg/ml timentin and the appropriate selection
695 agent. The plates were incubated at 23°C for four weeks, after which they were scored for callus
696 development on the ends of the roots. Stable transformation efficiency was calculated as the
697 percentage of total segments showing calli. Transient and stable transformation assays were
698 conducted in triplicate, with >100 root segments per replicate.
699
700 **Bimolecular fluorescence complementation (BiFC).** A VirE2 coding sequence was fused with
701 cEYFP (C-terminal 64 amino acid residues of an *EYFP* gene) and under the control of a β-
702 estradiol-inducer promoter in the vector pSAT1 to make pSAT1-Pi-VirE2-cEYFP. cDNAs
703 encoding myosin VIII CBDs were amplified using the appropriate primers (Supplemental Table
704 S3), fused with nVenus (N-terminal 174 amino acids of a *Venus* gene) and cloned, under the
705 control of a β-estradiol-inducer promoter in pSAT6, to make pSAT6-Pi-nVenus-myosin VIII
706 CBD. The Pi-VirE2-cEYFP expression cassette and the Pi-nVenus-myosin VIII CBD
707 expression cassettes were digested with *Asc*I and PI-*Psp*I, respectively, and cloned into the same
708 sites in the binary vector pE4437. pE4437 also contains a *hptII* plant selection marker, an
709 expression cassette for a nuclear marker (P_{35S}-Cerulean-NLS), and an actin cytoskeleton marker
710 (P_{35S}-mCherry-actin binding domain2, ABD2). These final constructs were introduced into *A.*
711 *tumefaciens* GV3101::pMP90 (Koncz and Schell, 1986) by electroporation to make *A.*
712 *tumefaciens* At2320-At2324, respectively, and used to generate transgenic Col-0 *Arabidopsis*
713 plants for *in vivo* BiFC assays.
714
715 **Yeast two hybrid assay**. An octopine-type VirE2 gene from pTiA6 was cloned into the bait
716 vector pGBKT7, and the myosin VIII and myosin XI CBD cDNAs were individually cloned into
717 the prey vector pGADT7 (Clontech). As negative controls, empty bait, empty prey, and Lamin
718 C prey plasmids were used (Krendel et al., 2007). A cDNA encoding the VirE2-interacting
719 protein 1 (VIP1) was used as a positive control (Tzfira et al., 2001). Yeast transformations were
720 performed using a lithium acetate method (Sato et al., 1994). Cells were plated onto synthetic

721 dropout (SD)-agar plates lacking tryptophan and leucine. Three days after transformation, yeast
722 cells from the resulting colonies were plated onto SD medium lacking tryptophan, leucine, and
723 histidine (-Trp-Leu-His) supplemented with 3-amino-1,2,4-triazole (3AT) to test for protein
724 interactions.
725
726 ***In vitro* protein pull-down assay.** The plasmid pET28a (Novagen, San Diego, CA) was used to
727 generate recombinant proteins fused in-frame with a Venus tag or a myc tag. A full-length
728 cDNA encoding VirE2 fused with Venus was cloned into pET28a with *Nco*I+*Not*I. cDNAs
729 encoding the CBDs (amino acids 953-1,166 for myosin VIII-1; amino acids 1,003-1,220 for
730 myosin VIII-2; amino acids 948-1,153 for myosin VIII-A; amino acids 954-1,136 for myosin
731 VIII-B; amino acids 808-1,531 for myosin XI-K) of myosin VIII and XI-K were amplified and
732 cloned into pET28a with *Nco*I+*Bam*HI (myosin VIII CBDs) or *Nco*I+*Not*I (myosin XI-K CBD)
733 to generate myc fusions. The full-length cDNA of VIP1 was cloned into pET28a with
734 *Nco*I+*Bam*HI to use as a myc-tagged positive control, and for negative controls Lamin C fused
735 with a myc tag, or Venus only, were cloned into pET28a with *Sma*I+*Bam*HI. The constructs
736 were transformed into *E. coli* BL21 (DE3). Bacteria were cultured at 16°C for 18 hours in the
737 presence of 0.5 mM isopropylthio-β-galactoside (IPTG). The cells were centrifuged and the
738 pellet was sonicated in cell lysis buffers (20 mM HEPES-KOH pH 7.2, 50 mM potassium acetate,
739 50 mM KCl, 1 mM EDTA, 1 mM EGTA, 1 mM DTT, 5% glycerol, 0.5% Triton X-100, 1 mM
740 phenylmethylsulfonylfluoride [PMSF]). VirE2-Venus and Venus cell lysates were incubated
741 with GFP-Trap magnetic agarose beads (Chromotek, USA) at 4°C for 2 hr with gentle shaking.
742 The beads were washed three times with cell lysate buffer (0.2% Triton X-100) and then
743 incubated with bacterial lysates from *E. coli* cells expressing myc-tagged VIP1, myc-tagged
744 Lamin C, or myc-tagged myosin VIII/XI-K CBDs proteins that were prepared as described
745 above. The binding reactions were incubated at 4°C for 1 hr with gentle shaking. The beads
746 were washed three times with cell lysate buffer (0.2% Triton X-100) followed by boiling in
747 sodium dodecyl sulfate polyacrylamide gel electrophoresis (SDS-PAGE) buffer for 10 min.
748 Protein samples were loaded onto 10% SDS polyacrylamide gels, subjected to electrophoresis
749 (60 Volts 1.5 hrs for the stacking gel and 100 Volts 4.5 hrs for the separating gel), then either
750 stained with Coomassie blue or subjected to western blot analysis using a 1:1000 dilution of

751 mouse anti-GFP or mouse anti-Myc antibodies (Cell Signaling Technology, USA). After
752 addition of a 1:5000 dilution of horseradish peroxidase-conjugated horse anti-mouse secondary
753 antibodies (Catalog #7076; Cell Signaling Technology, USA), proteins were detected using an
754 ECL kit (LI-COR Biosciences, Lincoln, NE, USA).
755
756 ***In vivo* co-immunoprecipitation (co-IP) assay.** Transgenic *Arabidopsis* plants (generated using
757 *Agrobacterium* strains At2423-At2427) harboring an inducible expression cassette of either
758 VirE2-Venus, or Venus, and of each myc-tagged myosin VIII or XI-K CBDs were used for *in*
759 *vivo* protein-protein interaction assays. Transgenic lines expressing, upon induction, myc-tagged
760 CBDs and Venus were used as negative controls (At2428). Four-week old plants were treated
761 with 5 μM β-estradiol for 24 hr, and roots were harvested and ground in liquid nitrogen using a
762 mortar and pestle. A total of 0.25 g of the ground tissue was transferred into a 2 ml tube and 500
763 μl of CoIP buffer (50 mM Tris-HCl, pH 7.5, 150 mM NaCl, 0.1% Triton X-100, 0.2% Nonidet
764 P-40, 0.6 mM PMSF, and 20 μM MG132 in a Roche protease inhibitor cocktail) was added. The
765 mixture was mixed thoroughly by repeated cycles of 30 sec vortexing followed by chilling on ice.
766 The samples were centrifuged at 4°C, 13000g for 5 min. A total of 20 μl of anti-GFP beads was
767 pre-washed with wash buffer (50 mM Tris-HCl, pH 7.5, 150 mM NaCl, 0.6 mM PMSF, and 20
768 μM MG132 with Roche protease inhibitor cocktail) three times, the beads were added to the
769 extracted supernatant solution, and the reactions were incubated at 4°C for 1 hr with gentle
770 shaking. The beads were washed five times with wash buffer, proteins were eluted by incubation
771 with 4x LDS sample loading buffer (Invitrogen, CA, USA) at 95℃ for 3 min. The proteins were
772 fractionated by SDS-PAGE and analyzed using western blots, with a 1:1000 dilution of anti-GFP
773 and anti-Myc antibodies, respectively. The proteins were detected using an ECL kit (LI-COR
774 Bioscienccs, Lincoln, NE, USA).
775
776 **Localization of VirE2-Venus after infection of *Arabidopsis* roots with *Agrobacterium* strains**
777 **harboring or lacking T-DNA.** Transgenic *A. thaliana* lines expressing a *VirE2-Venus* gene
778 under the control of a β-estradiol inducible promoter were treated with 5 μM β-estradiol for 24 hr.
779 Roots were infected with a *virE2* mutant strain *A. tumefaciens* strain (*A. tumefaciens* EHA105
780 containing a non-polar deletion of *virE2*; At1872) containing the plasmid pBBR1-
781 MCS2::mCherry to track red fluorescent bacteria (At2405). The *Agrobacterium* cells either

782 contained or lacked the T-DNA binary vector pE4672 (*A. tumefaciens* At2404 and At2403,
783 respectively). Overnight bacterial cultures were transferred to fresh AB-glucose medium and
784 grown until the cell density reached an A_{600}=0.83. The bacteria were centrifuged and
785 resuspended in induction medium (1x AB salts, 2% glucose, 30 mM MES, 2 mM Na_2HPO4, 2
786 mM NaH_2PO4) containing 100 μM acetosyringone and cultured for 16-20 hr. Six hr after
787 cocultivation with bacteria at 10^8 cfu/ml, root segments were observed by confocal microscopy
788 (Zesis 880 Upright Confocal microscope with a Plan-Apo 20×/0.8 objective). Images from 100
789 cells of each infection were analyzed using Image J.
790
791 **Confocal microscopy imaging.** For VirE2-Venus trafficking, transgenic plantlets harboring an
792 inducible *Venus-VirE2* transgene (generated using *A. tumefaciens* At2365-At2369) were placed
793 on B5 agar plates containing 100 μg/ml timentin and 20 μg/ml hygromycin and grown vertically
794 for one week. The plants were treated with 10 μM β-estradiol for 9 hr, washed with sterile water,
795 and time lapse images of the roots were taken using a Zeiss 880 confocal microscope equipped
796 with a 20 X water objective. For VirE2 relocalization assays, similarly grown plants were
797 treated with 5 μM β-estradiol for 24 hr, washed with sterile water, and infected with 10^8 cfu/ml
798 of a *virE2* mutant *Agrobacterium* strain containing or lacking a T-DNA binary vector. Infections
799 were conducted for 8 hr as described above, and images were taken using a Zeiss 880 confocal
800 microscope equipped with a Plan-Apo 20×/0.8 objective.
801

802 ## SUPPLEMENTAL DATA

803 **Supplemental Figure S1.** Most *myosin VIII* and *myosin XI* single mutants are not deficient in
804 stable transformation.
805 **Supplemental Figure S2.** Growth and morphology of wild-type and higher order *myosin VIII*
806 and *XI* mutant plants.
807 **Supplemental Figure S3.** Effect on transformation of expressing full-length myosin cDNAs in
808 wild-type and *myosin VIII-1/2/a/b* mutant plants.
809 **Supplemental Figure S4.** Effect on transformation of expressing full-length inducible myosin
810 cDNAs in wild-type and *myosin VIII-1/2/a/b* mutant plants.

Supplemental Figure S5. Effect on transformation of expressing pairs of full-length myosin cDNAs in wild-type and *myosin VIII-1/2/a/b* mutant plants.

Supplemental Figure S6. Inducible expression of myosin VIII, but not myosin XI-K, CBDs inhibits transformation.

Supplemental Figure S7. Co-localization of VirE2-Venus and FM4-64.

Supplemental Figure S8. Subcellular localization of VirE2-Venus in transgenic plants.

Supplemental Figure S9. Myosin VIII CBDs colocalize with the plasma membrane marker PIP2A.

Supplemental Figure S10. VirE2 re-localizes to the perinuclear area after infection by an *Agrobacterium* strain that can transfer T-DNA.

Supplemental Figure S11. Infection of root cells with an *Agrobacterium* strain capable of transferring T-DNA re-localizes VirE2-Venus from the cellular periphery into the cytoplasm.

Supplemental Figure S12. Infection of root cells with an *Agrobacterium* strain capable of transferring T-DNA does not re-localizes VirE2-Venus from the cellular periphery into the cytoplasm when the myosin VIII-1 CBD is expressed.

Supplemental Figure S13. Infection of root cells with an *Agrobacterium* strain capable of transferring T-DNA re-localizes VirE2-Venus from the cellular periphery into the cytoplasm.

Supplemental Figure S14. Infection of root cells with an *Agrobacterium* strain capable of transferring T-DNA re-localizes VirE2-Venus from the cellular periphery into the cytoplasm.

Supplemental Figure S15. Infection of root cells with an *Agrobacterium* strain capable of transferring T-DNA re-localizes VirE2-Venus from the cellular periphery into the cytoplasm.

Supplemental Figure S16. Expression of the myosin XI-K CBD does not affect VirE2-Venus localization upon infection by *Agrobacterium.*

Supplemental Figure S17. Expression of the myosin XI-K CBD inhibits movement of VirE2-Venus.

ACKNOWLEDGEMENTS

The authors thank Dr. Valerian V. Dolja, Oregon State University, for providing the *Arabidopsis* mutant lines. We thank the Purdue University Imaging Facility for use of their confocal microscope. We also thank Dr. Kiran Mysore for critical reading of the manuscript.

842 **FUNDING**

843 This project was supported by grants from the US National Science Foundation: IOS 1725122
844 and IOS-2006668. DNA sequence data were obtained with partial support from a P30 grant
845 (CA023168) to the Purdue University Cancer Center.

846

847

REFERENCES

Amari K, Di Donato M, Dolja VV, Heinlein M. (2014) Myosins VIII and XI play distinct roles in reproduction and transport of tobacco mosaic virus. PLoS Pathog 10: e1004448

Avisar D, Prokhnevsky AI, Dolja VV. (2008a) Class VIII myosins are required for plasmodesmatal localization of a closterovirus Hsp70 homolog. J Virol 82: 2836-2843

Avisar D, Prokhnevsky AI, Makarova KS, Koonin EV, Dolja VV. (2008b) Myosin XI-K is required for rapid trafficking of Golgi stacks, peroxisomes, and mitochondria in leaf cells of *Nicotiana benthamiana*. Plant Physiol 146: 1098-1108

Bar-Sinai S, Belausov E, Dwivedi V, Sadot,E. (2022) Collisions of cortical microtubules with membrane associated myosin VIII tail. Cells 11:145

Bezanilla M, Horton AC, Sevener HC, Quatrano RS. (2003) Phylogenetic analysis of new plant myosin sequences. J Mol Evol 57: 229-239

Bhattacharjee S, Lee L-Y, Oltmanns H, Cao H, Veena, Cuperus J, Gelvin SB. (2008) IMPa-4, an *Arabidopsis* importin alpha isoform, is preferentially involved in *Agrobacterium*-mediated plant transformation. Plant Cell 20: 2661-2680

Bichet A, Desnos T, Turner S, Grandjean O, Hofte H. (2001) BOTERO1 is required for normal orientation of cortical microtubules and anisotropic cell expansion in *Arabidopsis*. Plant J 25: 137-148

Bundock P, den Dulk-Ras A, Beijersbergen A, Hooykaas PJ. (1995) Trans-kingdom T-DNA transfer from *Agrobacterium tumefaciens* to *Saccharomyces cerevisiae*. EMBO J 14: 3206-3214

Cascales E, Christie,PJ. (2004) Definition of a bacterial type IV secretion pathway for a DNA substrate. Science 304: 1170-1173

Chang CW, Williams SJ, Counago RM, Kobe B. (2014) Structural basis of interaction of bipartite nuclear localization signal from *Agrobacterium* VirD2 with rice importin-alpha. Mol Plant 7: 1061-1064

Chilton M-D, Drummond MH, Merio DJ, Sciaky D, Montoya AL, Gordon MP, Nester EW. (1977) Stable incorporation of plasmid DNA into higher plant cells: The molecular basis of crown gall tumorigenesis. Cell 11: 263-271

Christie PJ, Atmakuri K, Krishnamoorthy V, Jakubowski S, Cascales E. (2005) Biogenesis, architecture, and function of bacterial type IV secretion systems. Annu Rev Microbiol 59: 451-485

Citovsky V, Liu B. (2017) Myosin-driven transport network in plants is functionally robust and distinctive. Proc Natl Acad Sci USA 114: 1756-1758

Citovsky V, Wong ML, Zambryski P. (1989) Cooperative interaction of *Agrobacterium* VirE2 protein with single-stranded DNA: Implications for the T-DNA transfer process. Proc Natl Acad Sci USA 86: 1193-1197

Citovsky V, Zupan J, Warnick D, Zambryski P. (1992) Nuclear localization of *Agrobacterium* VirE2 protein in plant cells. Science 256: 1802-1805

Clough SJ, Bent AF. (1998) Floral dip: A simplified method for *Agrobacterium*-mediated transformation of *Arabidopsis thaliana*. Plant J 16: 735-743

de Groot MJ, Bundock P, Hooykaas PJ, Beijersbergen AG. (1998) *Agrobacterium tumefaciens*-mediated transformation of filamentous fungi. Nat Biotechnol 16: 839-842

Djamei A, Pitzschke A, Nakagami H, Rajh I, Hirt H. (2007) Trojan horse strategy in *Agrobacterium* transformation: abusing MAPK defense signaling. Science 318: 453-456

Duan Z, Tominaga M. (2018) Actin-myosin XI: An intracellular control network in plants. Biochem Biophys Res Commun 506: 403-408

Duckely M, Oomen C, Axthelm F, Van Gelder P, Waksman G, Engel A. (2005) The VirE1VirE2 complex of *Agrobacterium tumefaciens* interacts with single-stranded DNA and forms channels. Mol Microbiol 58: 1130-1142

Dumas F, Duckely M, Pelczar P, Van Gelder P, Hohn B. (2001) An *Agrobacterium* VirE2 channel for transferred-DNA transport into plant cells. Proc Natl Acad Sci USA 98: 485-490

Dym O, Albeck S, Unger T, Jacobovitch J, Branzburg A, Michael Y, Frenkiel-Krispin D, Wolf S., Elbaum M. (2008) Crystal structure of the *Agrobacterium* virulence complex VirE1-VirE2 reveals a flexible protein that can accommodate different partners. Proc Natl Acad Sci USA 105: 11170-11175

Embley TM, Martin W. (2006) Eukaryotic evolution, changes and challenges. Nature 440: 623-630

908 Engstrom P, Zambryski P, Van Montagu M, Stachel S. (1987) Characterization of
909 *Agrobacterium tumefaciens* virulence proteins induced by the plant factor acetosyringone.
910 J Mol Biol 197: 635-645
911 Foth BJ, Goedecke MC, Soldati D. (2006) New insights into myosin evolution and classification.
912 Proc Natl Acad Sci USA 103: 3681-3686
913 Geeves MA. (2016) Review: The ATPase mechanism of myosin and actomyosin. Biopolymers
914 105: 483-491
915 Gelvin SB. (1998) *Agrobacterium* VirE2 proteins can form a complex with T strands in the plant
916 cytoplasm. J Bacteriol 180: 4300-4302
917 Gelvin SB. (2000) *Agrobacterium* and plant genes involved in T-DNA transfer and integration.
918 Annu Rev Plant Physiol Plant Mol Biol 51: 223-256
919 Gelvin SB. (2003) *Agrobacterium* and plant transformation: The biology behind the "gene-
920 jockeying" tool. Microbiol Mol Biol Rev 67: 16-37
921 Gelvin, SB. (2006) *Agrobacterium* transformation of *Arabidopsis thaliana* roots: A quantitative
922 assay. Methods Mol Biol 343: 105-113
923 Gelvin SB. (2010) Finding a way to the nucleus. Curr Opin Microbiol 13: 53-58
924 Gelvin SB. (2017) Integration of *Agrobacterium* T-DNA into the plant genome. Annual review
925 of genetics 51: 22
926 Golomb L, Abu-Abied M, Belausov E, Sadot E. (2008) Different subcellular localizations and
927 functions of *Arabidopsis* myosin VIII. BMC Plant Biol 8: 3
928 Grange W, Duckely M, Husale S, Jacob S, Engel A, Hegner M. (2008) VirE2: A unique ssDNA-
929 compacting molecular machine. PLoS Biol 6: e44
930 Haraguchi T, Tominaga M, Matsumoto R, Sato K, Nakano A, Yamamoto K, Ito K. (2014)
931 Molecular characterization and subcellular localization of *Arabidopsis* class VIII myosin,
932 ATM1. J Biol Chem 289: 12343-12355
933 Hodges L, Cuperus J, Ream W. (2004) *Agrobacterium rhizogenes* GALLS protein
934 substitutes for *Agobacterium tumefaciens* single-stranded DNA-binding protein VirE2. J
935 Bacteriol 186: 3065-3077
936 Hodges LD, Vergunst AC, Neal-McKinney J, den Dulk-Ras A, Moyer DM,

Hooykaas PJJ, Ream W. (2006) *Agrobacterium rhizogenes* GALLS protein contains domains for ATP binding, nuclear localization, and type IV secretion. J Bacteriol 188: 8222-8230

Howard E, Citovsky V. (1990) The emerging structure of the *Agrobacterium* T-DNA transfer complex. Bioessays 12: 103-108

Huang S, An YQ, McDowell JM, McKinney EC, Meagher RB. (1996) The *Arabidopsis thaliana* ACT4/ACT12 actin gene subclass is strongly expressed throughout pollen development. Plant J 10: 189-202

Hussey,PJ, Ketelaar T, Deeks MJ. (2006) Control of the actin cytoskeleton in plant cell growth. Annu Rev Plant Biol 57: 109-125

Hwang H-H, Gelvin SB. (2004) Plant proteins that interact with VirB2, the *Agrobacterium tumefaciens* pilin protein, mediate plant transformation. Plant Cell 16: 3148-3167

Koncz C, Schell J. (1986) The promoter of TL-DNA gene 5 controls the tissue-specific expression of chimaeric genes carried by a novel type of *Agrobacterium* binary vector. Mol Gen Genet 204: 383-396

Krendel M, Osterweil EK, Mooseker MS. (2007) Myosin 1E interacts with synaptojanin-1 and dynamin and is involved in endocytosis. FEBS Lett 581: 644-650

Lacroix B, Citovsky V. (2013) The roles of bacterial and host plant factors in *Agrobacterium*-mediated genetic transformation. Int J Dev Biol 57: 467-481

Lacroix B, Vaidya M, Tzfira T, Citovsky V. (2005) The VirE3 protein of *Agrobacterium* mimics a host cell function required for plant genetic transformation. EMBO J 24: 428-437

Lapham RA, Lee L-Y, Xhako E, Gomez EG, Nivya VM., and Gelvin, S.B. (2021). *Agrobacterium* VirE2 protein modulates plant gene expression and mediates transformation from its location outside the nucleus. Front Plant Sci 12, 684192

Lee L-Y, Wu F-H, Hsu C-T, She, S-C, Yeh,HY, Liao D-C, Fang M-J, Liu N-T, Yen Y-C, Dokládal L, Sýkorová E, Gelvin SB, Lin C-S (2012) Screening a cDNA library for protein-protein interactions directly *in planta*. Plant Cell. 24: 1746-1759

Lee YR, Liu B. (2004) Cytoskeletal motors in *Arabidopsis*. Sixty-one kinesins and seventeen myosins. Plant Physiol 136: 3877-3883

Li X, Pan SQ. (2017) *Agrobacterium* delivers VirE2 protein into host cells via clathrin-mediated endocytosis. Sci Adv 3: e1601528

Li X, Tu H, Pan SQ. (2018) *Agrobacterium* delivers anchorage protein VirE3 for companion VirE2 to aggregate at host entry sites for T-DNA protection. Cell Rep 25: 302-311 e306

Li X, Yang Q, Peng L, Tu H, Lee L-Y, Gelvin SB, Pan SQ. (2020) *Agrobacterium*-delivered VirE2 interacts with host nucleoporin CG1 to facilitate the nuclear import of VirE2-coated T complex. Proc Natl Acad Sci USA 117: 26389-26397

Li X, Zhu T, Tu H, Pan SQ. (2020) *Agrobacterium* VirE3 uses its two tandem domains at the C-terminus to retain its companion VirE2 on the cytoplasmic side of the host plasma membrane. Front Plant Sci 11:464

Madison SL, Nebenfuhr A. (2013) Understanding myosin functions in plants: Are we there yet? Curr Opin Plant Biol 16: 710-717

Madison SL, Buchanan ML, Glass JD, McClain TF, Park E, Nebenfuhr A. (2015) Class XI myosins move specific organelles in pollen tubes and are required for normal fertility and pollen tube growth in *Arabidopsis*. Plant Physiol 169: 1946-1960

McCullen CA, Binns AN. (2006) *Agrobacterium tumefaciens* and plant cell interactions and activities required for interkingdom macromolecular transfer. Annu Rev Cell Dev Biol 22: 101-127

Meagher RB, McKinney EC, Kandasamy MK. (1999) Isovariant dynamics expand and buffer the responses of complex systems: The diverse plant actin gene family. Plant Cell 11: 995-1006

Narasimhulu SB, Deng XB, Sarria R, Gelvin SB. (1996) Early transcription of *Agrobacterium* T-DNA genes in tobacco and maize. Plant Cell 8: 873-886

Ojangu EL, Jarve K, Paves H, Truve E. (2007) *Arabidopsis thaliana* myosin XIK is involved in root hair as well as trichome morphogenesis on stems and leaves. Protoplasma 230: 193-202

Otten L, DeGreve H, Leemans J, Hain R, Hooykaas P, Schell J. (1984) Restoration of virulence of *vir* region mutants of *Agrobacterium tumefaciens* strain B6S3 by coinfection with normal and mutant *Agrobacterium* strains. Mol Gen Genet 195: 159-163

Peremyslov VV, Prokhnevsky AI, Dolja VV. (2010) Class XI myosins are required for development, cell expansion, and F-Actin organization in *Arabidopsis*. Plant Cell 22: 1883-1897

998 Peremyslov VV, Prokhnevsky AI, Avisar D, Dolja VV. (2008) Two class XI myosins function in
999 organelle trafficking and root hair development in *Arabidopsis*. Plant Physiol 146: 1109-
1000 1116
1001 Peremyslov,VV, Mockler TC, Filichkin S., Fox SE, Jaiswal P, Makarova K., Koonin .V,
1002 Dolja,VV. (2011) Expression, splicing, and evolution of the myosin gene family in plants.
1003 Plant Physiol 155: 1191-1204
1004 Piers KL, Heath JD, Liang X, Stephens KM, Nester EW. (1996) *Agrobacterium tumefaciens*-
1005 mediated transformation of yeast. Proc Natl Acad Sci USA 93: 1613-1618
1006 Prokhnevsky AI, Peremyslov,VV, Dolja VV. (2008) Overlapping functions of the four class XI
1007 myosins in *Arabidopsis* growth, root hair elongation, and organelle motility. Proc Natl
1008 Acad Sci USA 105: 19744-19749
1009 Radford JE, White RG. (1998) Localization of a myosin-like protein to plasmodesmata. Plant J
1010 14: 743-750
1011 Ream W. (2009) *Agrobacterium tumefaciens* and *A. rhizogenes* use different proteins to transport
1012 bacterial DNA into the plant cell nucleus. Micro Biotechnol 2: 416-42.
1013 Reichelt S, Knight AE, Hodge TP, Baluska F, Samaj J, Volkmann D, Kendrick-Jones J. (1999)
1014 Characterization of the unconventional myosin VIII in plant cells and its localization at
1015 the post-cytokinetic cell wall. Plant J 19: 555-567
1016 Reisen D, Hanson MR. (2007) Association of six YFP-myosin XI-tail fusions with mobile plant
1017 cell organelles. BMC Plant Biol 7: 6
1018 Richards TA, Cavalier-Smith T. (2005) Myosin domain evolution and the primary divergence of
1019 eukaryotes. Nature 436: 1113-1118
1020 Rossi L, Hohn B, Tinland B. (1996) Integration of complete transferred DNA units is dependent
1021 on the activity of virulence E2 protein of *Agrobacterium tumefaciens*. Proc Natl Acad Sci
1022 USA 93: 126-130
1023 Roushan MR, deZeeuw MAM, Hooykaas PJJ, van Heusden GPH. (2018) Application
1024 of phiLOV2.1 as a fluorescent marker for visualization of *Agrobacterium* effector protein
1025 translocation. Plant J 96: 685-699
1026 Sakalis,PA, van Heusden GP, Hooykaas PJ. (2014) Visualization of VirE2 protein translocation
1027 by the *Agrobacterium* type IV secretion system into host cells. Microbiologyopen 3: 104-
1028 117

1029 Salman H, Abu-Arish A, Oliel S, Loyter A, Klafter J, Granek R, Elbaum M. (2005) Nuclear
1030 localization signal peptides induce molecular delivery along microtubules. Biophys J 89:
1031 2134-2145
1032 Sato T, Hanada M, Bodrug S, Irie, S, Iwama N, Boise LH, Thompson CB, Golemis E, Fong L,
1033 Wang HG. (1994) Interactions among members of the Bcl-2 protein family analyzed with
1034 a yeast two-hybrid system. Proc Natl Acad Sci U S A 91: 9238-9242
1035 Sattarzadeh A, Franzen R, Schmelzer E. (2008) The *Arabidopsis* class VIII myosin ATM2 is
1036 involved in endocytosis. Cell Motil Cytoskeleton 65: 457-468
1037 Schrammeijer B, den Dulk-Ras A, Vergunst AC, Jurado Jacome E, Hooykaas PJ. (2003)
1038 Analysis of Vir protein translocation from *Agrobacterium tumefaciens* using
1039 *Saccharomyces cerevisiae* as a model: Evidence for transport of a novel effector protein
1040 VirE3. Nucleic Acids Res 31: 860-868
1041 Sen P, Pazour GJ, Anderson D, Das A. (1989) Cooperative binding of *Agrobacterium*
1042 *tumefaciens* VirE2 protein to single-stranded DNA. J Bacteriol 171: 2573-2580
1043 Shi Y, Lee L-Y, Gelvin SB. (2014) Is VIP1 important for *Agrobacterium*-mediated
1044 transformation? Plant J 79: 848-860
1045 Simone M, McCullen CA, Stahl LE, Binns AN. (2001) The carboxy-terminus of VirE2 from
1046 *Agrobacterium tumefaciens* is required for its transport to host cells by the virB-encoded
1047 type IV transport system. Mol Microbiol 41: 1283-1293
1048 Smith LG, Oppenheimer .G. (2005) Spatial control of cell expansion by the plant cytoskeleton.
1049 Annu Rev Cell Dev Biol 21: 271-295
1050 Sparkes I, Runions J, Hawes C, Griffing L. (2009) Movement and remodeling of the
1051 endoplasmic reticulum in nondividing cells of tobacco leaves. Plant Cell 21: 3937-3949
1052 Stachel SE, Nester EW. (1986) The genetic and transcriptional organization of the vir region of
1053 the A6 Ti plasmid of *Agrobacterium tumefaciens*. EMBO J 5: 1445-1454
1054 Staiger CJ, Sheahan MB, Khurana P, Wang X, McCurdy DW, Blanchoin L. (2009) Actin
1055 filament dynamics are dominated by rapid growth and severing activity in the
1056 *Arabidopsis* cortical array. J Cell Biol 184: 269-280
1057 Szymanski DB, Cosgrove DJ. (2009) Dynamic coordination of cytoskeletal and cell wall systems
1058 during plant cell morphogenesis. Curr Biol 19: R800-811

1059 Tenea GN, Spantzel J, Lee L-Y, Zhu Y, Lin K, Johnson SJ, Gelvin SB. (2009) Over-expression
1060 of several *Arabidopsis* histone genes increases *Agrobacterium*-mediated transformation
1061 and transgene expression in plant cells. Plant Cell 21: 3350–3367
1062 Trybus KM. (2008) Myosin V from head to tail. Cell Mol Life Sci 65: 1378-1389
1063 Tu H, Li X, Yang Q, Peng L, Pan SQ. (2018) Real-time trafficking of *Agrobacterium* virulence
1064 protein VirE2 inside host cells. Curr Top Microbiol Immunol 418: 261-286
1065 Tzfira T, Vaidya M, Citovsky V. (2001) VIP1, an *Arabidopsis* protein that interacts with
1066 *Agrobacterium* VirE2, is involved in VirE2 nuclear import and *Agrobacterium* infectivity.
1067 EMBO J 20: 3596-3607
1068 Tzfira T, Li J, Lacroix B, Citovsky V. (2004) *Agrobacterium* T-DNA integration: Molecules and
1069 models. Trends Genet 20: 375-383
1070 Ueda H, Tamura K, Hara-Nishimura I. (2015) Functions of plant-specific myosin XI: from
1071 intracellular motility to plant postures. Curr Opin Plant Biol 28: 30-38
1072 Ueda H, Yokota E, Kutsuna N, Shimada T, Tamura K, Shimmen T, Hasezawa S, Dolja VV.,
1073 Hara-Nishimura I. (2010) Myosin-dependent endoplasmic reticulum motility and F-actin
1074 organization in plant cells. Proc Natl Acad Sci USA 107: 6894-6899
1075 Ueki S, Citovsky V. (2005) Identification of an interactor of cadmium ion-induced glycine-rich
1076 protein involved in regulation of callose levels in plant vasculature. Proc Natl Acad Sci
1077 USA 102: 12089-12094
1078 Vale RD. (2003) The molecular motor toolbox for intracellular transport. Cell 112: 467-480
1079 Vergunst AC, van Lier MC, den Dulk-Ras A, Stuve TA, Ouwehand A, Hooykaas PJ. (2005)
1080 Positive charge is an important feature of the C-terminal transport signal of the VirB/D4-
1081 translocated proteins of *Agrobacterium*. Proc Natl Acad Sci USA 102: 832-837
1082 Wang H, Han S, Siao W, Song C, Xiang Y, Wu X, Cheng P, Li H, Jasik J, Micieta K, Turna J,
1083 Voigt B, Baluska F, Liu J, Wang Y, Zhao H. (2015) *Arabidopsis* synaptotagmin 2
1084 participates in pollen germination and tube growth and is delivered to plasma membrane
1085 via conventional secretion. Mol Plant 8: 1737-1750
1086 Wang P, Hawkins TJ, Richardson C, Cummins I, Deeks MJ, Sparkes I, Hawes C, Hussey PJ.
1087 (2014) The plant cytoskeleton, NET3C, and VAP27 mediate the link between the plasma
1088 membrane and endoplasmic reticulum. Curr Biol 24: 1397-1405

Wojtaszek P, Anielska-Mazur A, Gabrys H, Baluska F, Volkmann D. (2005) Recruitment of myosin VIII towards plastid surfaces is root-cap specific and provides the evidence for actomyosin involvement in root osmosensing. Funct Plant Biol 32: 721-736

Wu Z, Bezanilla M. (2014) Myosin VIII associates with microtubule ends and together with actin plays a role in guiding plant cell division. Elife 3:e03498

Yang L, Qin L, Liu G, Peremyslov VV, Dolja VV, Wei Y. (2014) Myosins XI modulate host cellular responses and penetration resistance to fungal pathogens. Proc Natl Acad Sci USA 111: 13996-14001

Yang Q, Li X, Tu H, Pan SQ. (2017) *Agrobacterium*-delivered virulence protein VirE2 is trafficked inside host cells via a myosin XI-K-powered ER/actin network. Proc Natl Acad Sci USA 114: 2982-2987

Yusibov VM, Steck TR, Gupta V, Gelvin, SB. (1994) Association of single-stranded transferred DNA from *Agrobacterium tumefaciens* with tobacco cells. Proc Natl Acad Sci USA 91: 2994-2998

Zuo J, Niu Q-W, Chua N-H. (2000) An estrogen receptor-based transactivator XVE mediates highy inducible gene expression in transgenic plants. Plant J 24: 265-273

Zupan JR, Citovsky V, Zambryski P. (1996) *Agrobacterium* VirE2 protein mediates nuclear uptake of single-stranded DNA in plant cells. Proc Natl Acad Sci USA 93: 2392-2397

1109 **FIGURE LEGENDS**

1110

1111 **Figure 1. Some *Arabidopsis* actin and myosin genes are important for *Agrobacterium*-**
1112 **mediated transformation. (A)** Root segments from *Arabidopsis* wild-type and *act2-1*, *act7-1*,
1113 *act7-4*, *act12*, *act7*-4 comp (complemented), or *bot1* mutants were infected with *A. tumefaciens*
1114 A208 (tumorigenic strain for stable transformation; left panel) or *A. tumefaciens* At849 (T-DNA
1115 contains a plant-active *gusA*-intron gene for transient transformation; right panel). After two
1116 days, the root segments were moved to medium (MS lacking phytohormones for stable
1117 transformation, CIM for transient transformation) containing timentin to kill the bacteria. For
1118 stable transformation, the presence of tumors was scored one month after infection. For transient
1119 transformation, root segments were stained with X-gluc after an additional four days, and the
1120 percentage of roots showing GUS activity was calculated. *act7-4* comp, *act7-4* mutant
1121 complemented with an *ACT7* cDNA. **(B and C)** Root segments from *Arabidopsis* wild-type and
1122 single or higher order *myosin VIII* or *XI* mutants were infected with *A. tumefaciens* At849
1123 transiently or *A. tumefaciens* A208 stably. A total of 10-15 plants and >100 segments per plant
1124 were tested for stable transformation. Values given are means ± SE. Asterisks indicate
1125 significant differences compared to wild-type plants. [*t-test*, $*P < 0.05$; $**P < 0.01$].

1126

1127 **Figure 2**. **All Myosin VIII family members can contribute to *Agrobacterium*-mediated**
1128 **transformation.** Root segments from transgenic *Arabidopsis* individually expressing either an
1129 empty vector or *myosin VIII* cDNAs in *myosin VIII-1/2/a/b* mutant plants **(A)**, or in wild-type
1130 plants **(B)**, were infected with *A. tumefaciens* At849. Transgenic *Arabidopsis* expressing cDNAs
1131 encoding *myosins VIII-2, VIII-A, VIII-B, VIII-2+VIII-B* or *VIII-A+VIII-B* in the *myosin VIII-*
1132 *1/2/a/b* mutant background **(C)** or in wild-type Col0 plants **(D)** were similarly infected with *A.*
1133 *tumefaciens* At849. Transient transformation efficiencies are indicated as the percentage of roots
1134 showing GUS activity six days after infection. A total of 10-15 plants and >100 segments per
1135 plant, from five independent transgenic lines, were tested for transient transformation. Values
1136 given are means ± SE Asterisks indicate significant differences compared to control plants that
1137 contain an empty vector (**A** and **B**), the *myosin VIII-1/2/a/b* quadruple mutant (**C**), or wild-type
1138 Col-0 plants (**D**). [*t-test*, $*P < 0.05$; $**P < 0.01$; $***P < 0.001$; $****P < 0.0001$].

1139

1140

1141 **Figure 3**. **Inducible expression of myosin VIII, but not the myosin XI-K, cargo binding**
1142 **domains (CBD) inhibits transient transformation.** Root segments from transgenic
1143 *Arabidopsis* expressing the cargo binding domain (CBD) of the indicated myosin protein, under
1144 the control of a β-estradiol inducible promoter, were treated with β-estradiol or control solutions
1145 for 24 hr before infection with *A. tumefaciens* At849. The percentage of roots showing GUS
1146 activity six days after infection indicates the transient transformation efficiency. A total of 10-15
1147 plants and >100 segments per plant, from five independent transgenic lines, were tested for
1148 transient transformation. Values given are means ± SE. Asterisks indicate significant
1149 differences compared to uninduced plants. [*t-test*, $^{**}P < 0.01$; $^{***}P < 0.001$].
1150

1151 **Figure 4**. **Expression of VirE2-Venus in the *myosin VIII-1/2/a/b* mutant cannot**
1152 **complement a *virE2* mutant *Agrobacterium* strain for transient transformation. (A)**
1153 *Agrobacterium*-mediated transient transformation assays were conducted on roots of four
1154 independent transgenic lines of wild-type (Lines 2, 4, 5 and 8) or **(B)** the *myosin VIII-1/2/a/b*
1155 mutant (Lines 2, 3, 12, and 13). Root segments were inoculated with 10^6, 10^7, or 10^8 cfu/ml of
1156 the *virE2* mutant strain *A. tumefaciens* At1879 containing the T-DNA binary vector pBISN2.
1157 Plants were treated with β-estradiol (gray bars) or control solution (black bars) for VirE2-Venus
1158 expression 24 hr before infection. The percentage of roots showing GUS activity was calculated
1159 as in Figure 1. A total of 10-15 plants from each line and >100 segments per plant were tested
1160 for transient transformation. Values given are means ± SE. Asterisks indicate significant
1161 differences compared to uninduced plants. [*t-test*, $^{*}P < 0.05$; $^{**}P < 0.01$]. **(C)** Confocal images
1162 showing aggregation of VirE2-Venus proteins in transgenic roots of either wild-type (top panel)
1163 or *myosin VIII 1/2/a/b* mutant backgrounds (bottom panel). **(D)** Quantitative analysis of the size
1164 of VirE2-Venus aggregates and the percentage of the cellular area occupied by the aggregates.
1165 Image J was used for analysis. The average VirE2-Venus aggregate size was 2.0±0.3 μm^2 in
1166 wild-type roots, and 6.2±0.6 μm^2 in *myosin VIII-1/2/a/b* quadruple mutant roots. **(E)** Western
1167 blot detection of VirE2-Venus proteins expressed in transgenic plants of either the Col-0 or the
1168 *myosin VIII-1/2/a/b* quadruple myosin mutant background. Mouse anti-GFP antibody was used
1169 to detect VirE2-Venus protein expressed after induction of individual transgenic lines. The

1170 house-keeping protein phosphoenolpyruvate carboxylase (PEPC) was detected using a rabbit
1171 anti-PEPC antibody and served as an internal control.

1172 **Figure 5**. **Analysis of VirE2-Venus aggregates in roots of transgenic *Arabidopsis* expressing**
1173 **the CBDs of various Myosin VIII proteins.** Roots were treated with β-estradiol for eight hr.
1174 Random areas of confocal images from roots expressing **(A)** Myosin VIII-1 or VIII-2 CBDs, or
1175 **(B)** Myosin VIII-A or VIII-B CBDs were analyzed using Image J. Both the sizes and the
1176 percentage of the cellular area occupied by the VirE2-Venus aggregates are shown.

1177 **Figure 6**. **VirE2-Venus interacts with some myosin cargo binding domains (CBDs) *in vitro*.**
1178 VirE2-Venus or Venus proteins were incubated with the indicated myc-tagged myosin CBD,
1179 VIP1, or Lamin C. Following binding to anti-GFP beads, proteins were eluted and subjected to
1180 Western blot analysis using anti-myc antibodies. Coomassie stained gels are shown in panels **A**,
1181 **C**, and **E**, and immunoblots in panels **B**, **D**, and **F**. VirE2-Venus interacts with the CBDs of
1182 myosins VIII-2, VIII-A, VIII-B, and XI-K, and with VIP1 (panels **B**, **D**, and **F**), but not with the
1183 CBD of myosin VIII-1 or with Lamin C (panels **D** and **F**). Venus, as a negative control, does not
1184 interact with any myc-tagged protein.

1185 **Figure 7**. **The cargo binding domains (CBD) of some myosins interact with VirE2 in yeast.**
1186 Yeast two-hybrid analysis was conducted with VirE2 as the bait and individual myosin CBDs as
1187 the prey. Following co-transformation of the bait and prey plasmids, single colonies were picked
1188 and serial dilutions of yeast were grown on **(A)** SD-Trp-Leu (-TL) medium, or **(B)** SD-Trp-Leu-
1189 His medium supplemented with 3 mM 3-amino-1,2,4-triazole (-TLH+3AT). Colony growth on
1190 SD-TLH+3AT indicates interaction between VirE2 and the myosin CBD. VIP1 was used as a
1191 positive control for interaction with VirE2. Lamin C and the empty vector were used as negative
1192 controls. SD, synthetic dropout medium.

1193 **Figure 8**. **Myosin cargo binding domains can form complexes with VirE2 when expressed**
1194 **in *Arabidopsis*. (A)** Protein extracts from roots of transgenic *Arabidopsis* plants expressing
1195 VirE2-Venus, or Venus, and the indicated myc-tagged myosin CBD transgenes were incubated
1196 with anti-GFP beads, the bound proteins eluted, and subjected to Western blot analysis using
1197 anti-myc antibodies. Myc-tagged VIP1 was used as a positive control. **(B)** Root extracts

1198 expressing VirE2-Venus or Venus and myc-tagged myosin VIII-2 CBD were incubated with
1199 anti-GFP beads, the bound proteins eluted, and subjected to Western blot analysis using anti-myc
1200 antibodies.

1201 **Figure 9**. **Co-localization of VirE2-Venus and mCherry-myosin CBDs in *Arabidopsis* roots.**
1202 **(A)** Roots of transgenic *Arabidopsis* plants containing VirE2-Venus and mCherry-myosin CBD
1203 genes, each under the control of a β-estradiol-inducible promoter, were treated with β-estradiol
1204 for 8 hr and examined by confocal microscopy. Bars indicate 50 μm. **(B)** Pearson's correlation
1205 and overlap coefficient of Venus and mCherry fluorescence. A total of 10-15 transgenic lines
1206 and >50 cells per construct were used for quantitative analysis using Image J. Values >0.5
1207 indicate co-localization of the two proteins for both methods of analysis. The red line indicates a
1208 co-localization ratio of 0.5.

1209 **Figure 10**. **Bimolecular fluorescence complementation (BiFC) of VirE2 with various**
1210 **myosin CBDs in *Arabidopsis* roots.** Transgenic *Arabidopsis* plants containing VirE2-cEYFP
1211 and the indicated myosin CBDs-nVenus, each under the control of a β-estradiol-inducible
1212 promoter, were treated with β-estradiol for 48 hr and the fluorescence signal detected by
1213 confocal microscopy. VirE2 interacts with the CBDs of **(A),** myosin VIII-2; **(B),** myosin VIII-A;
1214 and **(D),** myosin VIII-B at the plasma membrane. VirE2 interacts with the myosin XI-K CBD at
1215 the plasma membrane and within the cytoplasm **(E)**. VirE2 does not interact with the myosin
1216 VIII-1 CBD **(C)** or Lamin C **(F)**. Yellow fluorescence indicates interaction of VirE2-Venus with
1217 the myosin CBD. Actin filaments are labeled by mCherry-ABD2. The figure shows merged
1218 images of the Venus and mCherry signals. Bars indicate 50 μm.
1219

1220 **Figure 11**. **Incubation of *Arabidopsis* roots with *Agrobacterium* that can transfer T-DNA**
1221 **results in increased VirE2-Venus in the perinuclear region.** **(A)** Transgenic *Arabidopsis*
1222 plants containing an inducible *VirE2-Venus* transgene were treated with 5 μm β-estradiol for 24
1223 hr, followed by inoculation with 10^8 cfu/ml of the *virE2* mutant *A. tumefaciens* At1872 without a
1224 binary vector (At2403, left panel) or with T-DNA on a binary vector (At2404, right panel). The
1225 percentage of total VirE2-Venus fluorescence in the perinuclear area was calculated. Images of
1226 10-15 transgenic lines and >50 cells were analyzed. The data indicate means ± SE. Asterisks

indicate significant differences between roots inoculated with the two *Agrobacterium* strains. **(B-F)** the relative distribution of VirE2-Venus at the cell poles or in the cytoplasm following infection with *A. tumefaciens* At2403 or At2404 of roots co-expressing CBDs of myosin VIII-1. myosin VIII-2, myosin VIII-A, myosin VIII-B, or myosin XI-K (B, C, D, E, F, respectively). Images of 10-15 transgenic lines and >50 cells were analyzed. The data indicate means ± SE. Asterisks indicate significant differences between roots inoculated with the two *Agrobacterium* strains. [*t-test*, $*P < 0.05$; $**P < 0.01$; $***P < 0.001$].

Figure 12. **Loss of function of myosin XI-K, but not myosin VIII, disrupts movement of VirE2-Venus along actin filaments.** Transgenic plants expressing mCherry-ABD2 constitutively and VirE2-Venus inducibly in Col-0, *myosin VIII-1/2/a/b*, and myosin XI-K CBD plants were used in this experiment. Roots of these plants were treated with 10 μm β-estradiol for 8 hr. Time lapse images were taken by confocal microscopy. Four images of each field are shown at the indicated times (0, 60, 90, and 120 seconds). Blue arrows indicate the initial position of a particular VirE2-Venus aggregate; white arrows indicate the position of the same aggregate at various times thereafter. Bars indicate 5 μm.

Figure 13. **Model of myosin VIII and myosin XI-K involvement in VirE2 trafficking to the perinuclear region.** **(A)** *Agrobacterium* virulence effector proteins, including VirE2 and VirE3, are secreted into host cells through a Type IV secretion system. VirE2 and VirE3 interact at the plant plasma membrane. Myosin VIII proteins localize at the plasma membrane and help tether VirE2 to the plasma membrane when no T-DNA is present. **(B)** When T-strands (as a VirD2/T-strand complex) enter the host cell, VirE2 molecules are released and some may bind T-DNA, following which VirE2 interacts with myosin XI-K and moves along actin filaments to the perinuclear region. Not shown are the *Agrobacterium* virulence effector proteins VirD5 and VirF which also are transferred to the plant.

1255 **Table 1.** Velocity of VirE2-Venus movement in leaf and root cells of various *Arabidopsis*
1256 transgenic lines

Transgene(s) in plant/ *Agrobacterium* infection[a]	***Arabidopsis* background**	**Velocity in leaves (µm/sec)**	**Velocity in roots (µm/sec)**
VirE2-Venus	Col-0	0.353± 0.06	0.312± 0.07
VirE2-Venus	myosin *VIII-1/2/a/b*	0.378± 0.02	0.318± 0.02
VirE2-Venus + Myosin VIII-1 CBD	Col-0	0.407 ± 0.06	0.341 ± 0.04
VirE2-Venus + Myosin VIII-2 CBD	Col-0	0.398 ± 0.07	0.321 ± 0.02
VirE2-Venus + Myosin VIII-A CBD	Col-0	0.387 ± 0.07	0.304 ± 0.01
VirE2-Venus + Myosin VIII-B CBD	Col-0	0.401 ± 0.05	0.328 ± 0.04
VirE2-Venus + Myosin XI-K CBD	Col-0	Not detectable	Not detectable
VirE2-Venus + Myosin XI-K CBD + *Agrobacterium* (- T-DNA)	Col-0	Not detectable	Not detectable
VirE2-Venus + Myosin XI-K CBD + *Agrobacterium* (+ T-DNA)	Col-0	Not detectable	Not detectable

1257 [a]All transgenes are under the control of a β-estradiol-inducible promoter; CBD, cargo binding
1258 domain. >50 cells of 10 independent transgenic lines were examined for each genotype of
1259 transgenic plant.
1260

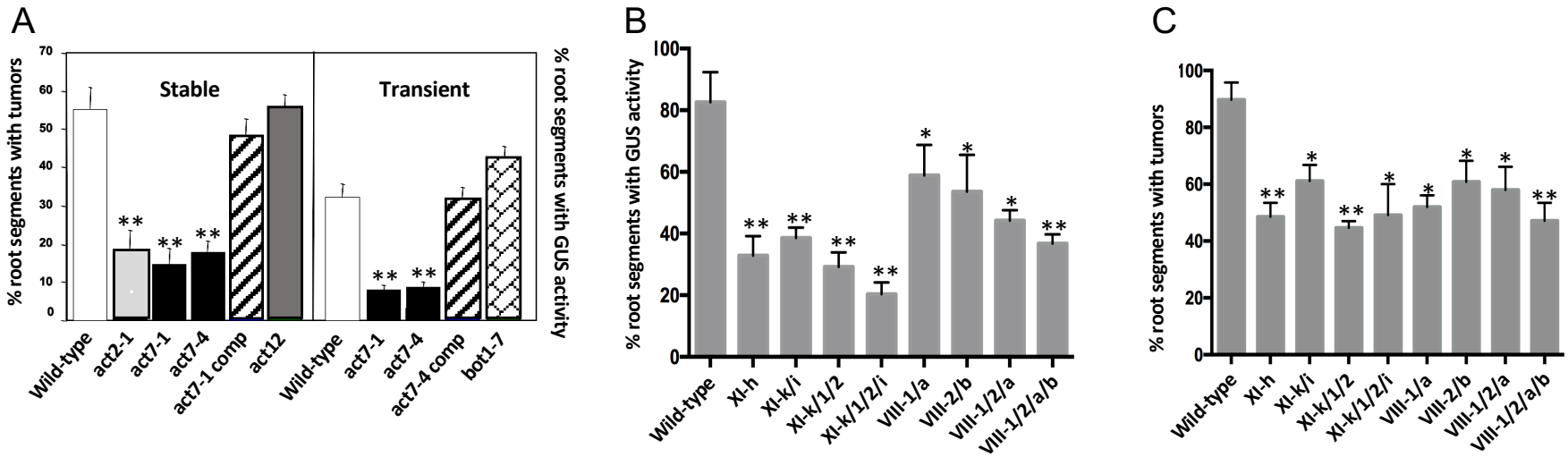

Figure 1. Some *Arabidopsis* actin and myosin genes are important for *Agrobacterium*-mediated root transformation. **(A)** Root segments from *Arabidopsis* wild-type and *act2-1*, *act7-1*, act7-4, *act12*, *act7*-4 comp, or *bot1* mutants were infected with *A. tumefaciens* A208 (tumorigenic strain for stable transformation; left panel) or *A. tumefaciens* At849 (T-DNA contains a plant-active *gusA*-intron gene for transient transformation; right panel). After two days, the root segments were moved to medium (MS lacking phytohormones for stable transformation, CIM for transient transformation) containing timentin to kill the bacteria. For stable transformation, the presence of tumors was scored one month after infection. For transient transformation, root segments were stained with X-gluc after an additional four days, and the percentage of roots showing GUS activity was calculated. *act7-4* comp, *act7-4* mutant complemented with an *ACT7* cDNA. **(B and C)** Root segments from *Arabidopsis* wild-type and single or higher order *myosin VIII* or *XI* mutants were infected with *A. tumefaciens* At849 transiently or *A. tumefaciens* A208 stably. A total of 10-15 plants and >100 segments per plant were tested for stable transformation. Values given are means ± SE. Asterisks indicate significant differences compared to wild-type plants. [*t-test*, $*P < 0.05$; $**P < 0.01$].

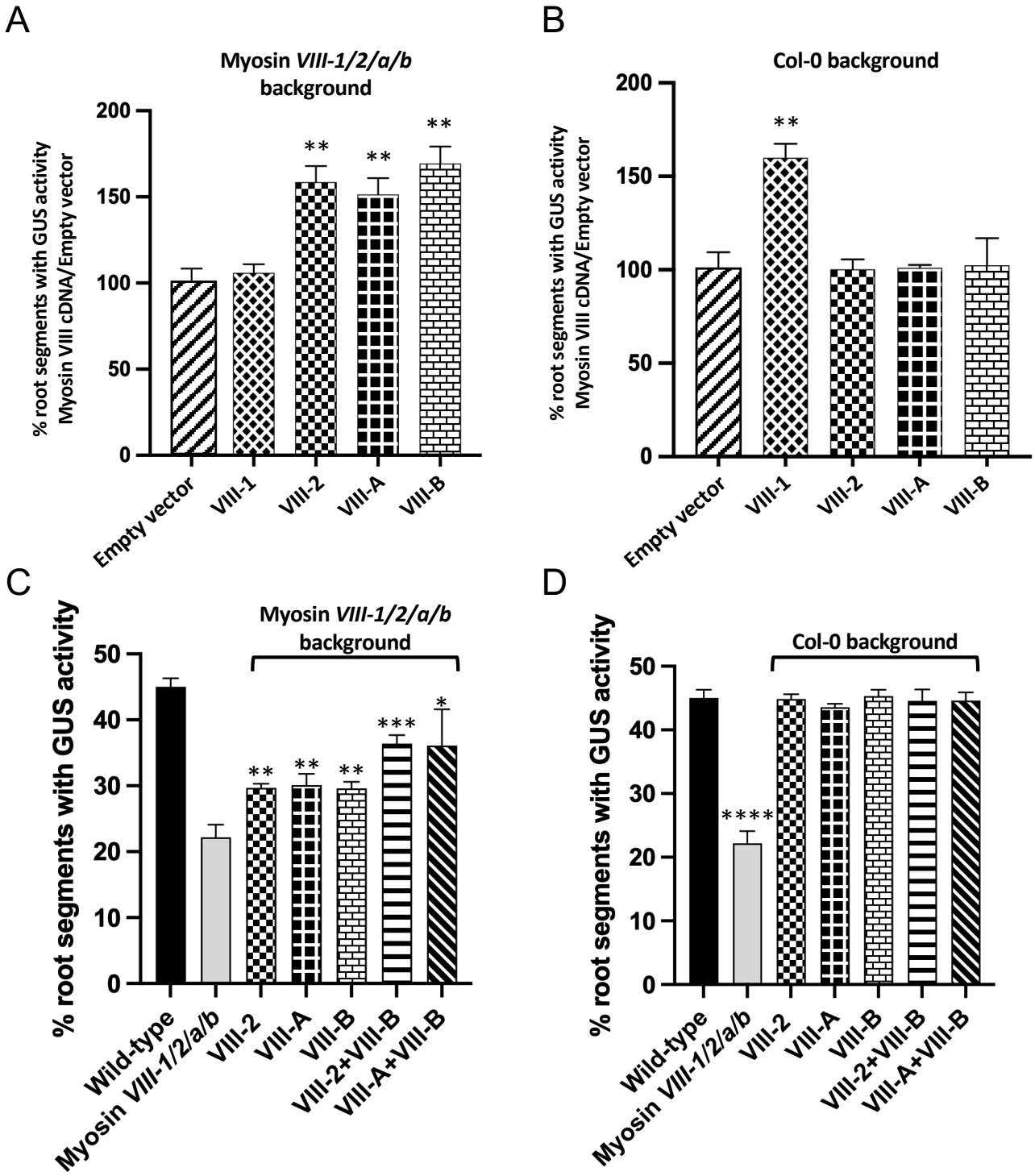
A
Myosin VIII-1/2/a/b background
% root segments with GUS activity
Myosin VIII cDNA/Empty vector
200
150
100
50
0
**
**
**
Empty vector
VIII-1
VIII-2
VIII-A
VIII-B
B
Col-0 background
% root segments with GUS activity
Myosin VIII cDNA/Empty vector
200
150
100
50
0
**
Empty vector
VIII-1
VIII-2
VIII-A
VIII-B
C
Myosin VIII-1/2/a/b background
% root segments with GUS activity
50
40
30
20
10
0
**
**
**
***
*
Wild-type
Myosin VIII-1/2/a/b
VIII-2
VIII-A
VIII-B
VIII-2+VIII-B
VIII-A+VIII-B
D
Col-0 background
% root segments with GUS activity
50
40
30
20
10
0
****
Wild-type
Myosin VIII-1/2/a/b
VIII-2
VIII-A
VIII-B
VIII-2+VIII-B
VIII-A+VIII-B

Figure 2. **All Myosin VIII family members can contribute to *Agrobacterium*-mediated transformation.** Root segments from transgenic *Arabidopsis* individually expressing either an empty vector or *myosin VIII* cDNAs in *myosin VIII-1/2/a/b* mutant plants **(A)**, or in wild-type plants **(B)**, were infected with *A. tumefaciens* At849. Transgenic *Arabidopsis* expressing cDNAs encoding *myosins VIII-2, VIII-A, VIII-B, VIII-2+VIII-B* or *VIII-A+VIII-B* in the *myosin VIII-1/2/a/b* mutant background **(C)** or in wild-type Col-0 plants **(D)** were similarly infected with *A. tumefaciens* At849. Transient transformation efficiencies are indicated as the percentage of roots showing GUS activity six days after infection. A total of 10-15 plants and >100 segments per plant, from five independent transgenic lines, were tested for transient transformation. Values given are means ± SE. Asterisks indicate significant differences compared to control plants that contain an empty vector (**A** and **B**), the *myosin VIII-1/2/a/b* quadruple mutant (**C**), or wild-type Col-0 plants (**D**). [*t-test*, $*P < 0.05$; $**P < 0.01$; $***P < 0.001$; $****P < 0.0001$].

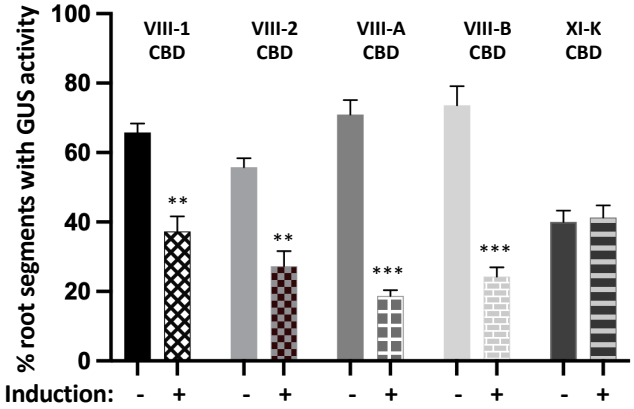

Figure 3. **Inducible expression of myosin VIII, but not the myosin XI-K, cargo binding domains (CBD) inhibits transient transformation.** Root segments from transgenic *Arabidopsis* expressing the cargo binding domain (CBD) of the indicated myosin protein, under the control of a β-estradiol inducible promoter, were treated with β-estradiol or control solutions for 24 hr before infection with *A. tumefaciens* At849. The percentage of roots showing GUS activity six days after infection indicates the transient transformation efficiency. A total of 10-15 plants and >100 segments per plant, from five independent transgenic lines, were tested for transient transformation. Values given are means ± SE. Asterisks indicate significant differences compared to uninduced plants. [*t-test*, $^{**}P < 0.01$; $^{***}P < 0.001$].

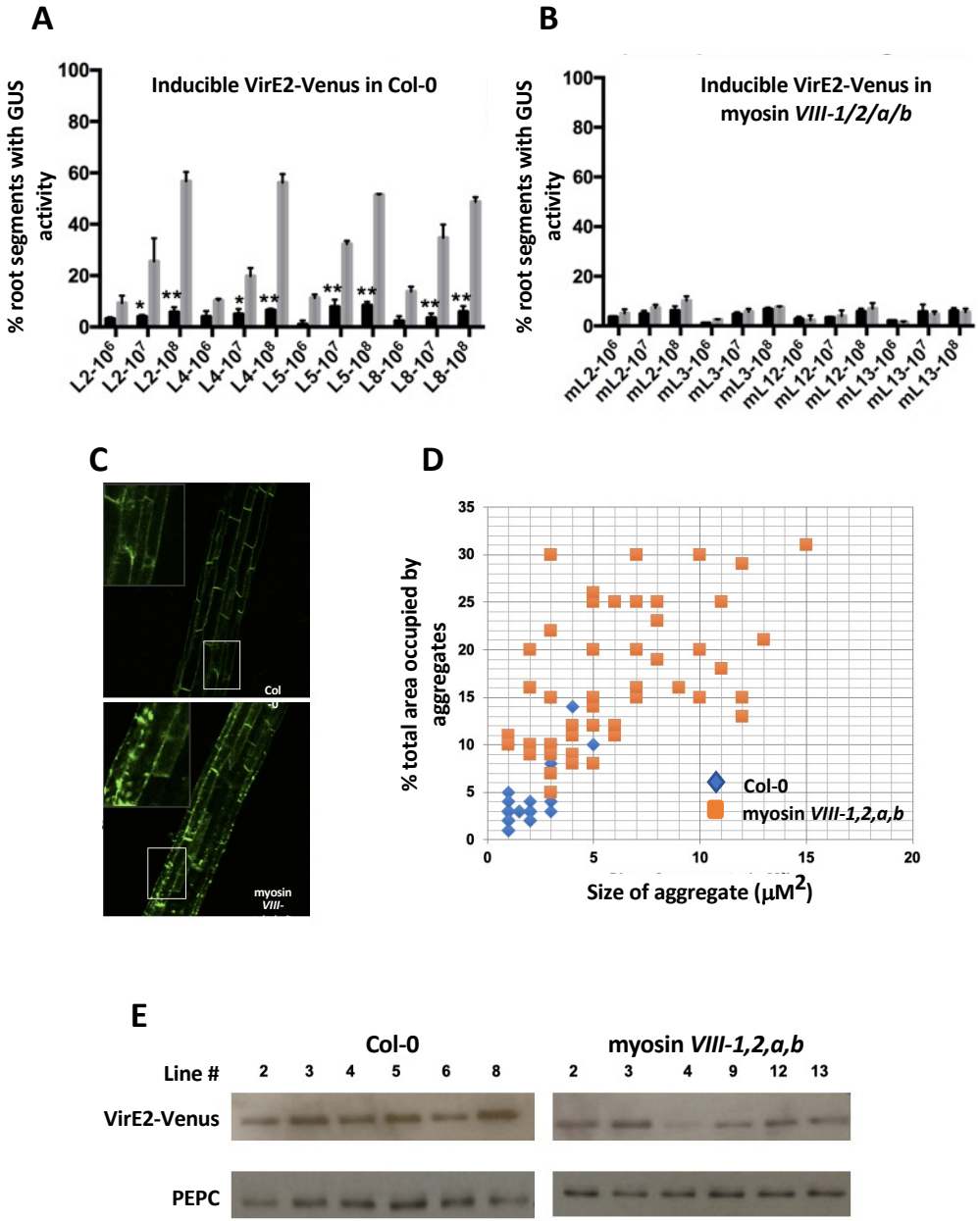
A
Inducible VirE2-Venus in Col-0
% root segments with GUS activity
100
80
60
40
20
0
L2-10^6
L2-10^7
L2-10^8
L4-10^6
L4-10^7
L4-10^8
L5-10^6
L5-10^7
L5-10^8
L8-10^6
L8-10^7
L8-10^8
B
Inducible VirE2-Venus in myosin VIII-1/2/a/b
% root segments with GUS activity
mL2-10^6
mL2-10^7
mL2-10^8
mL3-10^6
mL3-10^7
mL3-10^8
mL12-10^6
mL12-10^7
mL12-10^8
mL13-10^6
mL13-10^7
mL13-10^8
C
Col -0
myosin VIII-
D
% total area occupied by aggregates
Size of aggregate (μM^2)
Col-0
myosin VIII-1,2,a,b
E
Col-0
myosin VIII-1,2,a,b
Line #
2 3 4 5 6 8
2 3 4 9 12 13
VirE2-Venus
PEPC

- **Figure 4**. **Expression of VirE2-Venus in the *myosin VIII-1/2/a/b* mutant cannot complement a *virE2* mutant *Agrobacterium* strain for transient transformation.** **(A)** *Agrobacterium*-mediated transient transformation assays were conducted on roots of four independent transgenic lines of wild-type (Lines 2, 4, 5 and 8) or **(B)** the *myosin VIII-1/2/a/b* mutant (Lines 2, 3, 12, and 13). Root segments were inoculated with 10^6, 10^7, or 10^8 cfu/ml of the *virE2* mutant strain *A. tumefaciens* At1879 containing the T-DNA binary vector pBISN2. Plants were treated with β-estradiol (gray bars) or control solution (black bars) for VirE2-Venus expression 24 hr before infection. The percentage of roots showing GUS activity was calculated as in Figure 1. A total of 10-15 plants from each line and >100 segments per plant were tested for transient transformation. Values given are means ± SE. Asterisks indicate significant differences compared to uninduced plants. [*t-test*, $*P < 0.05$; $**P < 0.01$]. **(C)** Confocal images showing aggregation of VirE2-Venus proteins in transgenic roots of either wild-type (top panel) or *myosin VIII 1/2/a/b* mutant backgrounds (bottom panel). **(D)** Quantitative analysis of the size of VirE2-Venus aggregates and the percentage of the cellular area occupied by the aggregates. Image J was used for analysis. The average VirE2-Venus aggregate size was 2.0±0.3 μm^2 in wild-type roots, and 6.2±0.6 μm^2 in *myosin VIII-1/2/a/b* quadruple mutant roots. **(E)** Western blot detection of VirE2-Venus proteins expressed in transgenic plants of either the Col-0 or the *myosin VIII-1/2/a/b* quadruple myosin mutant background. Mouse anti-GFP antibody was used to detect VirE2-Venus protein expressed after induction of individual transgenic lines. The house-keeping protein phosphoenolpyruvate carboxylase (PEPC) was detected using a rabbit anti-PEPC antibody and served as an internal control.

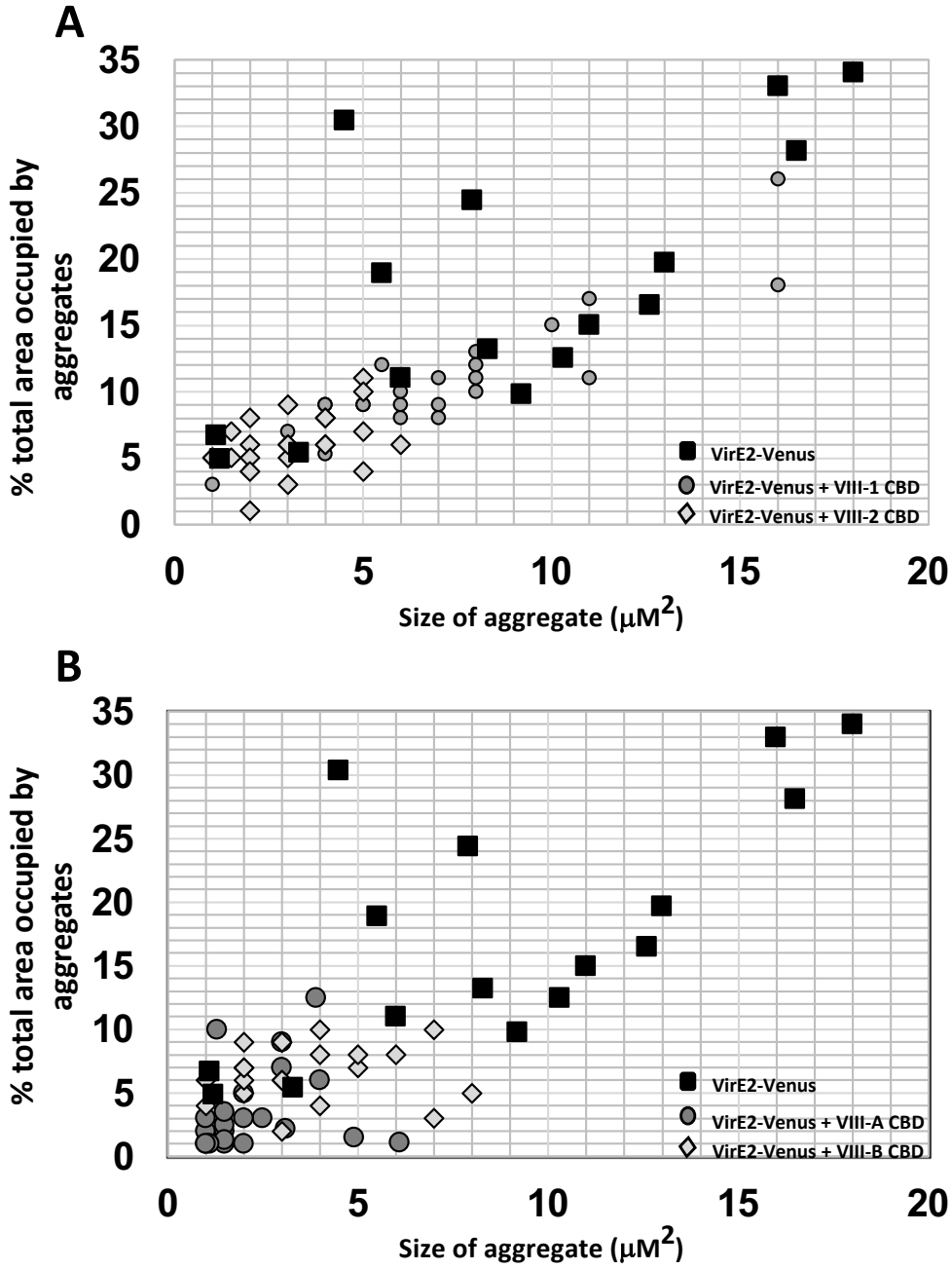

Figure 5. **Analysis of VirE2-Venus aggregates in roots of transgenic *Arabidopsis* expressing the CBDs of various Myosin VIII proteins.** Roots were treated with β-estradiol for eight hr. Random areas of confocal images from roots expressing **(A)** Myosin VIII-1 or VIII-2 CBDs, or **(B)** Myosin VIII-A or VIII-B CBDs were analyzed using Image J. Both the sizes and the percentage of the cellular area occupied by the VirE2-Venus aggregates are shown.

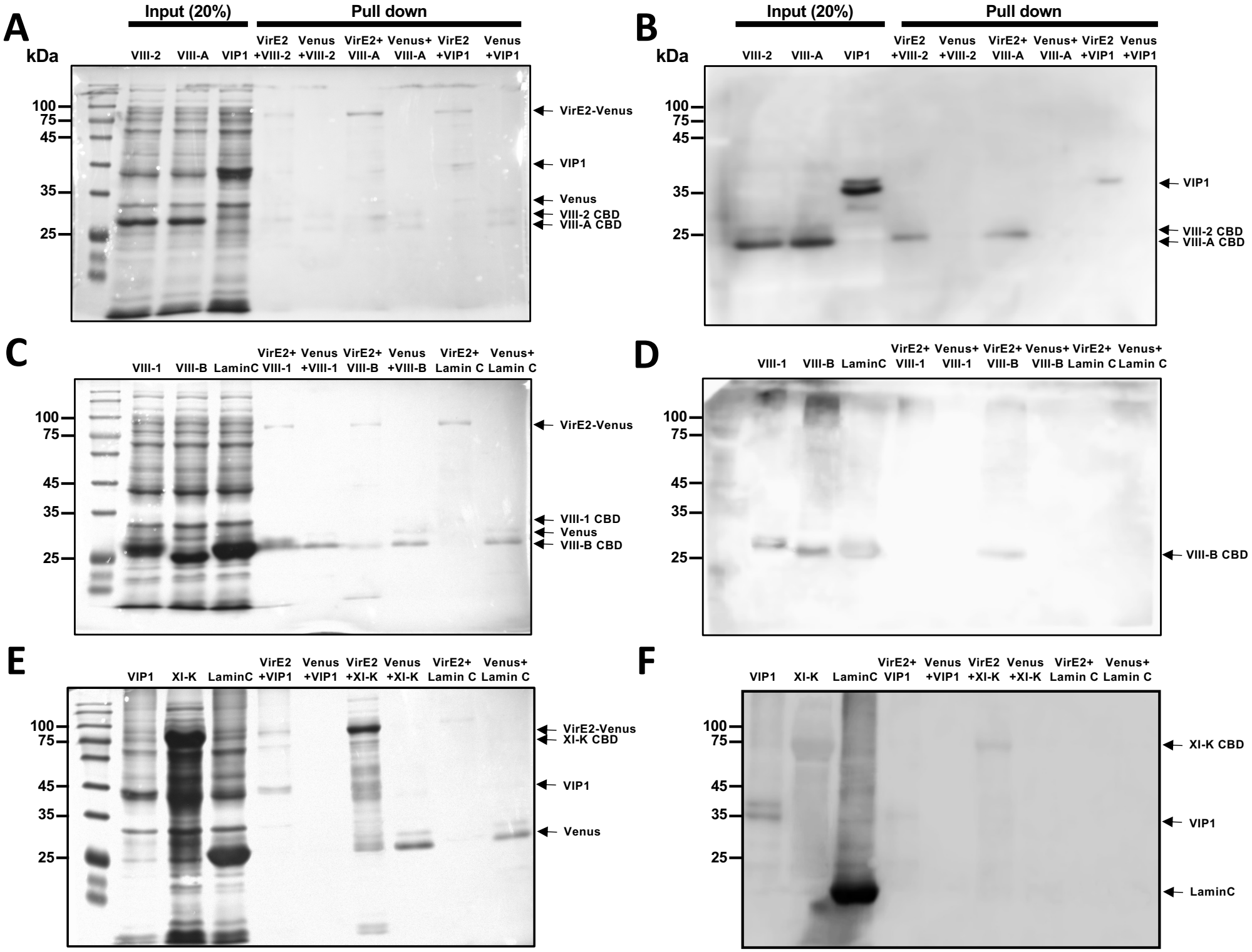
A
Input (20%)
Pull down
kDa
VIII-2
VIII-A
VIP1
VirE2 +VIII-2
Venus +VIII-2
VirE2+ VIII-A
Venus+ VIII-A
VirE2 +VIP1
Venus +VIP1
100
75
45
35
25
VirE2-Venus
VIP1
Venus
VIII-2 CBD
VIII-A CBD
B
Input (20%)
Pull down
kDa
VIII-2
VIII-A
VIP1
VirE2 +VIII-2
Venus +VIII-2
VirE2+ VIII-A
Venus+ VIII-A
VirE2 +VIP1
Venus +VIP1
100
75
45
35
25
VIP1
VIII-2 CBD
VIII-A CBD
C
VIII-1
VIII-B
LaminC
VirE2+ VIII-1
Venus +VIII-1
VirE2+ VIII-B
Venus +VIII-B
VirE2+ Lamin C
Venus+ Lamin C
100
75
45
35
25
VirE2-Venus
VIII-1 CBD
Venus
VIII-B CBD
D
VIII-1
VIII-B
LaminC
VirE2+ VIII-1
Venus+ VIII-1
VirE2+ VIII-B
Venus+ VIII-B
VirE2+ Lamin C
Venus+ Lamin C
100
75
45
35
25
VIII-B CBD
E
VIP1
XI-K
LaminC
VirE2 +VIP1
Venus +VIP1
VirE2 +XI-K
Venus +XI-K
VirE2+ Lamin C
Venus+ Lamin C
100
75
45
35
25
VirE2-Venus
XI-K CBD
VIP1
Venus
F
VIP1
XI-K
LaminC
VirE2+ VIP1
Venus +VIP1
VirE2 +XI-K
Venus +XI-K
VirE2+ Lamin C
Venus+ Lamin C
100
75
45
35
25
XI-K CBD
VIP1
LaminC

Figure 6. **VirE2-Venus interacts with some myosin cargo binding domains (CBDs) *in vitro*.** VirE2-Venus or Venus proteins were incubated with the indicated myc-tagged myosin CBD, VIP1, or Lamin C. Following binding to anti-GFP beads, proteins were eluted and subjected to Western blot analysis using anti-myc antibodies. Coomassie stained gels are shown in panels **A**, **C**, and **E**, and immunoblots in panels **B**, **D**, and **F**. VirE2-Venus interacts with the CBDs of myosins VIII-2, VIII-A, VIII-B, and XI-K, and with VIP1 (panels **B**, **D**, and **F**), but not with the CBD of myosin VIII-1 or with Lamin C (panels **D** and **F**). Venus, as a negative control, does not interact with any myc-tagged protein.

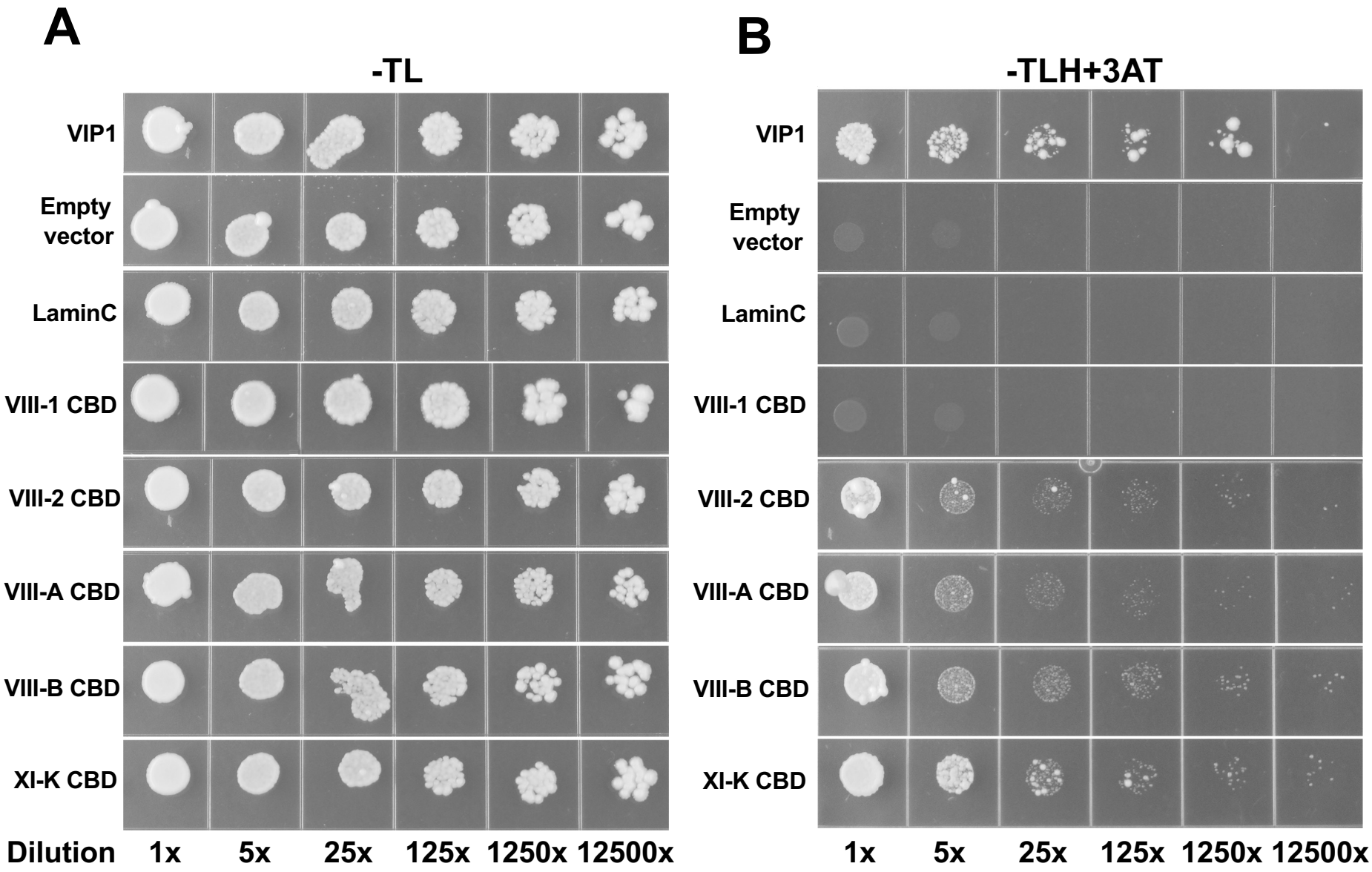

Figure 7. The cargo binding domains (CBD) of some myosins interact with VirE2 in yeast. Yeast two-hybrid analysis was conducted with VirE2 as the bait and individual myosin CBDs as the prey. Following co-transformation of the bait and prey plasmids, single colonies were picked and serial dilutions of yeast were grown on **(A)** SD-Trp-Leu (-TL) medium, or **(B)** SD-Trp-Leu-His medium supplemented with 3 mM 3-amino-1,2,4-triazole (-TLH+3AT). Colony growth on SD-TLH+3AT indicates interaction between VirE2 and the myosin CBD. VIP1 was used as a positive control for interaction with VirE2. Lamin C and the empty vector were used as negative controls. SD, synthetic dropout medium.

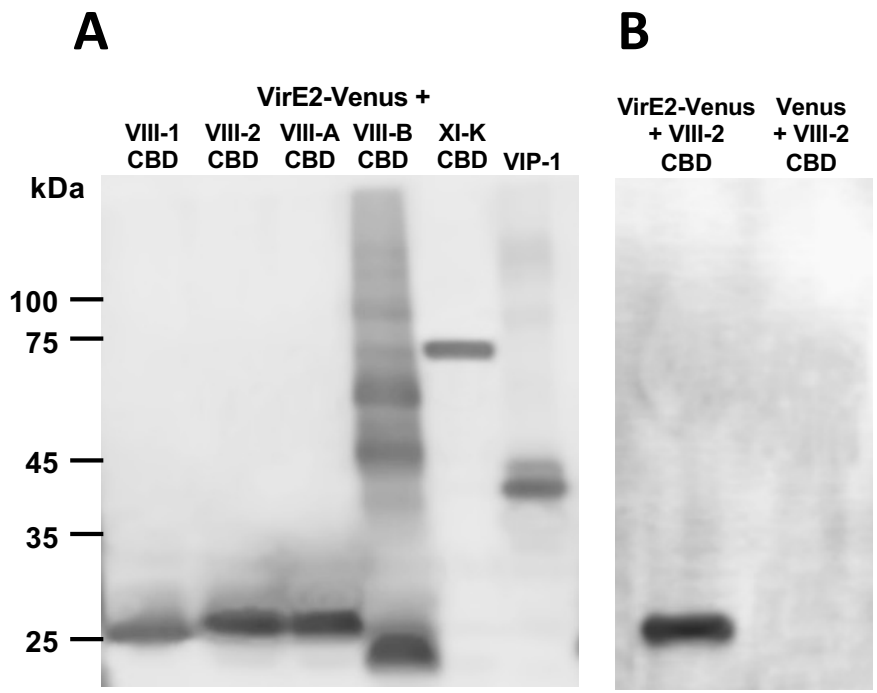

Figure 8. **Myosin cargo binding domains can form complexes with VirE2 when expressed in *Arabidopsis*. (A)** Protein extracts from roots of transgenic *Arabidopsis* plants expressing VirE2-Venus, or Venus, and the indicated myc-tagged myosin CBD transgenes were incubated with anti-GFP beads, the bound proteins eluted, and subjected to Western blot analysis using anti-myc antibodies. Myc-tagged VIP1 was used as a positive control. **(B)** Root extracts expressing VirE2-Venus or Venus and myc-tagged myosin VIII-2 CBD were incubated with anti-GFP beads, the bound proteins eluted, and subjected to Western blot analysis using anti-myc antibodies.

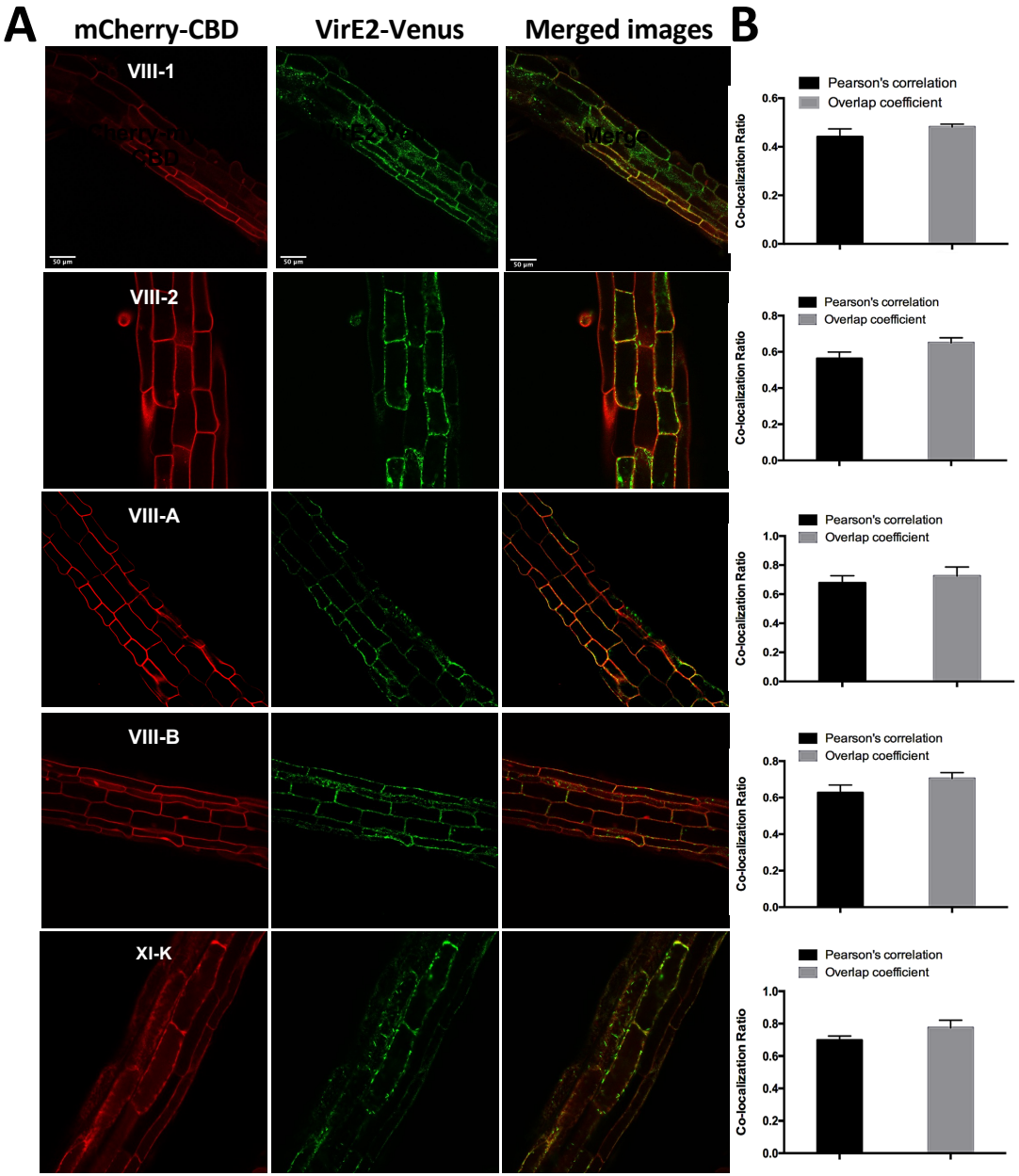

Figure 9. **Co-localization of VirE2-Venus and mCherry-myosin CBDs in *Arabidopsis* roots. (A)** Roots of transgenic *Arabidopsis* plants containing VirE2-Venus and mCherry-myosin CBD genes, each under the control of a β-estradiol-inducible promoter, were treated with β-estradiol for 8 hr and examined by confocal microscopy. Bars indicate 50 µm. **(B)** Pearson's correlation and overlap coefficient of Venus and mCherry fluorescence. A total of 10-15 transgenic lines and >50 cells per construct were used for quantitative analysis using Image J. Values >0.5 indicate co-localization of the two proteins for both methods of analysis. The red line indicates a co-localization ratio of 0.5.

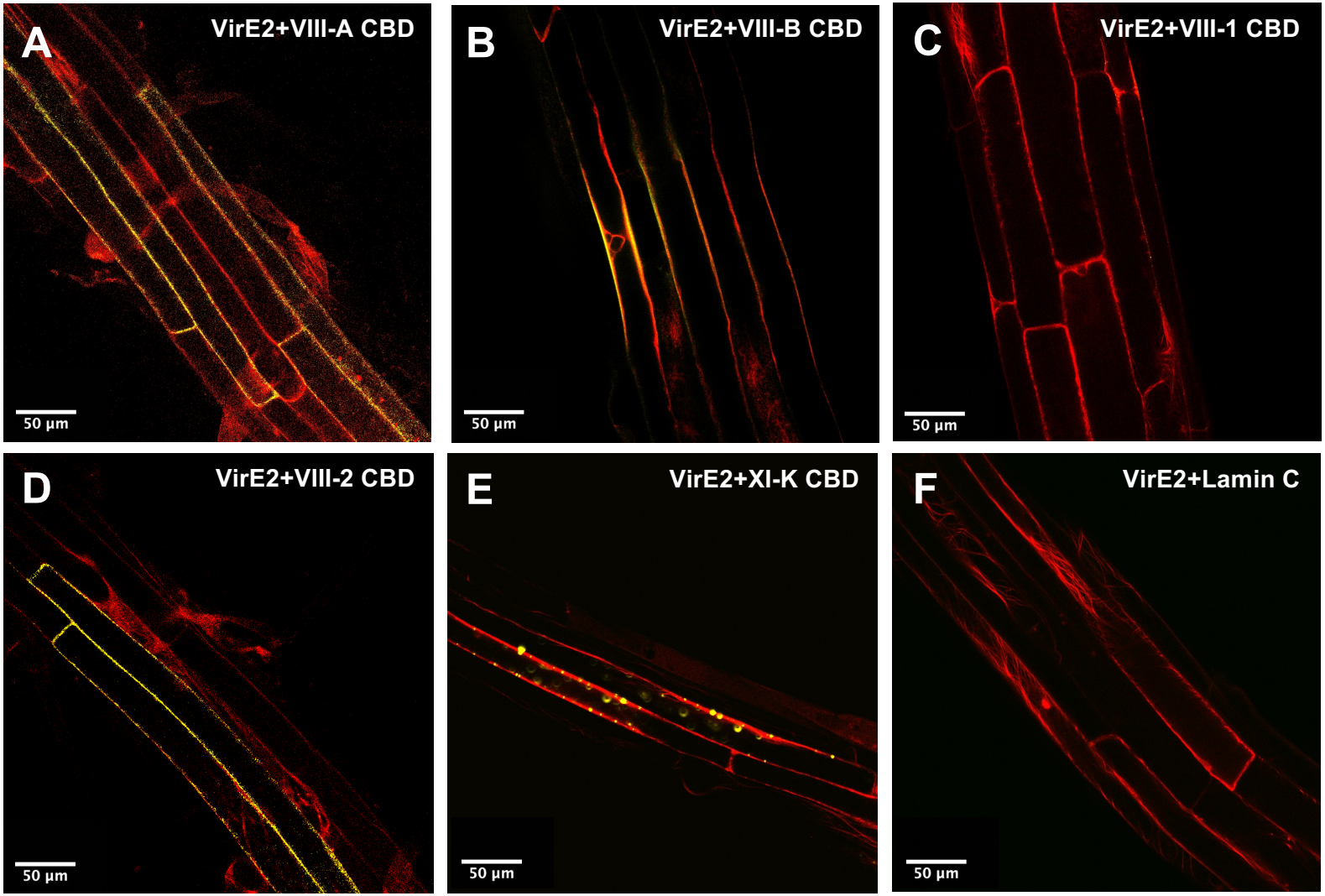
A
VirE2+VIII-A CBD
50 µm
B
VirE2+VIII-B CBD
50 µm
C
VirE2+VIII-1 CBD
50 µm
D
VirE2+VIII-2 CBD
50 µm
E
VirE2+XI-K CBD
50 µm
F
VirE2+Lamin C
50 µm

Figure 10. **Bimolecular fluorescence complementation (BiFC) of VirE2 with various myosin CBDs in *Arabidopsis* roots.** Transgenic *Arabidopsis* plants containing VirE2-cEYFP and the indicated myosin CBDs-nVenus, each under the control of a β-estradiol-inducible promoter, were treated with β-estradiol for 48 hr and the fluorescence signal detected by confocal microscopy. VirE2 interacts with the CBDs of **(A),** myosin VIII-2; **(B),** myosin VIII-A; and **(D),** myosin VIII-B at the plasma membrane. VirE2 interacts with the myosin XI-K CBD at the plasma membrane and within the cytoplasm **(E)**. VirE2 does not interact with the myosin VIII-1 CBD **(C)** or Lamin C **(F)**. Yellow fluorescence indicates interaction of VirE2-Venus with the myosin CBD. Actin filaments are labeled by mCherry-ABD2. The figure shows merged images of the Venus and mCherry signals. Bars indicate 50 μm.

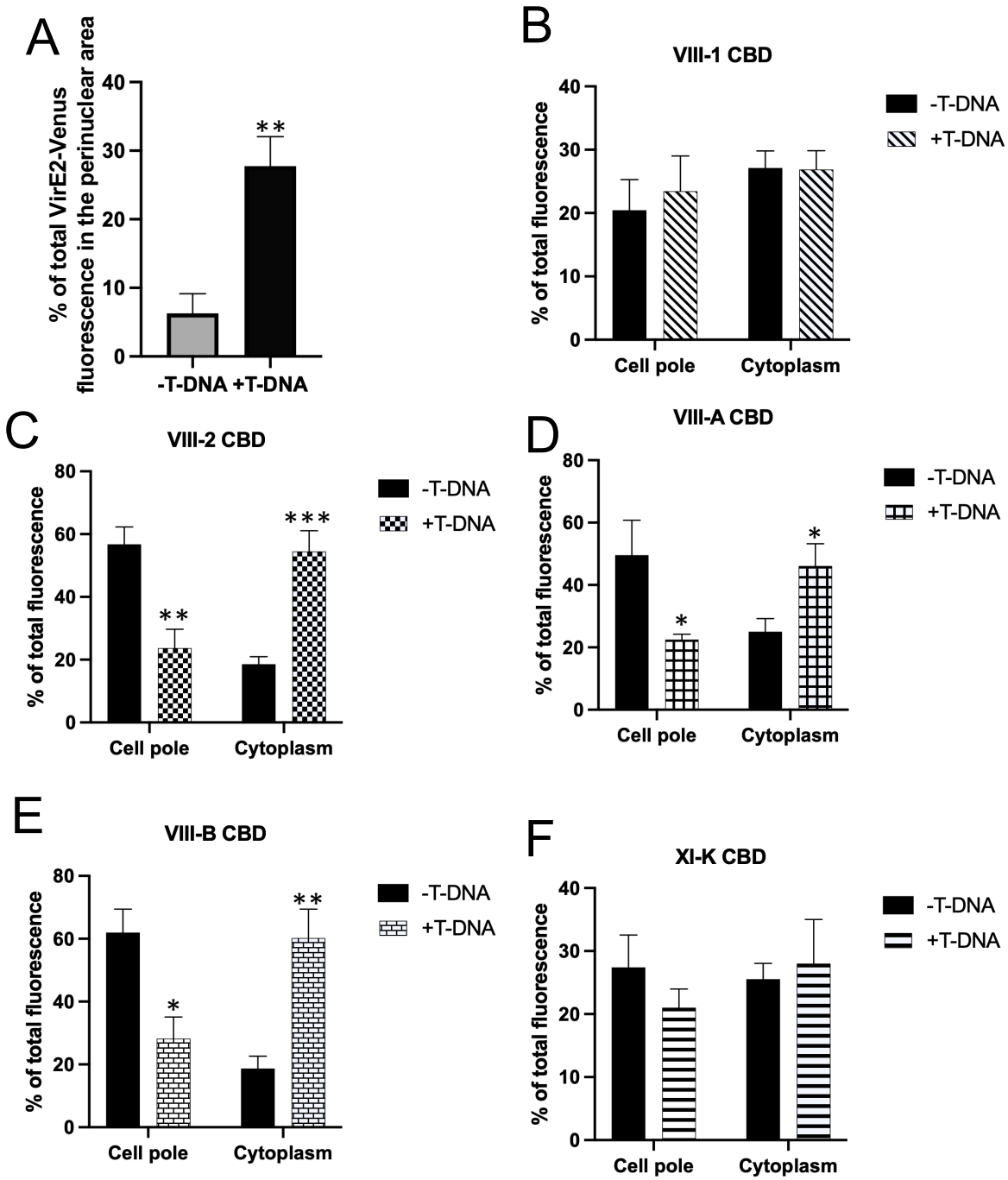
A
% of total VirE2-Venus fluorescence in the perinuclear area
40
30
20
10
0
**
-T-DNA +T-DNA
B
VIII-1 CBD
% of total fluorescence
40
30
20
10
0
Cell pole
Cytoplasm
-T-DNA
+T-DNA
C
VIII-2 CBD
% of total fluorescence
80
60
40
20
0
**
***
Cell pole
Cytoplasm
-T-DNA
+T-DNA
D
VIII-A CBD
% of total fluorescence
80
60
40
20
0
*
*
Cell pole
Cytoplasm
-T-DNA
+T-DNA
E
VIII-B CBD
% of total fluorescence
80
60
40
20
0
*
**
Cell pole
Cytoplasm
-T-DNA
+T-DNA
F
XI-K CBD
% of total fluorescence
40
30
20
10
0
Cell pole
Cytoplasm
-T-DNA
+T-DNA

Figure 11. **Incubation of *Arabidopsis* roots with *Agrobacterium* that can transfer T-DNA results in increased VirE2-Venus in the perinuclear region. (A)** Transgenic *Arabidopsis* plants containing an inducible *VirE2-Venus* transgene were treated with 5 μm β-estradiol for 24 hr, followed by inoculation with 10^8 cfu/ml of the *virE2* mutant *A. tumefaciens* At1872 without a binary vector (At2403, left panel) or with T-DNA on a binary vector (At2404, right panel). The percentage of total VirE2-Venus fluorescence in the perinuclear area was calculated. Images of 10-15 transgenic lines and >50 cells were analyzed. The data indicate means ± SE. Asterisks indicate significant differences between roots inoculated with the two *Agrobacterium* strains. **(B-F)** the relative distribution of VirE2-Venus at the cell poles or in the cytoplasm following infection with *A. tumefaciens* At2403 or At2404 of roots co-expressing CBDs of myosin VIII-1. myosin VIII-2, myosin VIII-A, myosin VIII-B, or myosin XI-K (B, C, D, E, F, respectively). Images of 10-15 transgenic lines and >50 cells were analyzed. The data indicate means ± SE. Asterisks indicate significant differences between roots inoculated with the two *Agrobacterium* strains. [*t-test*, $*P < 0.05$; $**P < 0.01$; $***P < 0.001$].

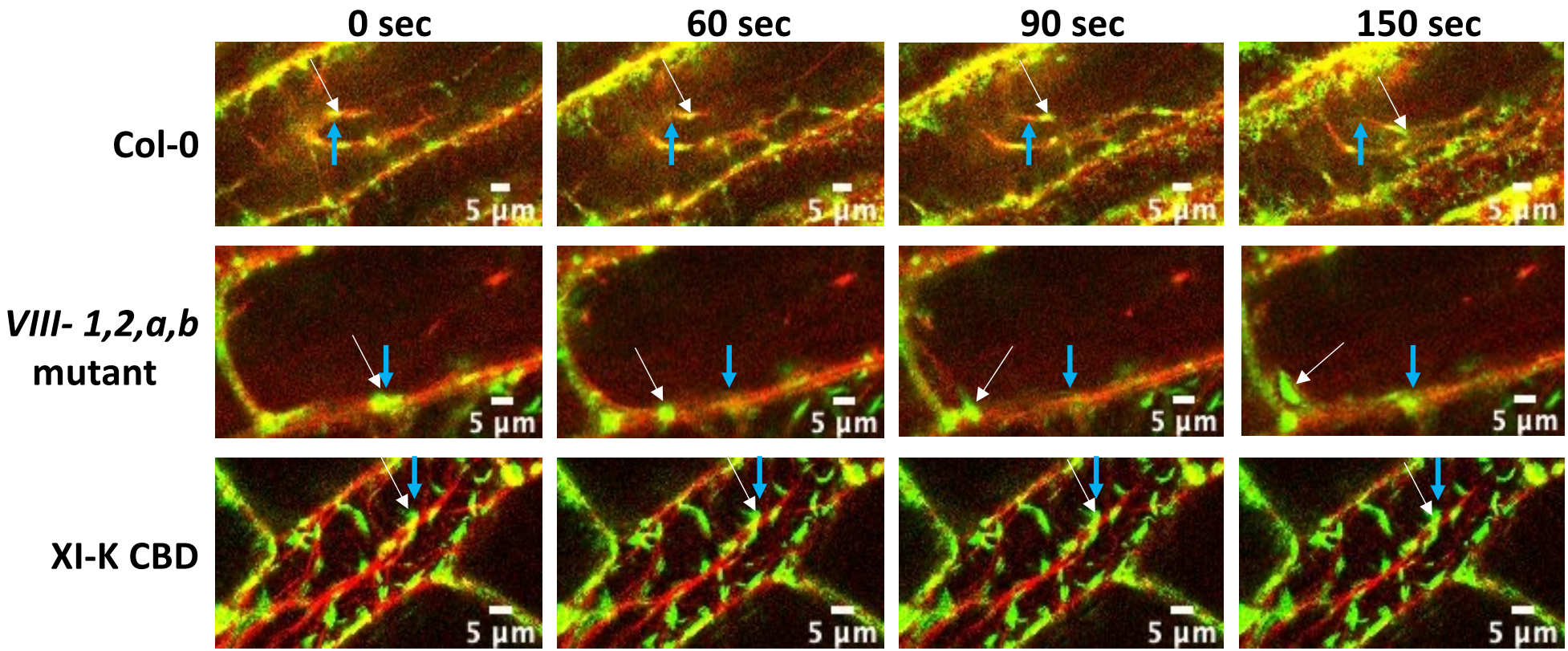

Figure 12. Loss of function of myosin XI-K, but not myosin VIII, disrupts movement of VirE2-Venus along actin filaments. Transgenic plants expressing mCherry-ABD2 constitutively and VirE2-Venus inducibly in Col-0, *myosin VIII-1/2/a/b*, and myosin XI-K CBD plants were used in this experiment. Roots of these plants were treated with 10 µM β-estradiol for 8 hr. Time lapse images were taken by confocal microscopy. Four images of each field are shown at the indicated times (0, 60, 90, and 120 seconds). Blue arrows indicate the initial position of a particular VirE2-Venus aggregate; white arrows indicate the position of the same aggregate at various times thereafter. Bars indicate 5 µm.

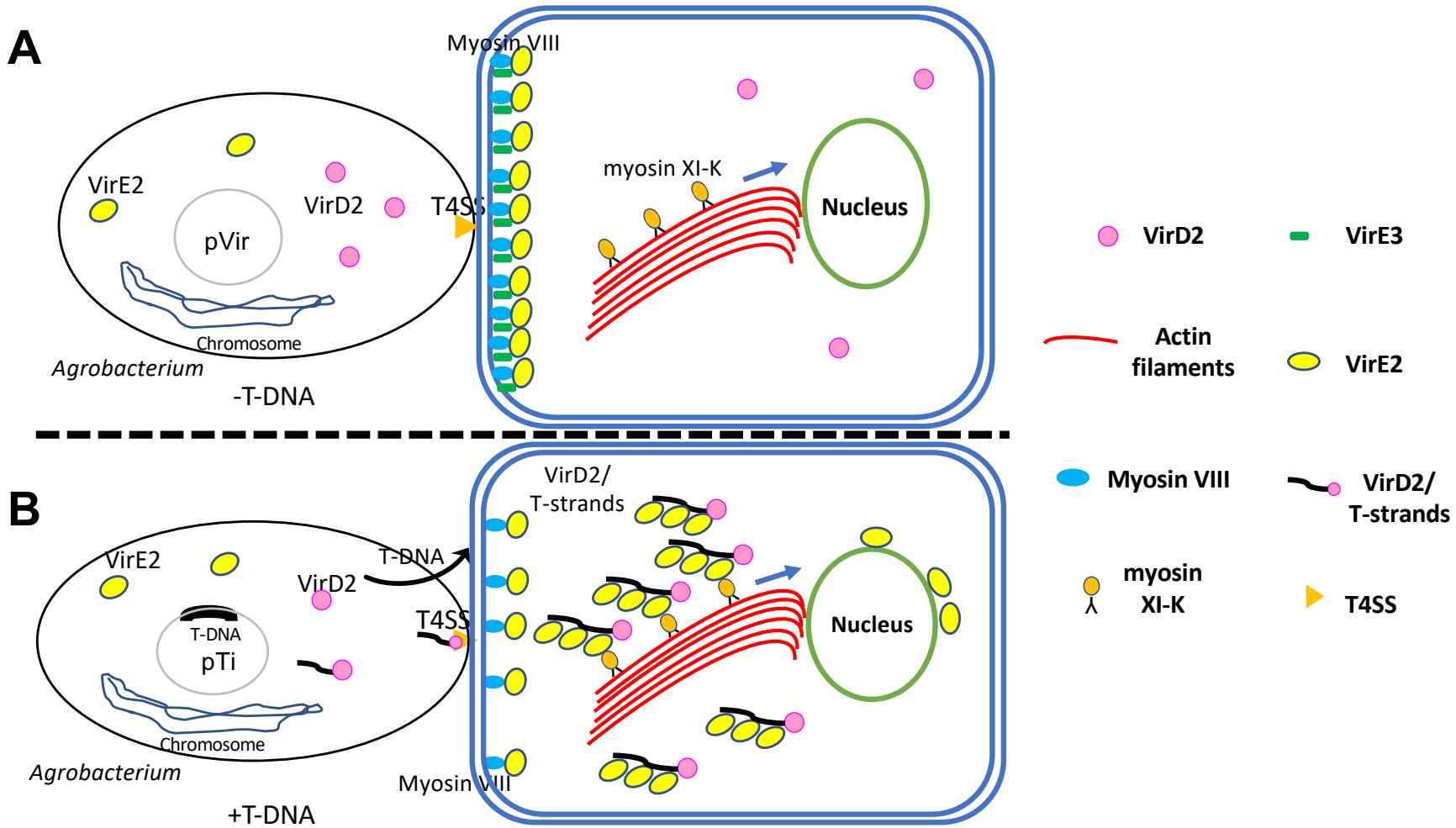

Figure 13. **Model of myosin VIII and myosin XI-K involvement in VirE2 trafficking to the perinuclear region. (A)** *Agrobacterium* virulence effector proteins, including VirE2 and VirE3, are secreted into host cells through a Type IV secretion system. VirE2 and VirE3 interact at the plant plasma membrane. Myosin VIII proteins localize at the plasma membrane and help tether VirE2 to the plasma membrane when no T-DNA is present. **(B)** When T-strands (as a VirD2/T-strand complex) enter the host cell, VirE2 molecules are released and some may bind T-DNA, following which VirE2 interacts with myosin XI-K and moves along actin filaments to the perinuclear region. Not shown are the *Agrobacterium* virulence effector proteins VirD5 and VirF which also are transferred to the plant.

Supplemental Table 1. Plasmids used in this study.

Plasmid	Important features/proteins	Plasmid description	Antibiotic resistance	Reference
pE886	Cloning vector	pBlusescript KS+	Amp	Kozaki et al., 2004
pE3086	EYFP	pSAT6-P_{35S}-cEYFP-N1	Amp	Citovsky et al., 2006
pE3129	PIP2A	pSAT6-PIP2A-mRFP	Amp	Gelvin lab strain
pE3183	myc	pSAT6-P_{35S}-myc-MCS	Amp	Gelvin lab strain
pE3230	nVenus	pSAT6-P_{35S}-nVenus-C	Amp	Lee and Gelvin 2014
pE3275	mCherry	pSAT6-P_{35S}-mCherry-C1-B	Amp	Lee and Gelvin 2014
pE3341	mCherry	pBBR1-MCS2::mCherry	Kan	From Clay Fuqua
pE3447	Lamin C	pBSKS-Lamin C	Amp	Gelvin lab strain
pE3519	Binary vector	pPZP-*bar*-RCS2	Spec	Gelvin lab strain
pE3522	Yeast bait vector	pGBKT7	Kan	Lu et al., 2010
pE3542	Venus	pSAT1-Venus-C	Amp	Lee and Gelvin 2014
pE3745	Yeast prey vector	pGADT7	Amp	Chien et al., 1991
pE3802	For N-terminal nVenus tagging of myosin XI-K CBD	pSAT6-P_{35S}-nVenus-Myosin XI-K CBD	Amp	Gelvin lab strain

pE3982	VirE2-cEYFP	pSAT1-P_{35S}-VirE2-cEYFP	Amp	Gelvin lab strain
pE4014	VirE2-cCFP	*Nco*I-*Bam*HI fragment from pSAT4-VirE2-cCFP cloned into the same sites in pGBKT7	Kan	Gelvin lab strain
pE4224	β-estradiol-inducible promoter	pSAT1-β-estradiol-inducible promoter	Amp	Gelvin lab strain
pE4282	VirE2-Venus	pSAT1-Pi-VirE2-Venus	Amp	Gelvin lab strain
pE4292	VirE2-Venus, mCherry-ABD2	pPZP-Pi-VirE2-Venus-P_{nos}-mCherry-ABD2	Spec	Gelvin lab strain
pE4317	Binary vector; VirE2-Venus, hptII	pPZP-Pi-VirE2-Venus-*hptII*	Spec	Gelvin lab strain
pE4381	mCherry-intron-NLS	pPZP-P_{35S}-mCherry-intron-NLS	Spec	Gelvin lab strain
pE4437	Binary vector; Cerulean-NLS, mCherry-ABD2	pPZP -P_{nos}-Cerulean-NLS-P_{35S}-mCherry-ABD2	Spec	Gelvin lab strain
pE4438	VirE2-Venus, Cerulean-NLS	pPZP-Pi-VirE2-Venus-P_{nos}-Cerulean-NLS	Spec	Gelvin lab strain
pE4515	pSAT1-P_{35S}	pSAT1-MCS	Kan	Gelvin lab strain
pE4672	Binary vector; *hptII*	pPZP-P_{nos}-*hptII*	Spec	Lee and Gelvin, 2014

pE4712	Myosin VIII-1 CBD	PCR fragment of Myosin VIII-1 CBD with *KpnI*/*Bam*HI sites, cloned into the *Eco*RV site of pBluescript KS+ to make pBS-Myosin VIII-1 CBD	Amp	This study
pE4713	Myosin VIII-2 CBD	PCR fragment of Myosin VIII-2 CBD with *Kpn*I/*Bam*HI sites, cloned into the *Eco*RV site of pBluescript KS+ to make pBS-Myosin VIII-2 CBD	Amp	This study
pE4714	Myosin VIII-A CBD	PCR fragment of Myosin VIII-A CBD with *Kpn*I/*Bam*HI sites, cloned into the *Eco*RV site of pBluescript KS+ to make pBS-Myosin VIII-A CBD	Amp	This study
pE4715	Myosin VIII-B CBD	PCR fragment of Myosin VIII-B CBD with *Kpn*I/*Bam*HI sites, cloned into the *Eco*RV site of pBluescript KS+ to make pBS-Myosin VIII-B CBD	Amp	This study
pE4716	β-estradiol-inducible promoter	PCR fragment of inducible promoter from pE4224 with *Age*I/*Eco*RV sites, cloned into the *Eco*RV site of pBluescript KS+ to make pBS-Pi promoter	Amp	This study
pE4720	pSAT6-Pi-mCherry-C	*Age*I+*Eco*RV digested pE4716, cloned into *Age*I+*Eco*RV digested pE3275, to make pSAT6-Pi-mCherry	Amp	This study
pE4721	mCherry-Myosin VIII-1 CBD	*Kpn*I+*Bam*HI digested pE4712 cloned into *Kpn*I+*Bam*HI digested pE4720 to make pSAT6-Pi-mCherry-Myosin VIII-1 CBD	Amp	This study
pE4722	mCherry-Myosin VIII-2 CBD	*Kpn*I+*Bam*HI digested pE4713 cloned into *Kpn*I+*Bam*HI digested pE4720 to make pSAT6-Pi-mCherry-Myosin VIII-2 CBD	Amp	This study
pE4723	mCherry-Myosin VIII-A CBD	*Kpn*I+*Bam*HI digested pE4714 cloned into *Kpn*I+*Bam*HI digested pE4720 to make pSAT6-Pi-mCherry-Myosin VIII-A CBD	Amp	This study
pE4724	mCherry-Myosin VIII-B CBD	*Kpn*I+*Bam*HI digested pE4715 cloned into *Kpn*I+*Bam*HI digested pE4720 to make pSAT6-Pi-mCherry-Myosin VIII-B CBD	Amp	This study

pE4725	mCherry-Myosin XI-K CBD	*Kpn*I+*Pst*I (Blunt) digested pE3802 cloned into *Kpn*I+*Bam*HI (Blunt) digested pE4720 to make pSAT6-Pi-mCherry-Myosin XI-K CBD	Amp	This study
pE4726	mCherry-Myosin VIII-1 CBD, VirE2-Venus, Cerulean-NLS	PI-*Psp*I digested pE4721 cloned into PI-*Psp*I digested pE4438 to make pPZP-Pi-VirE2-Venus-P_{nos}-Cerulean-NLS-Pi-mCherry-Myosin VIII-1 CBD	Spec	This study
pE4727	mCherry-Myosin VIII-2 CBD, VirE2-Venus, Cerulean-NLS	PI-*Psp*I digested pE4722 cloned into PI-*Psp*I digested pE4438 to make pPZP-Pi-VirE2-Venus-P_{nos}-Cerulean-NLS-Pi-mCherry-Myosin VIII-2 CBD	Spec	This study
pE4728	mCherry-Myosin VIII-A CBD, VirE2-Venus, Cerulean-NLS	PI-*Psp*I digested pE4723 cloned into PI-*Psp*I digested pE4438 to make pPZP-Pi-VirE2-Venus-P_{nos}-Cerulean-NLS-Pi-mCherry-Myosin VIII-A CBD	Spec	This study
pE4729	mCherry-Myosin VIII-B CBD, VirE2-Venus, Cerulean-NLS	PI-*Psp*I digested pE4724 cloned into PI-*Psp*I digested pE4438 to make pPZP-Pi-VirE2-Venus-P_{nos}-Cerulean-NLS-Pi-mCherry-Myosin VIII-B CBD	Spec	This study
pE4730	mCherry-Myosin XI-K CBD, VirE2-Venus, Cerulean-NLS	PI-*Psp*I digested pE4725 cloned into PI-*Psp*I digested pE4438 to make pPZP-Pi-VirE2-Venus-P_{nos}-Cerulean-NLS-Pi-mCherry-Myosin XI-K CBD	Spec	This study
pE4731	pSAT6-Pi-nVenus-C	*Age*I+*Eco*RV digested pE4716 cloned into *Age*I+*Eco*RV digested pE3230 to make pSAT6-Pi-nVenus	Amp	This study
pE4732	VirE2-cEYFP	*Age*I+*Swa*I digested pE4731 cloned into *Age*I+*Swa*I digested pE3982 to make pSAT1-Pi-VirE2-cEYFP	Amp	This study
pE4733	nVenus-Myosin VIII-1 CBD	*Kpn*I+*Bam*HI digested pE4712 cloned into *Kpn*I+*Bam*HI digested pE4731 to make pSAT6-Pi-nVenus-Myosin VIII-1 CBD	Amp	This study
pE4734	nVenus-Myosin VIII-2 CBD	*Kpn*I+*Bam*HI digested pE4713 cloned into *Kpn*I+*Bam*HI digested pE4731 to make pSAT6-Pi-nVenus-Myosin VIII-2 CBD	Amp	This study
pE4735	nVenus-Myosin VIII-A CBD	*Kpn*I+*Bam*HI digested pE4714 cloned into *Kpn*I+*Bam*HI digested pE4731 to make pSAT6-Pi-nVenus-Myosin VIII-A CBD	Amp	This study
pE4736	nVenus-Myosin VIII-B CBD	*Kpn*I+*Bam*HI digested pE4715 cloned into *Kpn*I+*Bam*HI digested pE4731 to make pSAT6-Pi-nVenus-Myosin VIII-B CBD	Amp	This study

pE4737	nVenus-Myosin XI-K CBD	*Kpn*I+*Not*I digested pE4725 cloned into *Kpn*I+*Not*I digested pE4731 to make pSAT6-Pi-nVenus-Myosin XI-K CBD	Amp	This study
pE4738	VirE2-cYFP, Cerulean-NLS, mCherry-ABD2	*Asc*I digested pE4732 cloned into *Asc*I digested pE4437, to make pPZP-Pi-VirE2-cYFP-P_{nos}-Cerulean-NLS-P_{35S}-mCherry-ABD2	Spec	This study
pE4739	pSAT1-Pi-mCherry	*Xho*I (Blunt)/*Not*I digested pE4424 cloned into *Nco*I (Blunt)/*Not*I digested pE3275 to make pSAT1-inducible promoter-mCherry	Amp	This study
pE4755	nVenus-Myosin VIII-A CBD, VirE2-cYFP, Cerulean-NLS, mCherry-ABD2	PI-*Psp*I digested pE4735 cloned into PI-*Psp*I digested pE4738 to make pPZP-Pi-VirE2-cYFP-P_{nos}-Cerulean-NLS-P_{35S}-mCherry-ABD2-Pi-nVenus-myosin VIII-A CBD	Spec	This study
pE4756	nVenus-Myosin VIII-B CBD, VirE2-cYFP, Cerulean-NLS, mCherry-ABD2	PI-*Psp*I digested pE4736 cloned into PI-*Psp*I digested pE4738 to make pPZP-Pi-VirE2-cYFP-P_{nos}-Cerulean-NLS-P_{35S}-mCherry-ABD2-Pi-nVenus-myosin VIII-B CBD	Spec	This study
pE4757	nVenus-Myosin XI-K CBD, VirE2-cYFP, Cerulean-NLS, mCherry-ABD2	PI-*Psp*I digested pE4737 cloned into PI-*Psp*I digested pE4738 to make pPZP-Pi-VirE2-cYFP-P_{nos}-Cerulean-NLS-P_{35S}-mCherry-ABD2-Pi-nVenus-myosin XI-K CBD	Spec	This study
pE4758	nVenus-Myosin VIII-1 CBD, VirE2-cYFP, Cerulean-NLS, mCherry-ABD2	PI-*Psp*I digested pE4733 cloned into PI-*Psp*I digested pE4738 to make pPZP-Pi-VirE2-cYFP-P_{nos}-Cerulean-NLS-P_{35S}-mCherry-ABD2-Pi-nVenus-myosin VIII-1 CBD	Spec	This study
pE4759	nVenus-Myosin VIII-2 CBD, VirE2-cYFP, Cerulean-NLS, mCherryABD2	PI-*Psp*I digested pE4734 cloned into PI-*Psp*I digested pE4738 to make pPZP-Pi-VirE2-cYFP-P_{nos}-Cerulean-NLS-P_{35S}-mCherry-ABD2-Pi-nVenus-myosin VIII-2 CBD	Spec	This study
pE4774	Myc	PCR fragment of myc tag (pE3183 as template) with *NcoI* and *Not*I (35S terminator), cloned into *Eco*RV site of pBlusescript KS+ (pE886) to make pBS-Myc	Amp	This study
pE4775	Myc	*Nco*I+*Not*I digested pBS-Myc cloned into *Nco*I+*Not*I digested pE4720, to make Pi-pSAT6-myc	Amp	This study

pE4776	Myc-Myosin VIII-1 CBD	*Kpn*I+*Bam*HI digested pE4712 cloned into *Kpn*I+*Bam*HI digested pE4775 to make pSAT6-Pi-myc-Myosin VIII-1 CBD	Amp	This study
pE4777	Myc-Myosin VIII-2 CBD	*Kpn*I+*Bam*HI digested pE4713 cloned into *Kpn*I+*Bam*HI digested pE4775 to make pSAT6-Pi-myc-Myosin VIII-2 CBD	Amp	This study
pE4778	Myc-Myosin VIII-A CBD	*Kpn*I+*Bam*HI digested pE4714 cloned into *Kpn*I+*Bam*HI digested pE4775 to make pSAT6-Pi-myc-Myosin VIII-A CBD	Amp	This study
pE4779	Myc-Myosin VIII-B CBD	*Kpn*I+*Bam*HI digested pE4715 cloned into *Kpn*I+*Bam*HI digested pE4775 to make pSAT6-Pi-myc-Myosin VIII-B CBD	Amp	This study
pE4780	Myc-Myosin XI-K CBD	*Kpn*I+*Not*I digested pE4725 cloned into *Kpn*I+*Not*I digested pE4775 to make pSAT6-Pi-myc-Myosin XI-K CBD	Amp	This study
pE4781	mCherry-Myosin VIII-1 CBD, Cerulean-NLS	*Asc*I digested pE4726 self-ligated to make pPZP-P_{nos}-Cerulean-NLS-Pi-mCherry-Myosin VIII-1 CBD	Spec	This study
pE4782	mCherry-Myosin VIII-2 CBD, Cerulean-NLS	*Asc*I digested pE4727 self-ligated to make pPZP-P_{nos}-Cerulean-NLS-Pi-mCherry-Myosin VIII-2 CBD	Spec	This study
pE4783	mCherry-Myosin VIII-A CBD, Cerulean-NLS	*Asc*I digested pE4728 self-ligated to make pPZP-P_{nos}-Cerulean-NLS-Pi-mCherry-Myosin VIII-A CBD	Spec	This study
pE4784	mCherry-Myosin VIII-B CBD, Cerulean-NLS	*Asc*I digested pE472 self-ligated to make pPZP-P_{nos}-Cerulean-NLS-Pi-mCherry-Myosin VIII-B CBD	Spec	This study
pE4785	mCherry-Myosin XI-K CBD, Cerulean-NLS	*Asc*I digested pE4730 self-ligated to make pPZP-P_{nos}-Cerulean-NLS-Pi-mCherry-Myosin XI-K CBD	Spec	This study
pE4786	Myc-Myosin VIII-1 CBD, VirE2-Venus	PI-*Psp*I digested pE4776 cloned into PI-*Psp*I digested pE4317 to make pPZP-Pi-VirE2-Venus-Pi-myc-myosin VIII-1 CBD	Spec	This study
pE4787	Myc-Myosin VIII-2 CBD, VirE2-Venus	PI-*Psp*I digested pE4777 cloned into PI-*Psp*I digested pE4317 to make pPZP-Pi-VirE2-Venus-Pi-myc-myosin VIII-2 CBD	Spec	This study

pE4788	Myc-Myosin VIII-A CBD, VirE2-Venus	PI-*Psp*I digested pE4778 cloned into PI-*Psp*I digested pE4317 to make pPZP-Pi-VirE2-Venus-Pi-myc-myosin VIII-A CBD	Spec	This study
pE4789	Myc-Myosin VIII-B CBD, VirE2-Venus	PI-*Psp*I digested pE4779 cloned into PI-*Psp*I digested pE4317 to make pPZP-Pi-VirE2-Venus-Pi-myc-myosin VIII-B CBD	Spec	This study
pE4790	Myc-Myosin XI-K CBD, VirE2-Venus	PI-*Psp*I digested pE4780 cloned into PI-*Psp*I digested pE4317 to make pPZP-Pi-VirE2-Venus-Pi-myc-myosin XI-K CBD	Spec	This study
pE4791	New inducible promoter	*Age*I+*Swa*I digested pE4754 cloned into *Age*I+*Swa*I digested pE4731 to make pSAT6-Pi(New)-nVenus	Amp	This study
pE4792	nVenus-Lamin C	*Sma*I+*Bam*HI digested pE3447 cloned into *Sma*I+*Bam*HI digested pE4791 to make pSAT6-Pi(new)-nVenus-Lamin C	Amp	This study
pE4814	Venus	*Nco*I+*Not*I digested pE3542 cloned into *Nco*I+*Not*I digested pET28a, to make pET28a-Venus	Kan	This study
pE4815	VirE2-Venus	*Nco*I+*Not*I digested pE4282 cloned into *Nco*I/+*Not*I digested pET28a, to make pET28a-VirE2-Venus	Kan	This study
pE4816	Myc-Myosin VIII-1 CBD	*Nco*I+*Bam*HI digested pE4776 cloned into *Nco*I+*Bam*HI digested pET28a to make pET28a-myc-myosin VIII-1 CBD	Kan	This study
pE4817	Myc-Myosin VIII-2 CBD	*Nco*I+*Bam*HI digested pE4777 cloned into *Nco*I+*Bam*HI digested pET28a to make pET28a-myc-myosin VIII-2 CBD	Kan	This study
pE4818	Myc-Myosin VIII-A CBD	*Nco*I+*Bam*HI digested pE4778 cloned into *Nco*I+*Bam*HI digested pET28a to make pET28a-myc-myosin VIII-A CBD	Kan	This study
pE4819	Myc-Myosin VIII-B CBD	*Nco*I+*Bam*HI digested pE4779 cloned into *Nco*I+*Bam*HI digested pET28a to make pET28a-myc-myosin VIII-B CBD	Kan	This study
pE4820	Myc-Myosin XI-K CBD	*Nco*I+*Not*I digested pE4780 cloned into *Nco*I+*Not*I digested pET28a to make pET28a-myc-myosin XI-K CBD	Kan	This study
pE4821	Myc-VIP1	*Xho*I+*Bam*HI digested pE3395 cloned into *Xho*I+*Bam*HI digested pE4775 to make Pi-pSAT6-myc-VIP1	Amp	This study

pE4822	Myc-VIP1	*Nco*I+*Bam*HI digested pE4821 cloned into *Nco*I+*Bam*HI digested pET28a to make pET28a-myc-VIP1	Kan	This study
pE4831	Gal4BD-Myosin VIII-1 CBD	*Nco*I+*Bam*HI digested pE4776 cloned into *Nco*I+*Bam*HI digested pE3745 to make pGADT7-myosin VIII-1 CBD	Amp	This study
pE4832	Gal4BD-Myosin VIII-2 CBD	*Nco*I+*Bam*HI digested pE4777 cloned into *Nco*I+*Bam*HI digested pE3745 to make pGADT7-myosin VIII-2 CBD	Amp	This study
pE4833	Gal4BD-Myosin VIII-A CBD	*Nco*I+*Bam*HI digested pE4778 cloned into *Nco*I+*Bam*HI digested pE3745 to make pGADT7-myosin VIII-A CBD	Amp	This study
pE4834	Gal4BD-Myosin VIII-B CBD	*Nco*I+*Bam*HI digested pE4779 cloned into *Nco*I+*Bam*HI digested pE3745 to make pGADT7-myosin VIII-B CBD	Amp	This study
pE4835	Gal4BD-Myosin XI-K CBD	*Pst*I-Blunt+*Bam*HI digested pE3082 cloned into *Eco*R53KI+*Bam*HI digested pE3745 to make pGADT7-myosin XI-K CBD	Amp	This study
pE4836	Gal4BD-VIP1	*Nco*I+*Bam*HI digested pE4821 cloned into *Nco*I+*Bam*HI digested pE3745 to make pGADT7-VIP1	Amp	This study
pE4837	Myc-Lamin C	*Sma*I+*Bam*HI digested pE4822 cloned into *Sma*I+*Bam*HI digested pE4792 to make pET28a-myc-Lamin C	Kan	This study
pE4843	Myosin VIII-1	PCR fragment of Myosin VIII-1 full length with *Kpn*I/*Bam*HI sites, cloned into *Eco*RV site of pBlusescript KS+ to make pBS-Myosin VIII-1 full length	Amp	This study
pE4844	Myosin VIII-2	PCR fragment of Myosin VIII-2 full length with *Kpn*I/*Sma*I sites, cloned into *Eco*RV site of pBlusescript KS+ to make pBS-Myosin VIII-2 full length	Amp	This study
pE4845	Myosin VIII-A	PCR fragment of Myosin VIII-A full length with *Kpn*I/*Bam*HI sites, cloned into *Eco*RV site of pBlusescript KS+ to make pBS-Myosin VIII-A full length	Amp	This study

pE4846	Myosin VIII-B	PCR fragment of Myosin VIII-B full length with *Kpn*I/*Sma*I sites, cloned into *Eco*RV site of pBlusescript KS+ to make pBS-Myosin VIII-B full length	Amp	This study
pE4847	Myosin VIII-1	*Kpn*I+*Bam*HI digested pE4843 cloned into *Kpn*I+*Bam*HI digested pE3086 to make pSAT6-myosin VIII-1 full length	Amp	This study
pE4848	Myosin VIII-B	*Kpn*I+*Sma*I digested pE4846 cloned into *Kpn*I+*Sma*I digested pE3086 to make pSAT6-myosin VIII-B full length	Amp	This study
pE4849	Myc-Myosin VIII-1 CBD, Venus	*Asc*I digested pE3542 cloned into *Asc*I digested pE4786 to make pPZP-35S-Venus-Pi-myc-myosin VIII-1 CBD	Spec	This study
pE4850	Myc-Myosin VIII-2 CBD, Venus	*Asc*I digested pE3542 cloned into *Asc*I digested pE4787 to make pPZP-35S-Venus-Pi-myc-myosin VIII-2 CBD	Spec	This study
pE4851	Myc-Myosin VIII-A CBD, Venus	*Asc*I digested pE3542 cloned into *Asc*I digested pE4788 to make pPZP-35S-Venus-Pi-myc-myosin VIII-A CBD	Spec	This study
pE4852	Myc-Myosin VIII-2 CBD, VirE2-Venus, mCherry-ABD2	PI-*Psp*I digested pE4777 cloned into PI-*Psp*I digested pE4292 to make pPZP-Pi-VirE2-Venus-P_{nos}-mCherry-ABD2-Pi-myc-myosin VIII-2 CBD	Spec	This study
pE4853	Myc-Myosin VIII-A CBD, VirE2-Venus, mCherry-ABD2	PI-*Psp*I digested pE4778 cloned into PI-*Psp*I digested pE4292 to make pPZP-Pi-VirE2-Venus-P_{nos}-mCherry-ABD2-Pi-myc-myosin VIII-A CBD	Spec	This study
pE4854	Myosin VIII-1, hptII	PI-*Psp*I digested pE4847 cloned into PI-*Psp*I digested pE4672 to make pPZP-hpt-XVE-P_{35S}-myosin VIII-1 full length	Spec	This study
pE4855	Myc-Myosin VIII-1 CBD, VirE2-Venus, mCherry-ABD2	PI-*Psp*I digested pE4776 cloned into PI-*Psp*I digested pE4292 to make pPZP-Pi-VirE2-Venus-P_{nos}-mCherry-ABD2-Pi-myc-myosin VIII-1 CBD	Spec	This study
pE4856	Myc-Myosin VIII-B CBD, VirE2-Venus, mCherry-ABD2	PI-*Psp*I digested pE4779 cloned into PI-*Psp*I digested pE4292 to make pPZP-Pi-VirE2-Venus-P_{nos}-mCherry-ABD2-Pi-myc-myosin VIII-B CBD	Spec	This study

pE4857	Myosin VIII-B, hptII	PI-*Psp*I digested pE4848 cloned into PI-*Psp*I digested pE4672 to make pPZP-*hptII*-XVE-P35S-myosin VIII-B full length	Spec	This study
pE4858	Myosin VIII-A	*Kpn*I+*Bam*HI digested pE4845 cloned into *Kpn*I+*Bam*HI digested pE4515 to make pSAT1-Myosin VIII-A full length	Kan	This study
pE4859	PIP2A-Venus	*Xho*I+*Bam*HI digested pE3129 (PIP2A) cloned into *Xho*I+*Bam*HI digested pE3758 to make pSAT1-PIP2A-Venus	Amp	This study
pE4874	Myosin VIII-A, *hptII*	*Asc*I digested pE4858 cloned into *Asc*I digested pE4672 to make pPZP-XVE-P35S-myosin VIII-A full length	Spec	This study
pE4875	Myosin VIII-2	*Kpn*I+*Sma*I digested pE4844 cloned into *Kpn*I+*Sma*I digested pE4515 to make pSAT1-Myosin VIII-2 full length	Kan	This study
pE4876	Myosin VIII-2, *hptII*	*Asc*I digested pE4875 cloned into *Asc*I digested pE4672 to make pPZP-XVE-P35S-myosin VIII-2 full length	Spec	This study
pE4877	mCherry-Myosin VIII-1 CBD, Cerulean, PIP2A-Venus	*Asc*I digested pE4859 cloned into *Asc*I digested pE4781 to make pPZP-P_{nos}-Cerulean-P35S-PIP2A-Venus-Pi-mCherry-myosin VIII-1 CBD	Spec	This study
pE4878	mCherry-Myosin VIII-A CBD, Cerulean, PIP2A-Venus	*Asc*I digested pE4859 cloned into *Asc*I digested pE4783 to make pPZP-P_{nos}-Cerulean-P35S-PIP2A-Venus-Pi-mCherry-myosin VIII-A CBD	Spec	This study
pE4879	mCherry-Myosin VIII-B CBD, Cerulean, PIP2A-Venus	*Asc*I digested pE4859 cloned into *Asc*I digested pE4784 to make pPZP-P_{nos}-Cerulean-P35S-PIP2A-Venus-Pi-mCherry-myosin VIII-B CBD	Spec	This study
pE4880	mCherry-Myosin XI-K CBD, Cerulean, PIP2A-Venus	*Asc*I digested pE4859 cloned into *Asc*I digested pE4785 to make pPZP-P_{nos}-Cerulean-P35S-PIP2A-Venus-Pi-mCherry-myosin XI-K CBD	Spec	This study
pE4889	Myc-Myosin XI-K CBD, VirE2-Venus, mCherry-ABD2	PI-*Psp*I digested pE4780 cloned into PI-*Psp*I digested pE4292 to make pPZP-Pi-VirE2-Venus-P_{nos}-mCherry-ABD2-Pi-myc-myosin XI-K CBD	Spec	This study

pE4890	mCherry-Myosin VIII-2 CBD, Cerulean, PIP2A-Venus	*Asc*I digested pE4859 cloned into *Asc*I digested pE4782 to make pPZP-P_{nos}-Cerulean-P_{35S}-PIP2A-Venus-Pi-mCherry-myosin VIII-2 CBD	Spec	This study
pE4891	Myosin VIII-A, Myosin VIII-B, hptII	*Asc*I digested pE4858 cloned into *Asc*I digested pE4857 to make pPZP-hpt-XVE-P_{35S}-myosin VIII-B full length-myosin VIII-A full length	Spec	This study
pE4892	Myosin VIII-2, Myosin VIII-B, hptII	*Asc*I digested pE4875 cloned into *Asc*I digested pE4857 to make pPZP-hpt-XVE-P_{35S}-myosin VIII-B full length-myosin VIII-2 full length	Spec	This study
pE4908	Myosin VIII-B	*Age*I+*Swa*I digested pE4848 cloned into *Age*I+*Swa*I digested pE4754 to make pSAT6-Pi-myosin VIII-B FL	Amp	This study
pE4909	Myosin VIII-1	*Swa*I+*Bam*HI digested pE4847 cloned into *Swa*I+*Bam*HI digested pE4754 to make pSAT1-Pi-myosin VIII-1 FL	Amp	This study
pE4910	Myosin VIII-2	*Kpn*I+*Sma*I digested pE4875 cloned into *Kpn*I+*Sma*I digested pE4908 to make pSAT6-Pi-Myosin VIII-2 full length	Amp	This study
pE4911	Myosin VIII-A	*Kpn*I+*Bam*HI digested pE4858 cloned into *Kpn*I+*Bam*HI digested pE4909 to make pSAT1-Pi-Myosin VIII-A full length	Amp	This study
pE4912	Myosin VIII-1, *hptII*	*Asc*I digested pE4909 cloned into *Asc*I digested pE4672 to make pPZP-*hptII*-XVE-Pi-myosin VIII-1 full length	Spec	This study
pE4913	Myosin VIII-A, *hptII*	*Asc*I digested pE4911 cloned into *Asc*I digested pE4672 to make pPZP-*hptII*-XVE-Pi-myosin VIII-A full length	Spec	This study
pE4914	Myosin VIII-B, *hptII*	PI-*Psp*I digested pE4908 cloned into PI-*Psp*I digested pE4672 to make pPZP-*hptII*-XVE-Pi-myosin VIII-B full length	Spec	This study
pE4915	Myosin VIII-2, *hptII*	PI-*Psp*I digested pE4910 cloned into PI-*Psp*I digested pE4672 to make pPZP-*hptII*-XVE-Pi-myosin VIII-2 full length	Spec	This study

Amp, ampicillin; Gent, gentamicin; Kan, kanamycin; Rif, rifampicin; Spec, spectinomycin; hpt/hptII, hyromycin phosphotransferase II

P_{35S}, CaMV 35S promoter; P_{nos}, nopaline synthase promoter; Pi, inducible promoter
CBD, cargo binding domain

Supplemental Table 2. Bacterial strains used in this study.
***Agrobacterium* strains**

Stock number	Bacterial host	Plasmid harbored	Important features	Antibiotic resistance	Reference
At1872	EHA105ΔVirE2	-----	Non-polar *virE2* deletion of pTiEHA105	Rif	Gelvin lab strain
At1879	At1872	pBISN2	pBISN2 *gusA-intron* gene	Kan, Rif, Spec	Gelvin lab strain
At2315	GV3101	pE4726	mCherry-Myosin VIII-1 CBD VirE2-Venus Cerulean-NLS	Rif, Spec	This study
At2316	GV3101	pE4727	mCherry-Myosin VIII-2 CBD VirE2-Venus Cerulean-NLS	Rif, Spec	This study
At2317	GV3101	pE4728	mCherry-Myosin VIII-A CBD VirE2-Venus Cerulean-NLS	Rif, Spec	This study
At2318	GV3101	pE4729	mCherry-Myosin VIII-B CBD VirE2-Venus Cerulean-NLS	Rif, Spec	This study
At2319	GV3101	pE4730	mCherry-Myosin XI-K CBD VirE2-Venus Cerulean-NLS	Rif, Spec	This study
At2320	GV3101	pE4758	nVenus-Myosin VIII-1 CBD VirE2-cYFP Cerulean-NLS mCherry-ABD2	Rif, Spec	This study
At2321	GV3101	pE4759	nVenus-Myosin VIII-2 CBD VirE2-cYFP Cerulean-NLS mCherryABD2	Rif, Spec	This study

At2322	GV3101	pE4755	nVenus-Myosin VIII-A CBD VirE2-cYFP Cerulean-NLS mCherry-ABD2	Rif, Spec	This study
At2323	GV3101	pE4756	nVenus-Myosin VIII-B CBD VirE2-cYFP Cerulean-NLS mCherry-ABD2	Rif, Spec	This study
At2324	GV3101	pE4757	nVenus-Myosin XI-K CBD VirE2-cYFP Cerulean-NLS mCherry-ABD2	Rif, Spec	This study
At2360	GV3101	pE4672	Binary vector; *hptII*	Rif, Spec	This study
At2361	GV3101	pE4854	Myosin VIII-1 *hptII*	Rif, Spec	This study
At2362	GV3101	pE4857	Myosin VIII-B *hptII*	Rif, Spec	This study
At2363	GV3101	pE4874	Myosin VIII-A *hptII*	Rif, Spec	This study
At2364	GV3101	pE4876	Myosin VIII-2 *hptII*	Rif, Spec	This study
At2365	GV3101	pE4852	myc-Myosin VIII-2 CBD VirE2-Venus mCherry-ABD2	Rif, Spec	This study
At2366	GV3101	pE4853	myc-Myosin VIII-A CBD VirE2-Venus mCherry-ABD2	Rif, Spec	This study
At2367	GV3101	pE4855	myc-Myosin VIII-1 CBD VirE2-Venus mCherry-ABD2	Rif, Spec	This study
At2368	GV3101	pE4856	myc-Myosin VIII-B CBD VirE2-Venus mCherry-ABD2	Rif, Spec	This study
At2369	GV3101	pE4889	myc-Myosin XI-K CBD VirE2-Venus mCherry-ABD2	Rif, Spec	This study
At2370	GV3101	pE4877	mCherry-Myosin VIII-1 CBD Cerulean PIP2A-Venus	Rif, Spec	This study

At2371	GV3101	pE4878	mCherry-Myosin VIII-A CBD Cerulean PIP2A-Venus	Rif, Spec	This study
At2372	GV3101	pE4879	mCherry-Myosin VIII-B CBD Cerulean PIP2A-Venus	Rif, Spec	This study
At2373	GV3101	pE4880	mCherry-Myosin XI-K CBD Cerulean PIP2A-Venus	Rif, Spec	This study
At2374	GV3101	pE4890	mCherry-Myosin VIII-2 CBD Cerulean PIP2A-Venus	Rif, Spec	This study
At2375	GV3101	pE4891	Myosin VIII-A Myosin VIII-B *hptII*	Rif, Spec	This study
At2376	GV3101	pE4892	Myosin VIII-2 Myosin VIII-B *hptII*	Rif, Spec	This study
At2389	GV3101	pE4912	Myosin VIII-1 *hptII*	Rif, Spec	This study
At2390	GV3101	pE4915	Myosin VIII-2 *hptII*	Rif, Spec	This study
At2391	GV3101	pE4913	Myosin VIII-A *hptII*	Rif, Spec	This study
At2392	GV3101	pE4914	Myosin VIII-B *hptII*	Rif, Spec	This study
At2403	At1872	pE3341	pBBR1-MCS2::mCherry	Kan	This study
At2404	At2403	pE4672	pPZP-RCS-P_{nos}-*hptII*	Kan, Spec	This study
At2405	At1872	pE4381	pPZP-P_{35S}-mCherry-intron-NLS	Spec	This study

At2423	GV3101	pE4786	Myc-Myosin VIII-1 CBD VirE2-Venus	Rif, Spec	This study
At2424	GV3101	pE4787	Myc-Myosin VIII-2 CBD VirE2-Venus	Rif, Spec	This study
At2425	GV3101	pE4788	Myc-Myosin VIII-A CBD VirE2-Venus	Rif, Spec	This study
At2426	GV3101	pE4789	Myc-Myosin VIII-B CBD VirE2-Venus	Rif, Spec	This study
At2427	GV3101	pE4790	Myc-Myosin XI-K CBD VirE2-Venus	Rif, Spec	This study
At2428	GV3101	pE4850	Myc-Myosin VIII-2 CBD Venus	Rif, Spec	This study

Kan, kanamycin; Rif, rifampicin; Spec, spectinomycin
CBD, cargo binding domain; FL, full-length

***E. coli* strains**

Stock number	Host	Description of strain	Antibiotic resistance	Reference
E4823	BL21(DE3)	pE4814 in BL21DE3	Kan	This study
E4824	BL21(DE3)	pE4815 in BL21DE3	Kan	This study
E4825	BL21(DE3)	pE4816 in BL21DE3	Kan	This study
E4826	BL21(DE3)	pE4817 in BL21DE3	Kan	This study
E4827	BL21(DE3)	pE4818 in BL21DE3	Kan	This study
E4828	BL21(DE3)	pE4819 in BL21DE3	Kan	This study
E4829	BL21(DE3)	pE4820 in BL21DE3	Kan	This study
E4830	BL21(DE3)	pE4822 in BL21DE3	Kan	This study
Top10	N/A	F^- *mcr*A Δ(*mrr-hsd*RMS-*mcr*BC) φ80 *lac*ZΔM15Δ *lac*X74 *rec*A1 *ara*Δ139Δ(*ara-leu*)7697 *gal*U *gal*K *rps*L (StrR) *end*A1 *nup*G	Str	Invitrogen
BL21(DE3)	N/A	*E. coli* B F^- *dcm ompT hsdS* (rB^-mB^-) *gal* λ(DE3)	None	Studier and Moffatt, 1986

Kan, kanamycin; Str, streptomycin; N/A, not applicable

Supplemental Table 3. Primers used in this study.

Purpose	Forward primer	Reverse primer
myosin cDNA amplification		
VIII-1 CBD	5'-CCGGGGTACCAAAGCATCA GTACTTTCCGAGCT-3'	5'-CCGCGGATCCTCAATACC TGGTGCTATTTCTCC-3'
VIII-2 CBD	5'-CCGGGGTACCTCTATGT CTGATCTCCAGAAACG-3'	5'-CCGCGGATCCCTAGCC TCTTTTTCCCCACCA-3'
VIII-A CBD	5'-CCGGGGTACCTATCTTT CCGATCTTCAGCGT-3'	5'-CCGCGGATCCTTAATACC TAGTACTCCTCAACCTC-3'
VIII-B CBD	5'-CCGGGGTACCGTTCTTG CTGATCTCCAGAGCC-3'	5'-CCGCGGATCCTCAATAAC TTTTCTTGCACCACCAA-3'
XI-K CBD	5'-CCGGGGTACCGCAAGG AAAGCTATTGAAGAAGC-3'	5'-CCGCGGATCCTTACGAT GTACTGCCTTCTTTAC-3'
VIII-1 FL	5'-AATTGGTACCATGTCTC AGAAGGTTACTCCATT-3'	5'-TTAAGGATCCTCAATAC CTGGTGCTATTTCTCC-3'
VIII-2 FL	5'-AATTGGTACCATGATGT TATCGGCATCGCCGAAC-3'	5'-TTAACCCGGGCTAGCCT CTTTTTCCCCACCA-3'
VIII-A FL	5'-AATTGGTACCATGGCAC ACAAGGTTAAGGCATC-3'	5'-TTAAGGATCCTTAATAC CTAGTACTCCTCAACCTC-3'
VIII-B FL	5'-AATTGGTACCATGATGA AAAGTTCAGTGAAGG-3'	5'-TTAACCCGGGTCAATAA CTTTTCTTGCACCACC-3'

Purpose	Forward primer	Reverse primer
Plant genotyping		
Myosin VIII-1	5’-TTCGTGTGAACGTTGATTCTG-3’	5’-TCCAGCTTGAATAGATGACGG-3’
Myosin VIII-2	5’-CTGAGTTCAGGAGTGTTTCCG-3’	5’-TGTACCTCCGAACTGGACAAG-3’
Myosin VIII-A	5’-AGGTTGTACAACACTGCTGGC-3’	5’-ACGAGAAATGGTCTTGTGCTG-3’
Myosin VIII-B	5’-AGTAAAGCAGGGCCAGTTTTG-3’	5’-CTACACTTTGCTTCAGCAGGG-3’
Myosin XI-1	5’-TCAAAACGTTGAACTAACCGG-3’	5’- TTGTTTGGACGGGTATCTCAG-3’
Myosin XI-2	5’-GTGCTCCCGAAGATCCTATT-3’	5’-CAGTGCAACCACATGAAGATG-3’
Myosin XI-B	5’-CAGAAGCAACCCACTTCAGTC-3’	5’-GCTACCGAAGGAAGGACTGTC-3’
Myosin XI-C	5’-TTATGATCACACCCGAGGAAG-3’	5’-AAAGACCCACAACAAAGGGAC-3’
Myosin XI-H	5’-AAATGCTTGAGCTGGAACATG -3’	5’-TGCCCTGATTTTTCATTTGTC-3’
Myosin XI-J	5’-CTCACCTTGCAAAGTGGAGTC-3’	5’-CTCAACTTGCAATAAGGCCTG-3’
Myosin XI-E	5’-TTGGGATGACCCAACTTGTAC-3’	5’-GCCTGGAATACACTGAAGCTG-3’
Myosin XI-I	5’-TTCTGCAATTTCAATTCAGGC-3’	5’-CAGCAGACTTCTCCTTCATGG-3’
Myosin XI-K	5’-GGGTAGCAAGATACTCCTCGG-3’	5’-GCAAGAGCAACTCAATTCTGG-3’
Salk T-DNA left border	5’-TGGTTCACGTAGTGGGCCATCG-3’	

CBD, cargo binding domain; FL, full-length

REFERENCES

Chien CT, Bartel PL, Sternglanz R, Fields F. (1991) The two-hybrid system: a method to identify and clone genes for proteins that interact with a protein of interest. Proc Natl Acad Sci USA **88:** 9578-9582

Citovsky V, Lee L-Y, Vyas S, Glick E, Chen M-H, Vainstein A, Gafni Y, Gelvin SB, Tzfira T. (2006) Subcellular localization of interacting proteins by bimolecular fluorescence complementation *in planta*. J Mol Biol **362**: 1120-1131

Koncz C, Schell J. (1986) The promoter of TL-DNA gene 5 controls the tissue-specific expression of chimaeric genes carried by a novel type of *Agrobacterium* binary vector. Mol Gen Genet **204**: 383-396

Kozaki A, Hake S, Colasanti J. (2004) The maize ID1 flowering time regulator is a zinc finger protein with novel DNA binding properties. Nucl Acids Res **32**: 1710-1720

Lee L-Y, Gelvin SB. (2014) Bimolecular fluorescence complementation for imaging protein-protein interactions in plant hosts of microbial pathogens. In Methods in Molecular Biology: Host-Bacteria Interactions. (A.C. Vergunst and D. O'Callaghan, eds.). Springer, Humana Press. Vol. 1197. pp. 185-208

Lu Q, Tang X, Tian G, Wang F, Liu K, Nguyen V, Kohalmi SE, Keller WA, Tsang EW, Harada JJ, Rothstein SJ, Cui Y. (2010) *Arabidopsis* homolog of the yeast TREX-2 mRNA export complex: Components and anchoring nucleoporin. Plant J **61:** 259-70

Studier FW, Moffatt BA. (1986) Use of bacteriophage T7 RNA polymerase to direct selective high-level expression of cloned genes. J Mol Biol **189**: 113-130

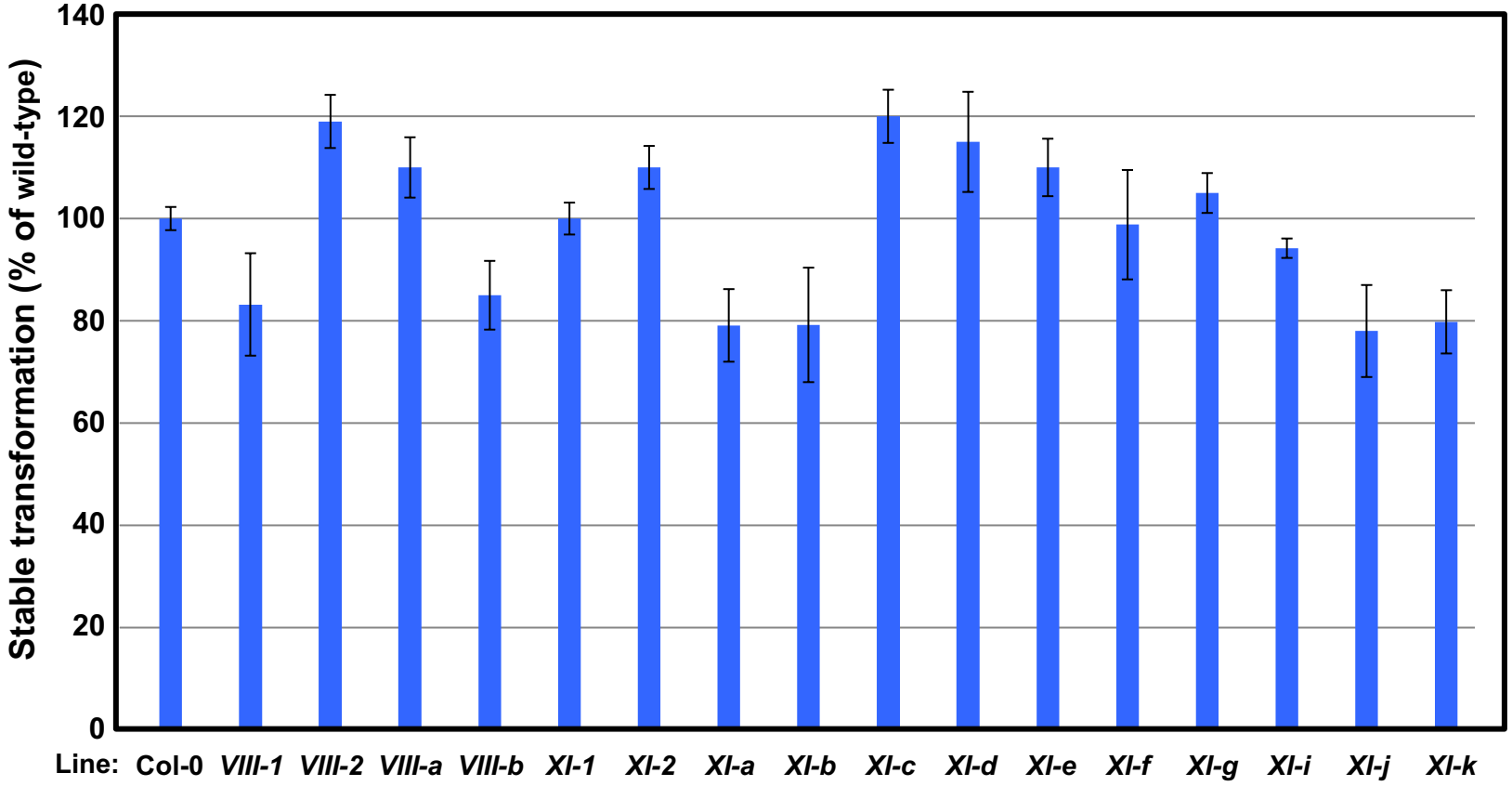

Supplemental Figure S1. Most *myosin VIII* and *myosin XI* single mutants are not deficient in stable transformation. Root segments from the indicated *Arabidopsis myosin VIII* or *myosin XI* single mutants, as well as control wild-type plants, were infected with the tumorigenic strain *A. tumefaciens* A208 at the concentration of 10^6 cfu/ml and the tumors were scored after 30 days of infection. A total of 10-15 plants and >100 segments per plant were tested for stable transformation. Values given are means ± SE. No significant differences were observed compared to wild-type plants.

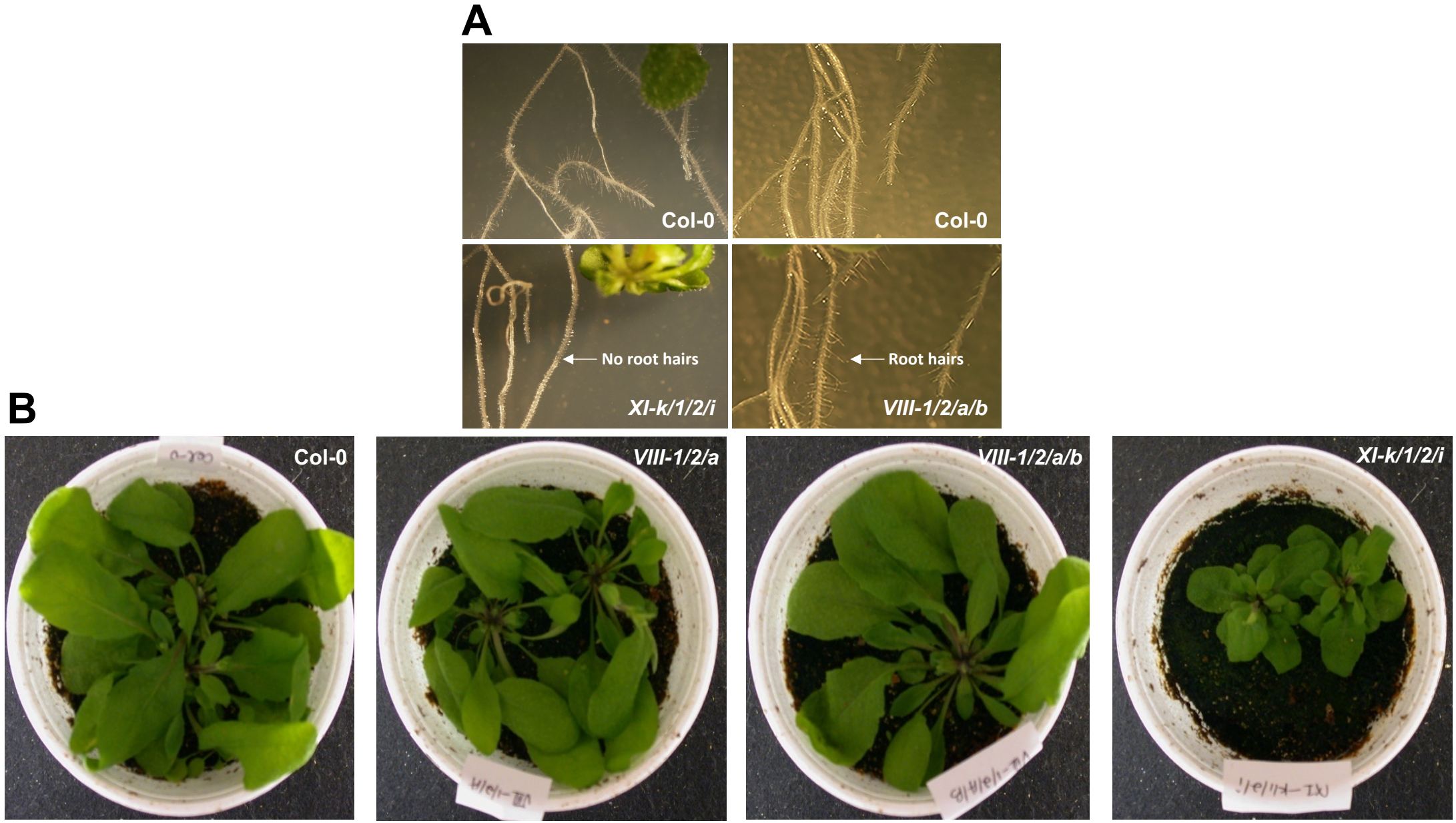

Supplemental Figure S2. Growth and morphology of wild-type and higher order *myosin VIII* and *XI* mutant plants. (A) Roots; **(B)** Above-ground tissues.

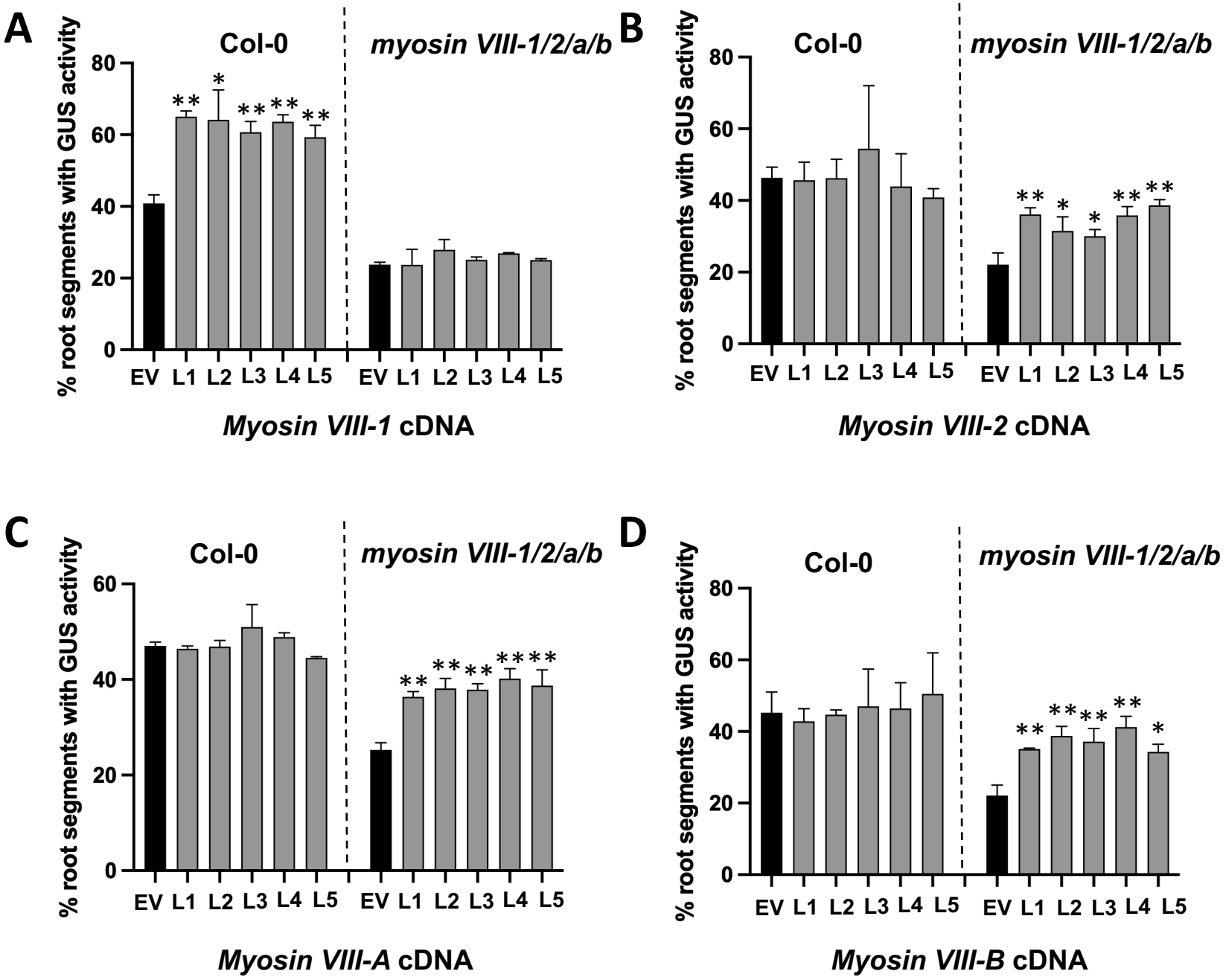

Supplemental Figure S3. Effect on transformation of expressing full-length myosin cDNAs in wild-type and *myosin VIII-1/2/a/b* mutant plants. Root segments of five transgenic plants of each independent line, expressing the indicated *myosin VIII* cDNAs in the indicated genetic backgrounds, were infected with *A. tumefaciens* At849 containing the binary vector pBISN1 with a *gusA*-intron gene in the T-DNA region, at 10^7 cfu/ml. Six days after infection the root segments were stained with X-gluc and the percentage of roots showing GUS activity was calculated. (**A**) *myosin VIII-1* cDNA; (**B**) *myosin VIII-2* cDNA; (**C**) *myosin VIII-A* cDNA; (**D**) *myosin VIII-B* cDNA. Each bar indicates the mean of five plants and >100 root segments/plant ± SE for each transgenic line. Asterisks indicate significant differences of the indicated *myosin VIII* cDNA transgenic plant compared with plants harboring an empty vector (EV). L, Independent transgenic line.
[*t-test*, $*P < 0.05$; $**P < 0.01$].

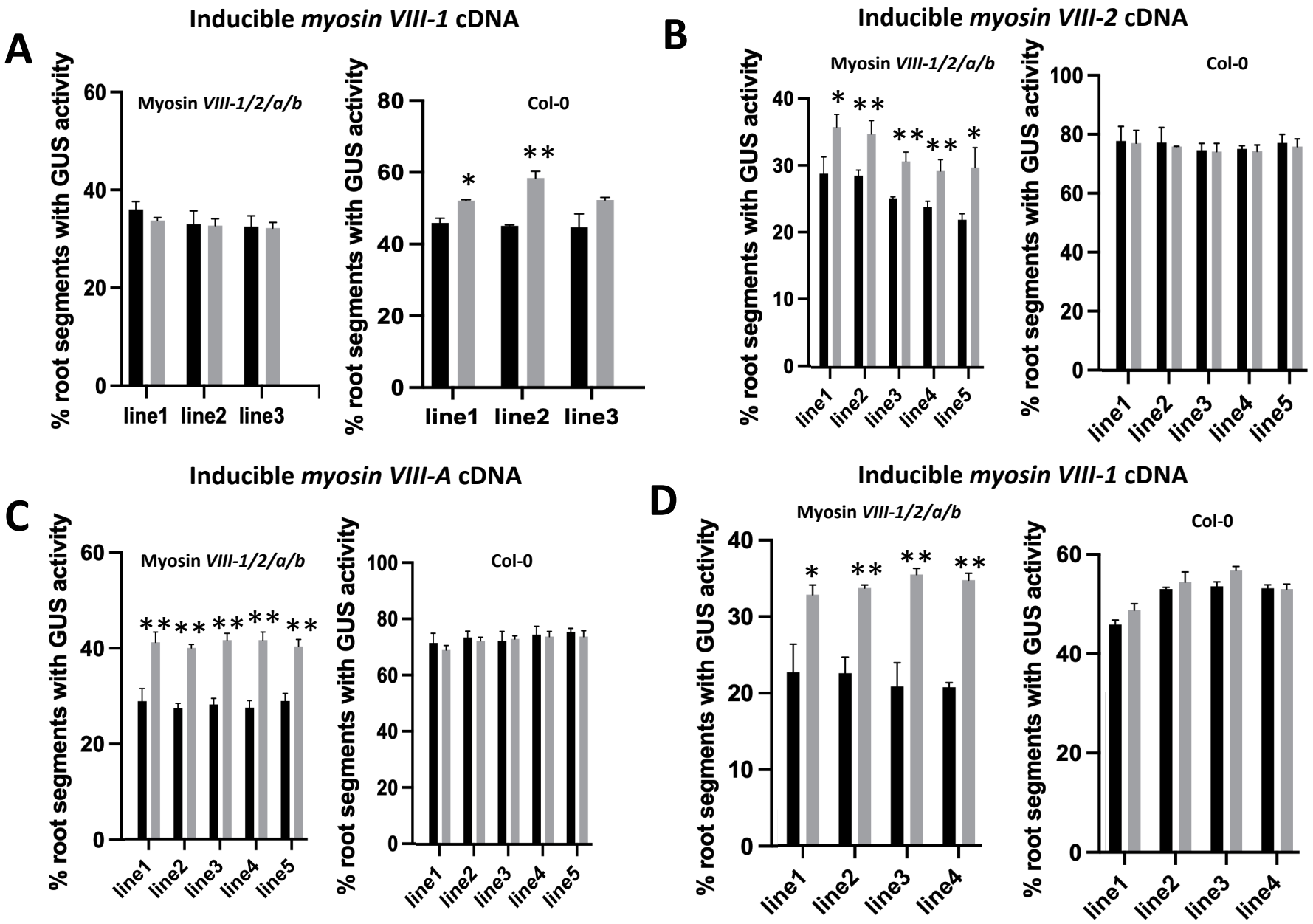

Supplemental Figure S4. Effect on transformation of expressing full-length inducible myosin cDNAs in wild-type and *myosin VIII-1/2/a/b* mutant plants. Root segments of five transgenic plants of each independent line, expressing the indicated inducible *myosin VIII* cDNAs in the indicated genetic backgrounds, treated with β-estradiol or control solution for 24 hr, then infected with *A. tumefaciens* At849 containing the binary vector pBISN1 with a *gusA*-intron gene in the T-DNA region, at 10^7 cfu/ml. Six days after infection the root segments were stained with X-gluc and the percentage of roots showing GUS activity was calculated. (**A**) *myosin VIII-1* cDNA; (**B**) *myosin VIII-2* cDNA; (**C**) *myosin VIII-A* cDNA; (**D**) *myosin VIII-B* cDNA. Each bar indicates the mean of five plants and >100 root segments/plant ± SE for each transgenic line. Asterisks indicate significant differences of the indicated *myosin VIII* cDNA transgenic plant compared with plants treated with control solution. [*t-test*, $*P < 0.05$; $**P < 0.01$].

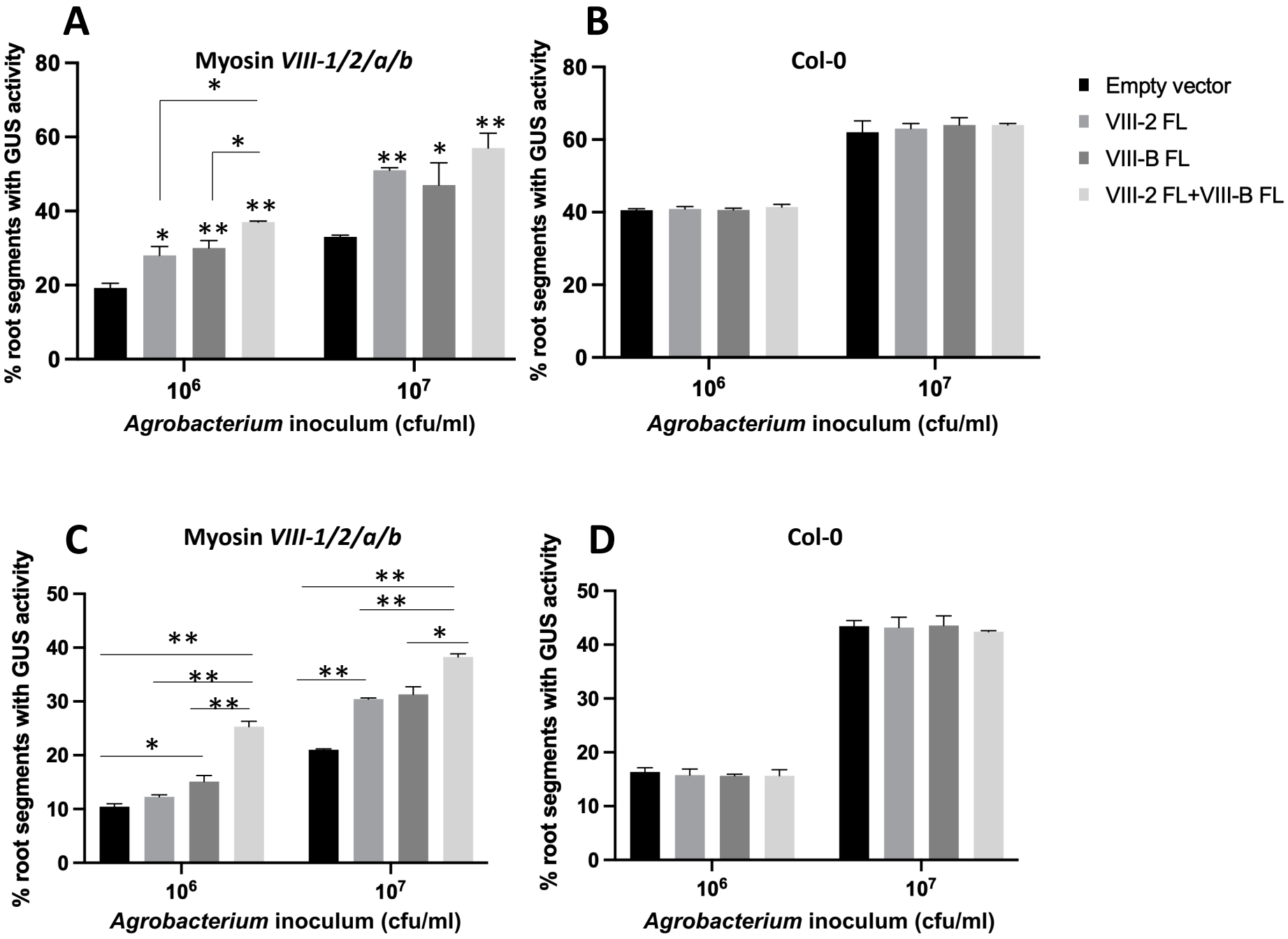

Supplemental Figure S5. Effect on transformation of expressing pairs of full-length myosin cDNAs in wild-type and *myosin VIII-1/2/a/b* mutant plants. Root segments of five transgenic plants of each independent line, expressing the indicated single and pairs of *myosin VIII* cDNAs in the indicated genetic backgrounds, were infected with *A. tumefaciens* At849 as mentioned above. The percentage of roots showing GUS activity was calculated. (**A**) *myosin VIII-2*, *myosin VIII-B*, and *myosin VIII-2+VIII-B* cDNAs in the *myosin VIII-1/2/a/b* mutant; (**B**) *myosin VIII-2, myosin VIII-B*, and *myosin VIII-2+VIII-B* cDNAs in Col-0; (**C**) *myosin VIII-A*, *myosin VIII-B*, and *myosin VIII-A+VIII-B* cDNAs in the *myosin VIII-1/2/a/b* mutant; (**D**) *myosin VIII-A*, *myosin VIII-B*, and *myosin VIII-A+VIII-B* cDNAs in Col-0. Each bar indicates the mean of five plants and >100 root segments/plant ± SE for each transgenic line. Except where otherwise indicated, asterisks indicate significant differences of the indicated *myosin VIII* cDNA transgenic plant compared with plants harboring an empty vector.
[*t-test*, $*P < 0.05$; $**P < 0.01$].

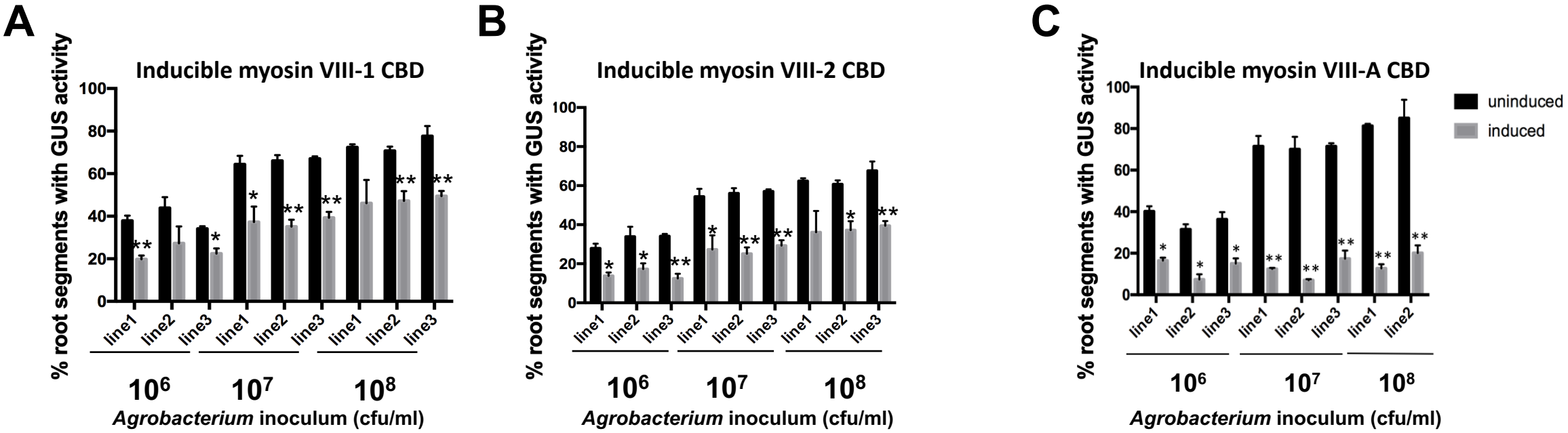

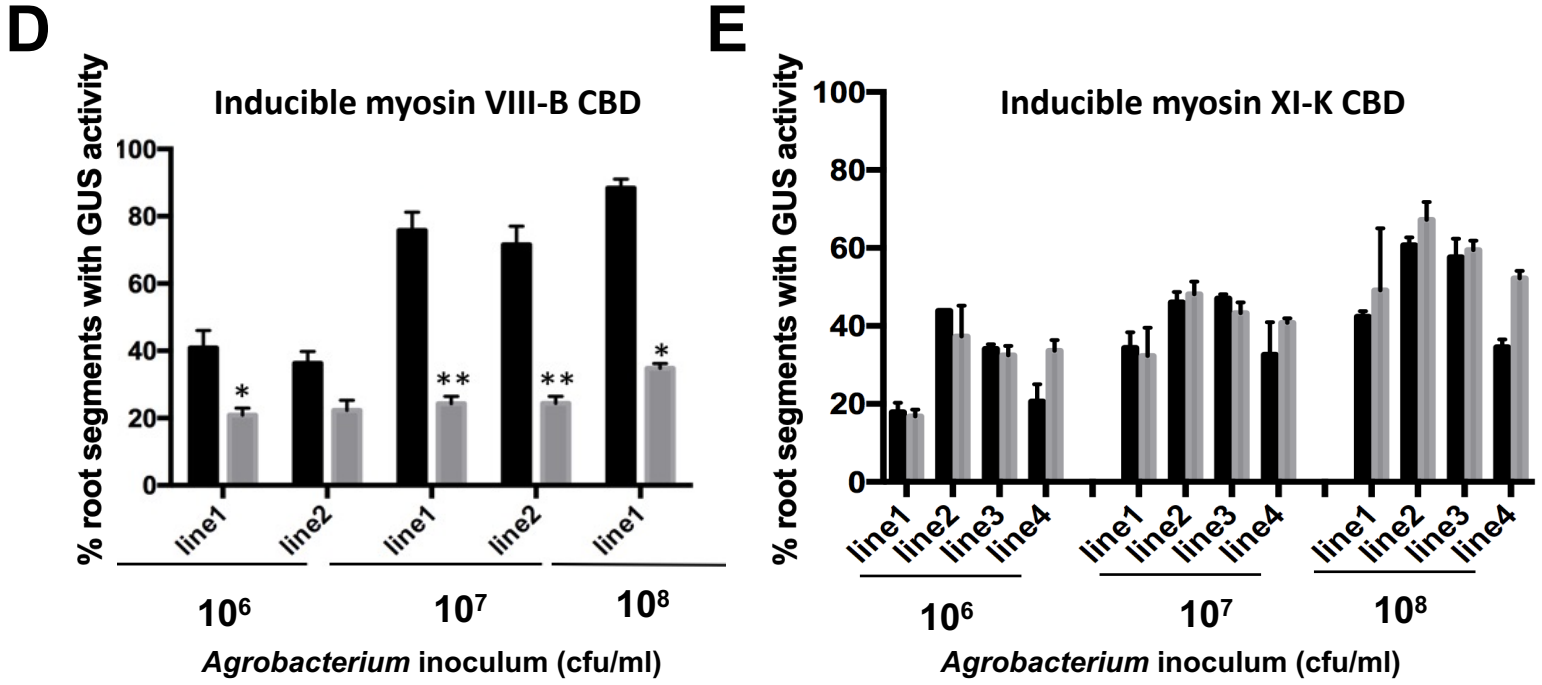

Supplemental Figure S6. Inducible expression of myosin VIII, but not myosin XI-K, CBDs inhibits transformation. Root segments of transgenic plants of each independent line, expressing the indicated inducible *myosin VIII* or *myosin XI-K* CBD cDNA, were treated with β-estradiol or control solution for 24 hr, then infected with *A. tumefaciens* At849 containing the binary vector pBISN1 with a *gusA*-intron gene in the T-DNA region, at the indicated 10^6, 10^7 and 10^8 cfu/ml. Six days after infection the root segments were stained with X-gluc and the percentage of roots showing GUS activity was calculated. (**A**) myosin VIII-1 CBD; (**B**) myosin VIII-2 CBD; (**C**) myosin VIII-A CBD; (**D**) myosin VIII-B CBD; (**E**) myosin XI-K CBD. Each bar indicates the mean of five plants and >100 root segments/plant ± SE for each transgenic line. Asterisks indicate significant differences of the indicated *myosin VIII* cDNA transgenic plant compared with plants treated with control solution. [*t-test*, $*P < 0.05$; $**P < 0.01$].

A

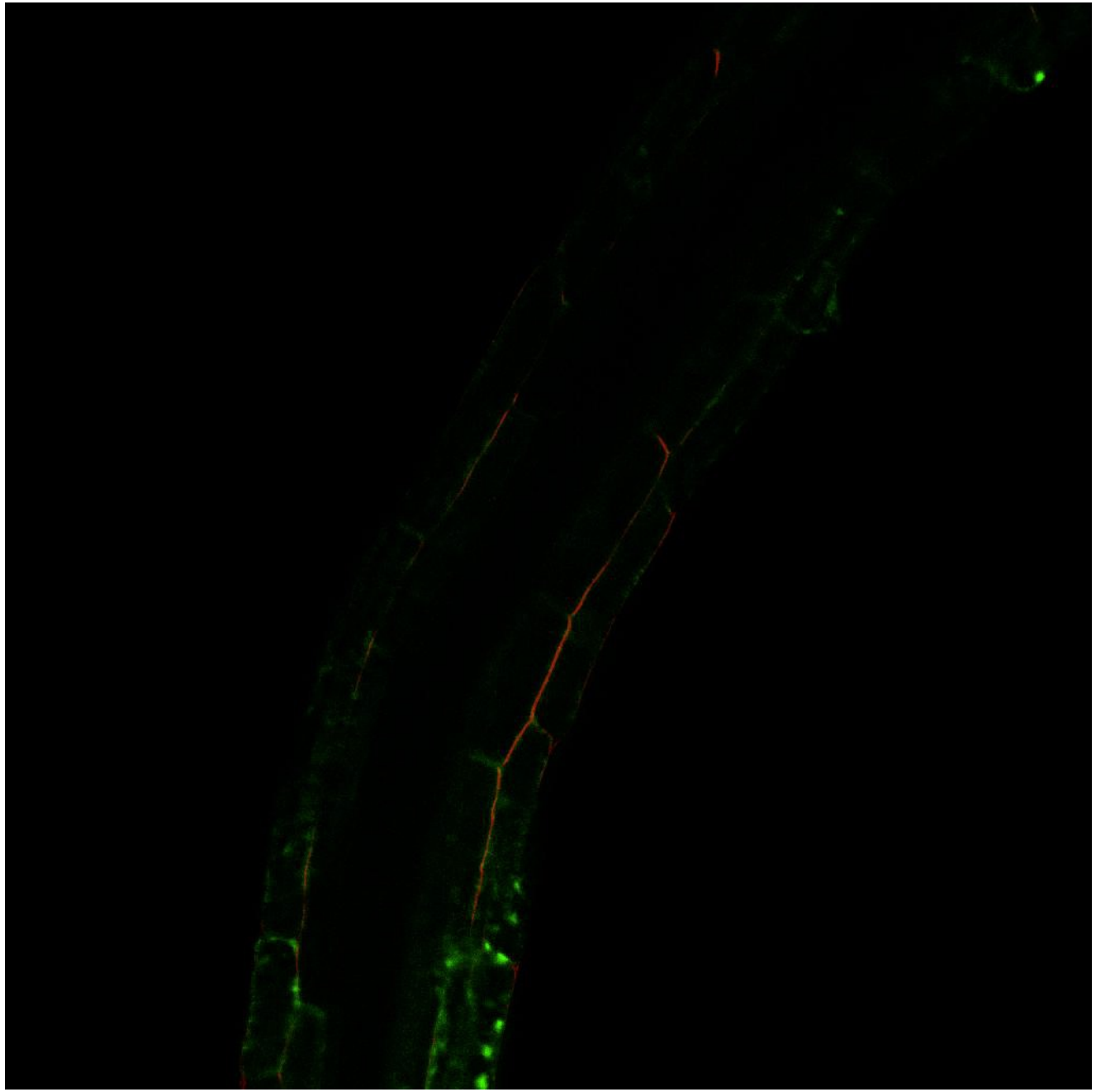

B

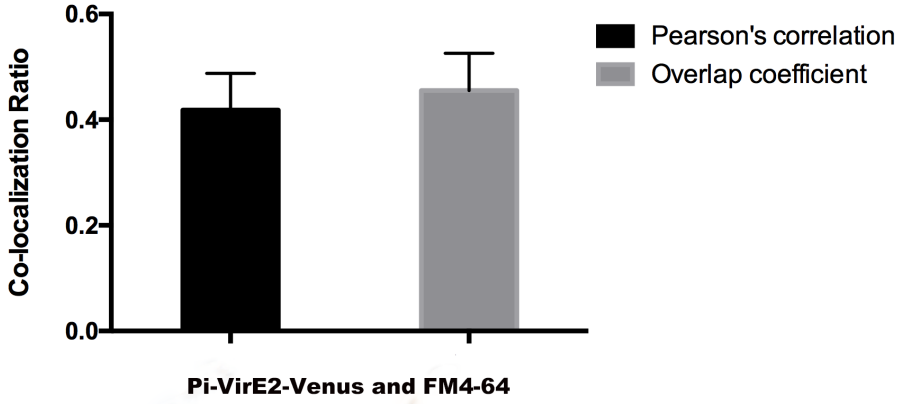

Supplemental Figure S7. Lack of co-localization of VirE2-Venus and FM4-64. (A) Inducible VirE2-Venus transgenic plants were treated with β-estradiol for 8 hr, then the root cells were stained with FM4-64 for 5 minutes before imaging. The Z-stack image was taken using a Zesis LSM 880 Upright Confocal Plan-Apo microscope with a 20×/0.8 objective. **(B)** Pearson's and overlap correlations of Venus and red FM4-64 fluorescence. A total of 10-15 transgenic lines and >50 cells were used for quantitative analysis using Image J. Values <0.5 indicate lack of co-localization of the two proteins.

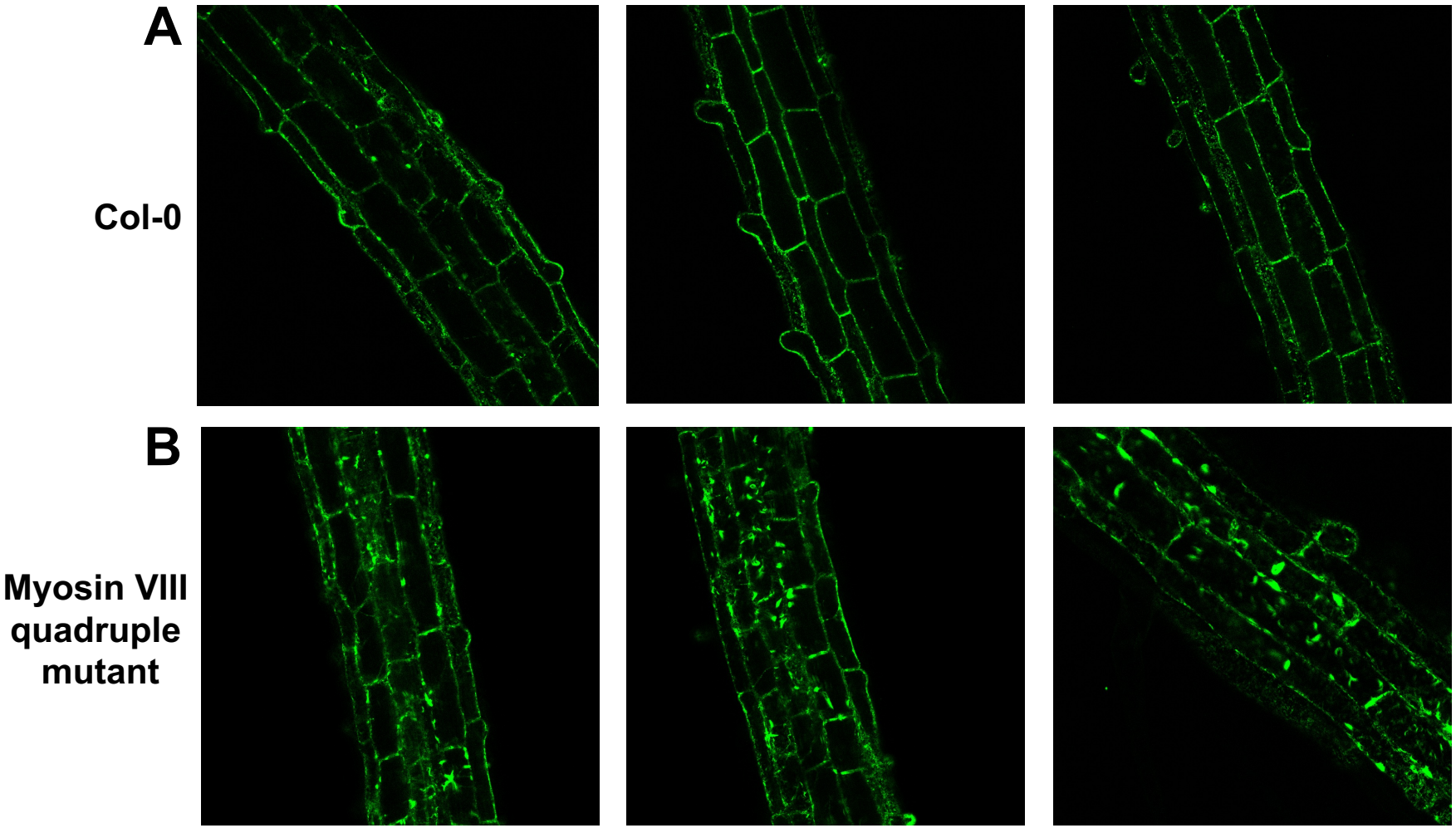

Supplemental Figure S8. Subcellular localization of VirE2-Venus in transgenic plants. (A) Inducible VirE2-Venus expressed in wild-type plants. **(B)** Inducible VirE2-Venus expressed in *myosin VIII-1/2/a/b* quadruple mutant plants. Roots from three independent transgenic plants were treated with β-estradiol for 8 hr, and the images were taken using a Zesis LSM 880 Upright Confocal Plan-Apo microscope with a 20×/0.8 objective.

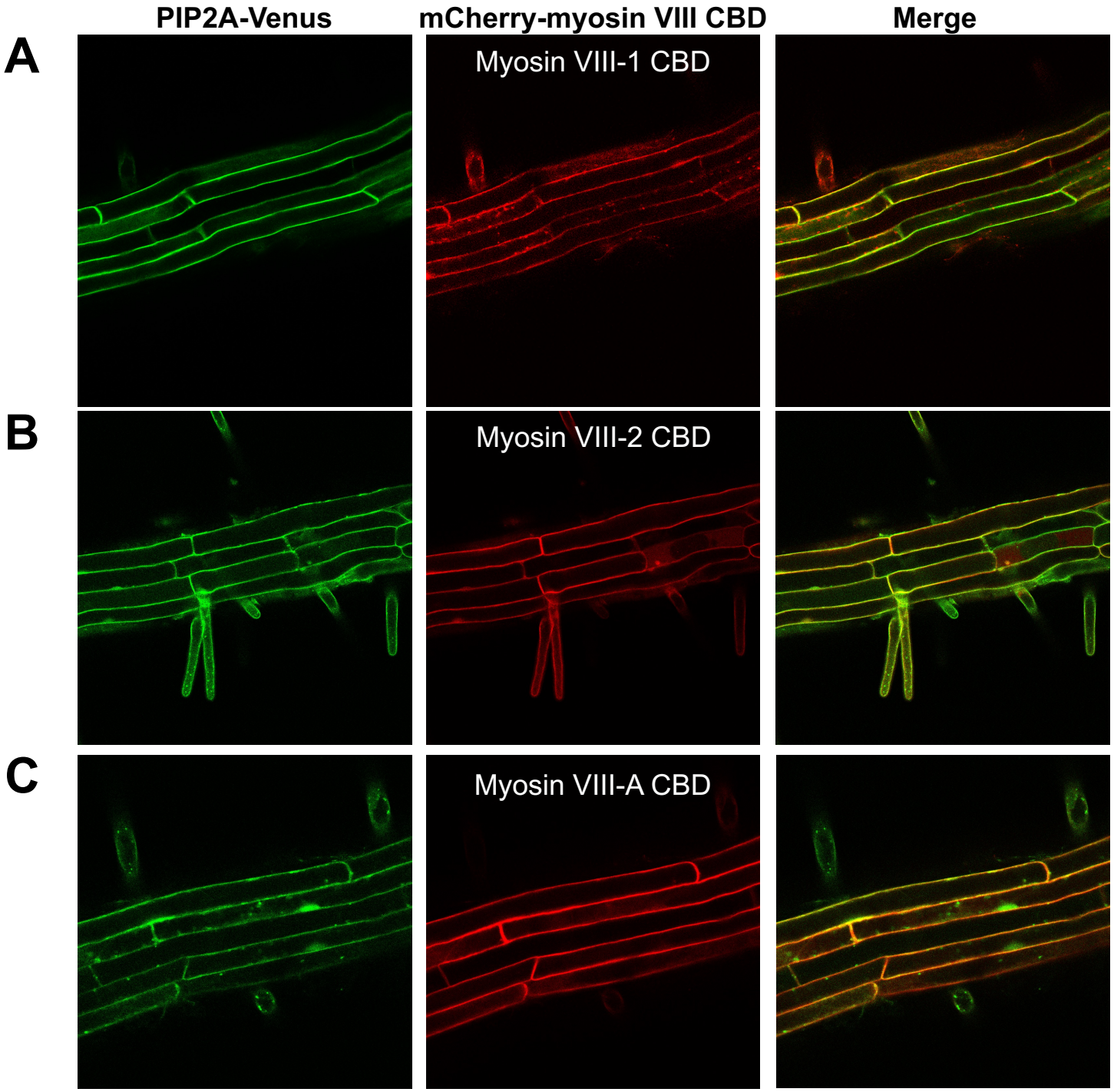

Supplemental Figure S9. Myosin VIII CBDs colocalize with the plasma membrane marker PIP2A. (A) Transgenic *Arabidopsis* plant roots that inducibly express an mCherry-myosin VIII-1 CBD and constitutively express PIP2A-Venus. **(B)** Transgenic *Arabidopsis* plants roots that inducibly express an mCherry-myosin VIII-2 CBD and constitutively express PIP2A-Venus. **(C)** Transgenic *Arabidopsis* plants roots that inducibly express an mCherry-myosin VIII-A CBD and constitutively express PIP2A-Venus. A total of 10 independent transgenic lines were treated with β-estradiol for 8 hr, and representative images were taken using a Zesis LSM 880 Upright Confocal Plan-Apo microscope with a 20×/0.8 objective.

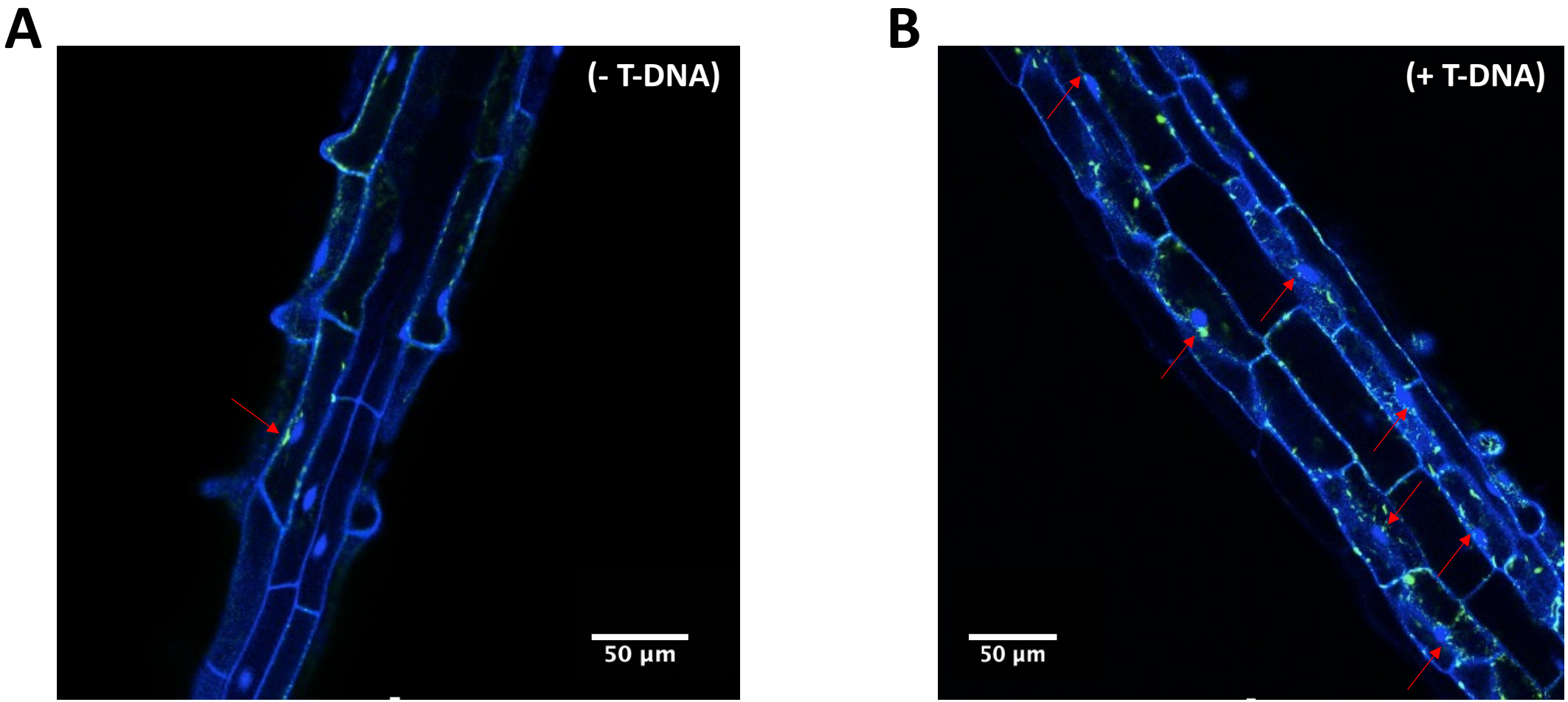

Supplemental Figure S10. VirE2 re-localizes to the perinuclear area after infection by an *Agrobacterium* strain that can transfer T-DNA. VirE2-Venus transgenic plants were treated with 5 µM β-estradiol for 24 hr. Root segments were inoculated with 10^8 cfu/ml of the *virE2* mutant strain *A. tumefaciens* At1872 **(A)** lacking or **(B)** containing a T-DNA region. Images of the elongation zone of the root were taken 8 hr after infection using a Zesis LSM 880 Upright Confocal microscope with a Plan-Apo 20×/0.8 objective. Statistical analysis of VirE2 localization is shown in Figure 11A. Red arrows indicate several examples of perinuclear VirE2-Venus. Bars indicate 50 µm.

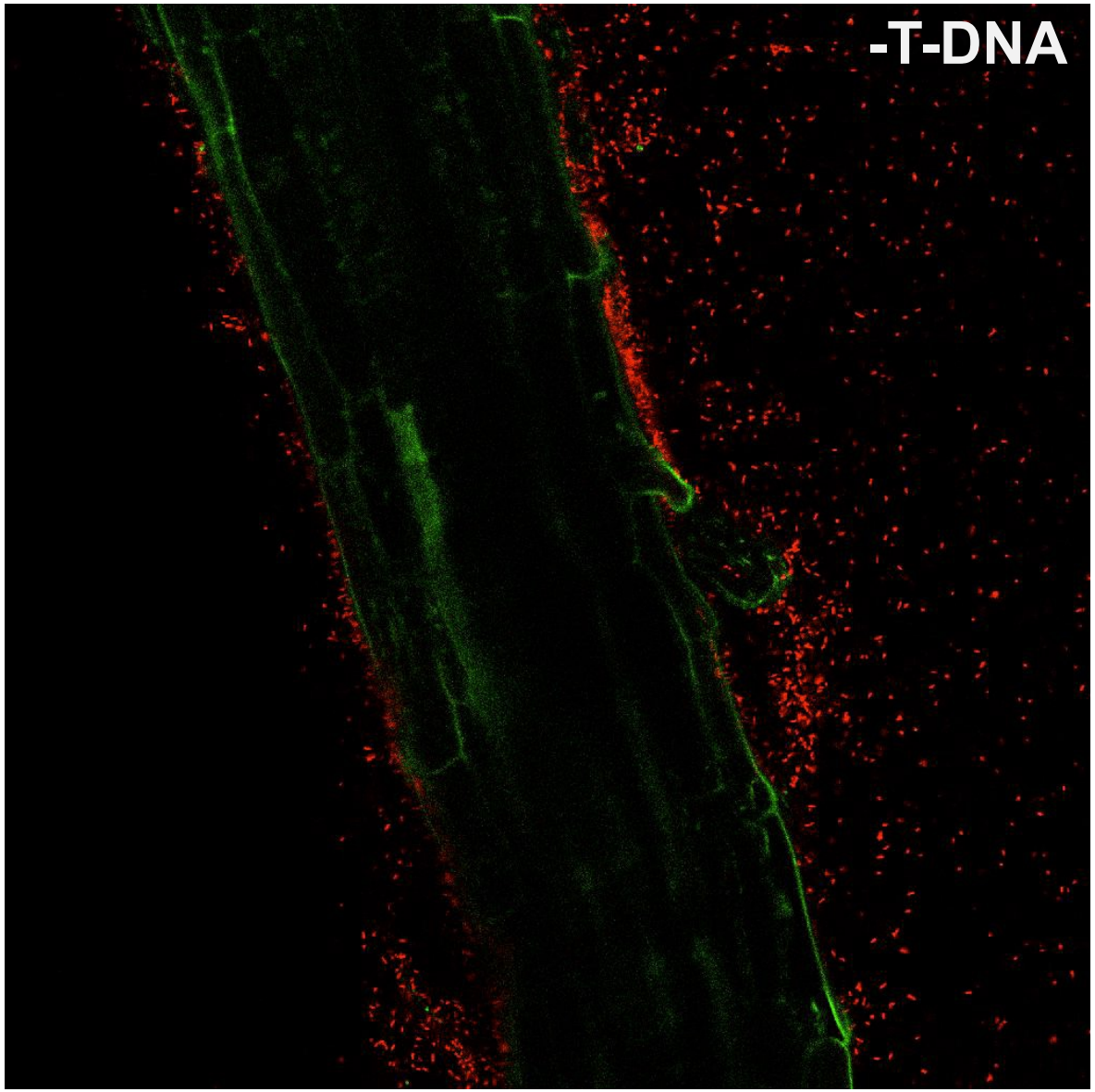

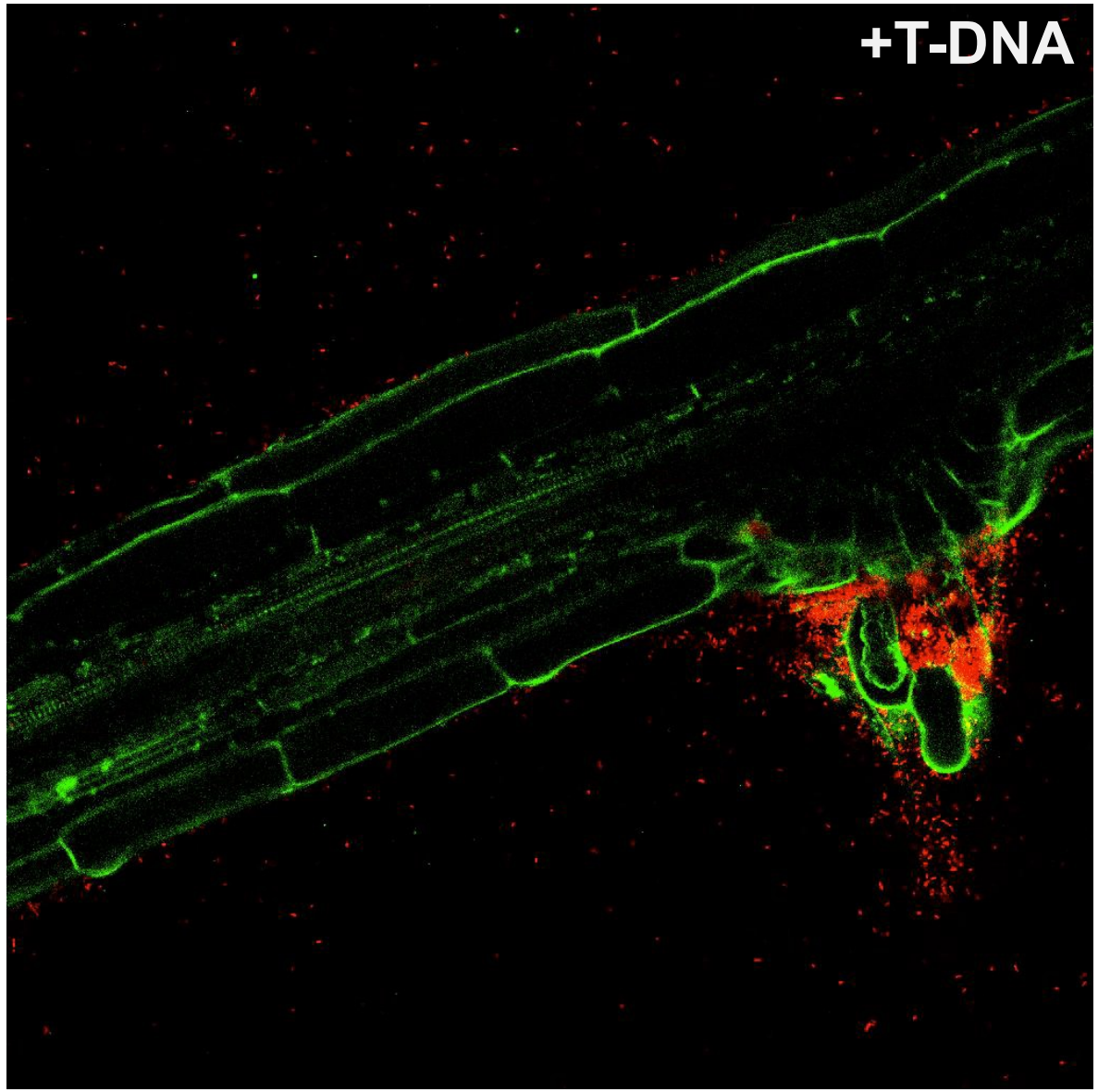

Supplemental Figure S11. Infection of root cells with an *Agrobacterium* strain capable of transferring T-DNA re-localizes VirE2-Venus from the cellular periphery into the cytoplasm. Transgenic plants inducibly expressing VirE2-Venus were treated with 5 μM β-estradiol for 24 hr, then inoculated with 10^8 cfu/ml of the *virE2* mutant strain *A. tumefaciens* At1872 without (left panel) or with (right panel) T-DNA. The *Agrobacterium* cells also expressed an mCherry protein. Z-stack images of cells in the root elongation zone were taken after 8 hr of infection using a Zesis LSM 880 Upright Confocal Plan-Apo microscope using a 20×/0.8 objective.

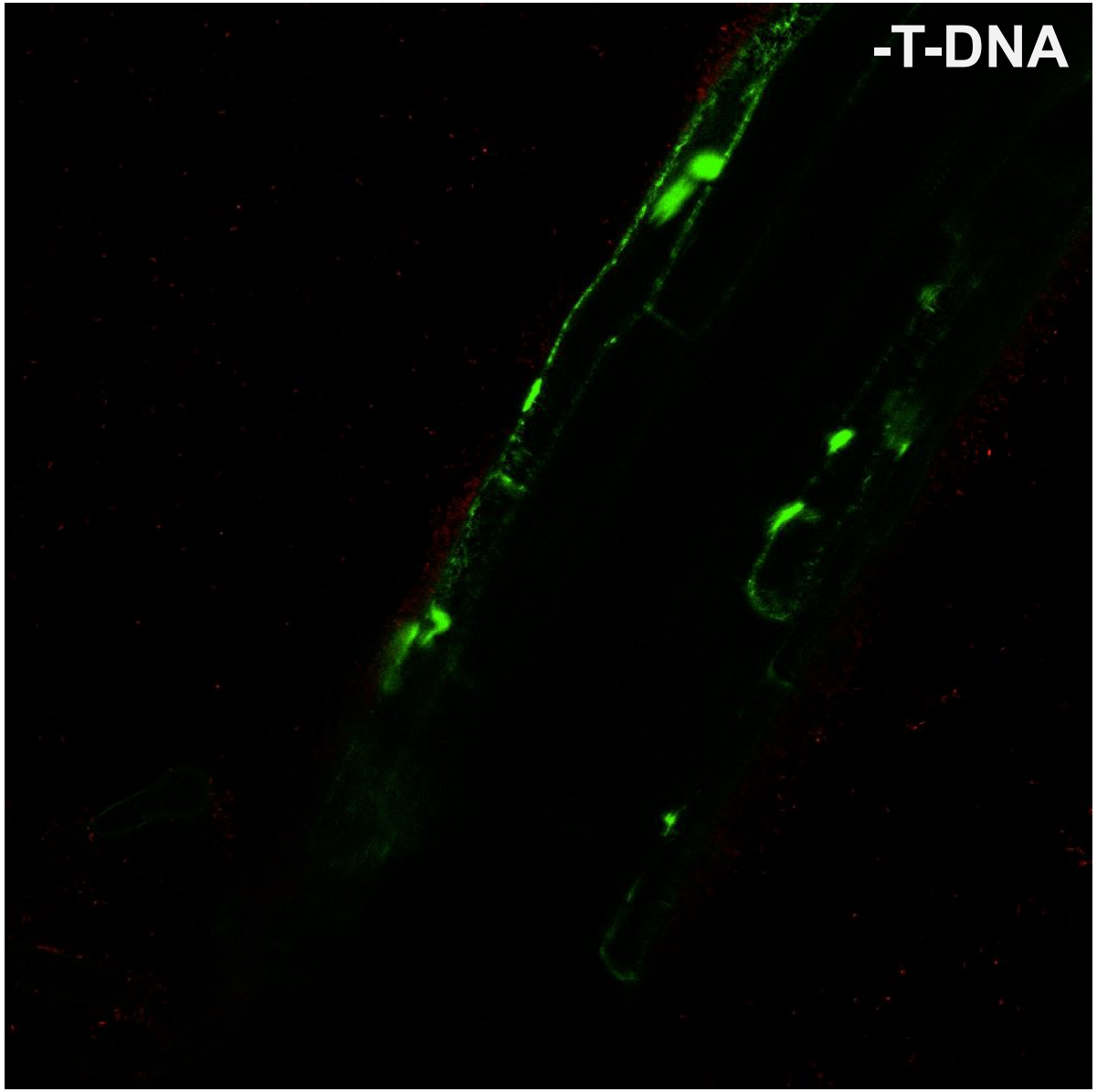

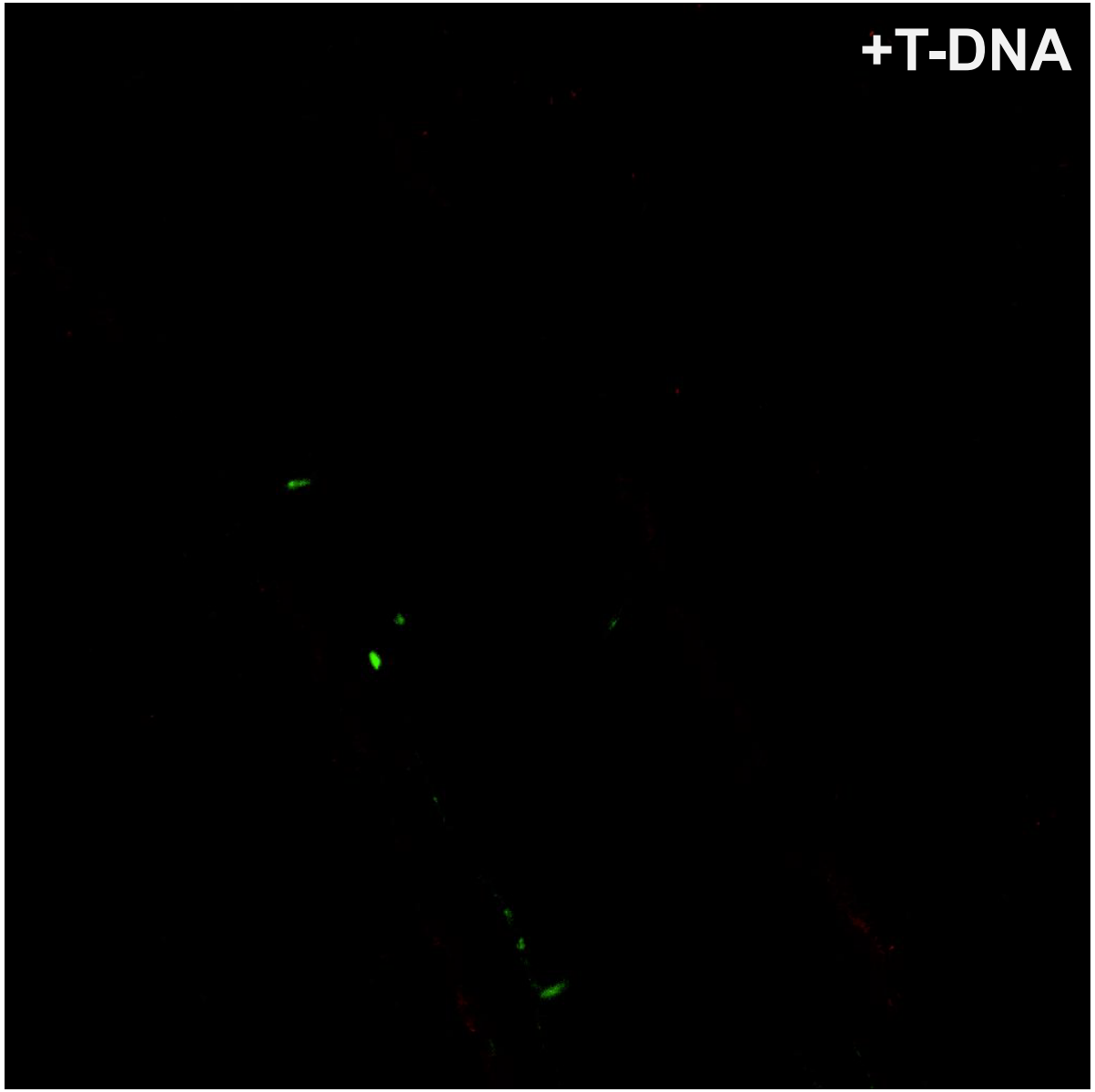

Supplemental Figure S12. Infection of root cells with an *Agrobacterium* strain capable of transferring T-DNA does not re-localize VirE2-Venus from the cellular periphery into the cytoplasm when the myosin VIII-1 CBD is expressed. Transgenic plants inducibly expressing the myosin VIII-1 CBD and VirE2-Venus were treated with 5 μM β-estradiol for 24 hr, then inoculated with 10^8 cfu/ml of the *virE2* mutant strain *A. tumefaciens* At1872 without (left panel) or with (right panel) T-DNA. Z-stack images of cells in the root elongation zone were taken after 8 hr of infection using a Zesis LSM 880 Upright Confocal Plan-Apo microscope using a 20×/0.8 objective.

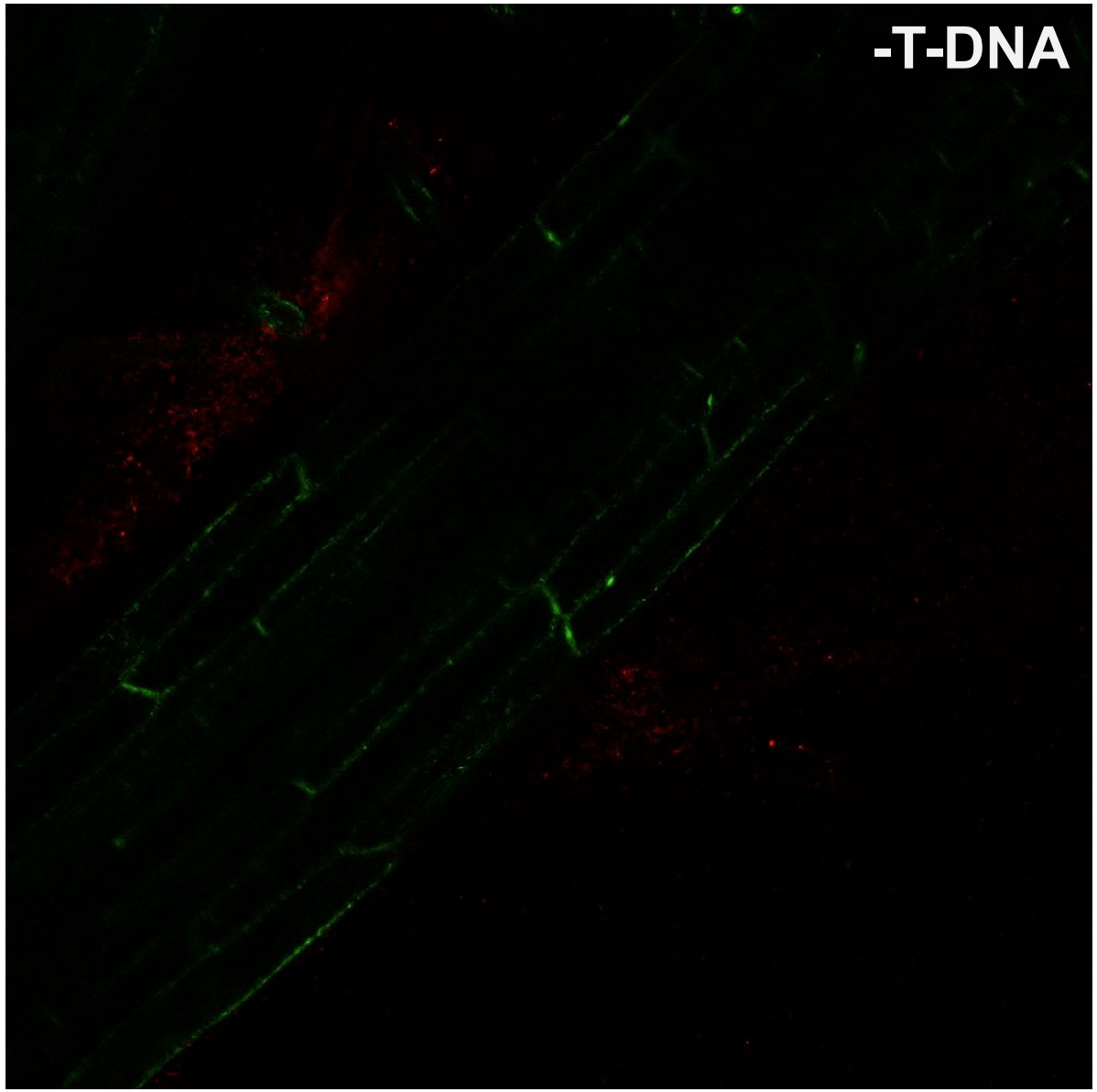

Supplemental Figure S13. Infection of root cells expressing the myosin VIII-2 CBD with an *Agrobacterium* strain capable of transferring T-DNA re-localizes VirE2-Venus from the cellular periphery into the cytoplasm. Transgenic plants inducibly expressing the myosin VIII-2 CBD and VirE2-Venus were treated with 5 μM β-estradiol for 24 hr, then inoculated with 10^8 cfu/ml of the *virE2* mutant strain *A. tumefaciens* At1872 without (left panel) or with (right panel) T-DNA. Z-stack images of cells in the root elongation zone were taken after 8 hr of infection using a Zesis LSM 880 Upright Confocal Plan-Apo microscope using a 20×/0.8 objective.

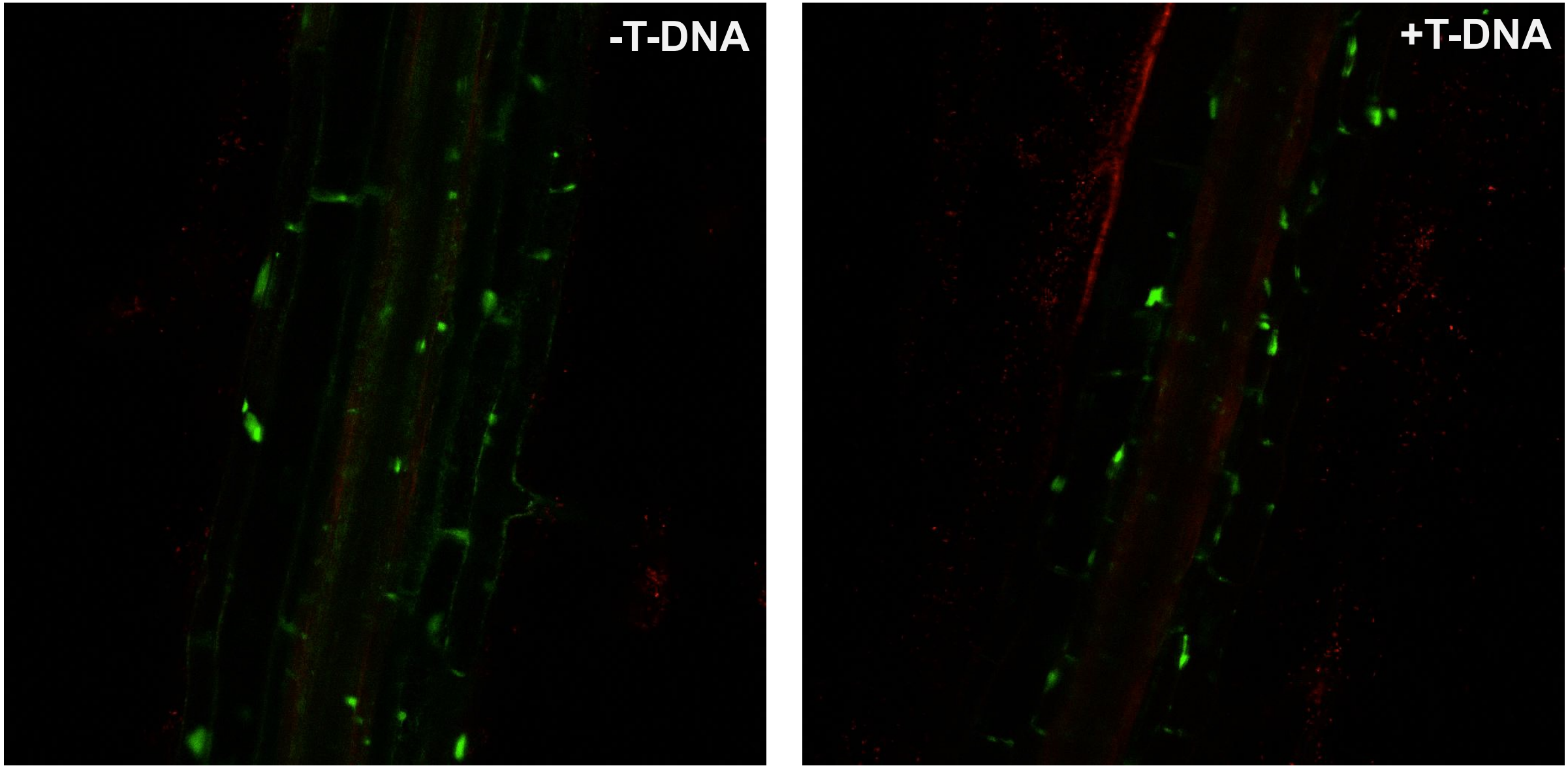

Supplemental Figure S14. Infection of root cells expressing the myosin VIII-A CBD with an *Agrobacterium* strain capable of transferring T-DNA re-localizes VirE2-Venus from the cellular periphery into the cytoplasm. Transgenic plants inducibly expressing the myosin VIII-A CBD and VirE2-Venus were treated with 5 μM β-estradiol for 24 hr, then inoculated with 10^8 cfu/ml of the *virE2* mutant strain *A. tumefaciens* At1872 without (left panel) or with (right panel) T-DNA. Z-stack images of cells in the root elongation zone were taken after 8 hr of infection using a Zesis LSM 880 Upright Confocal Plan-Apo microscope using a 20×/0.8 objective.

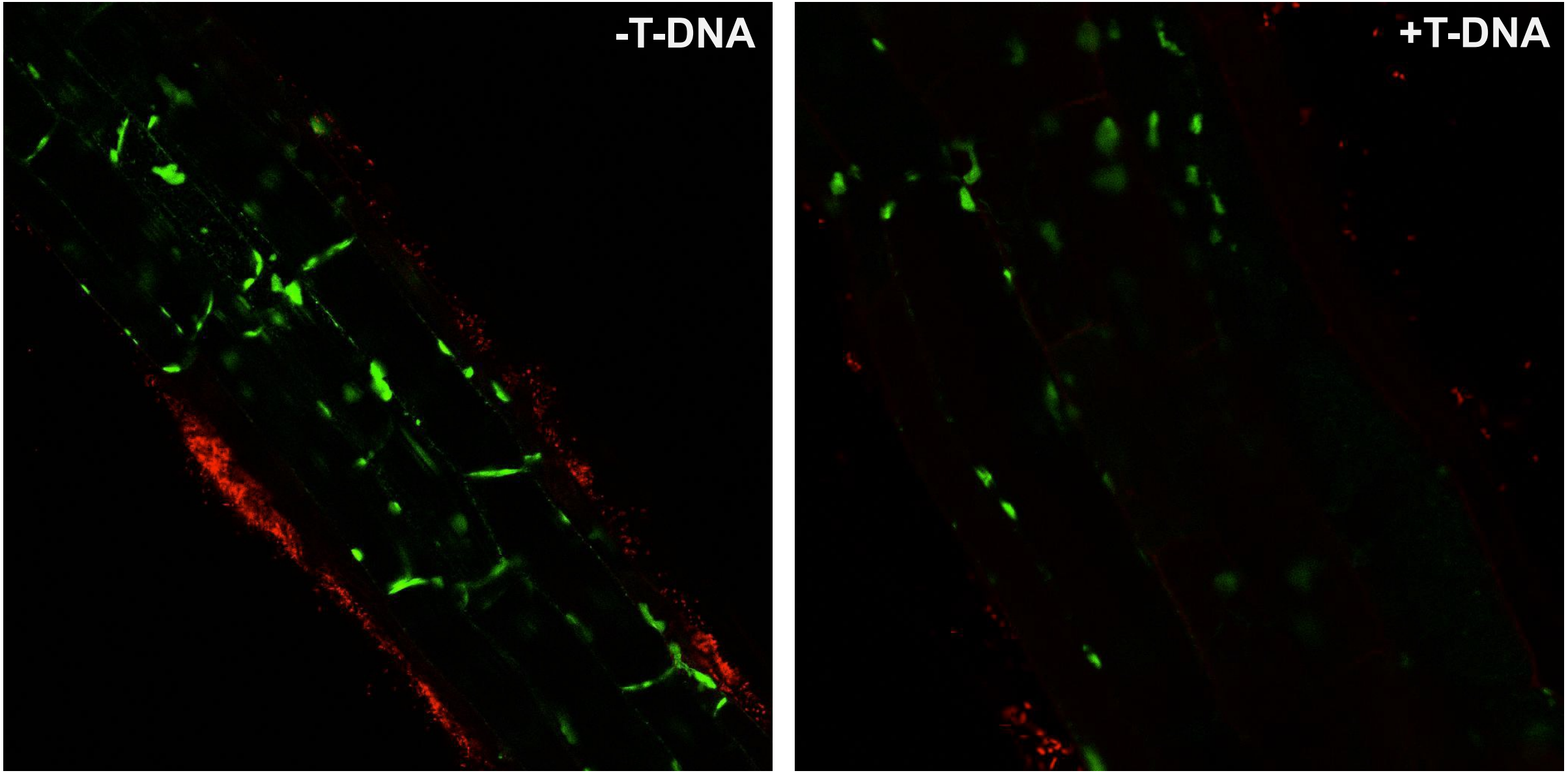

Supplemental Figure S15. Infection of root cells expressing the myosin VIII-B CBD with an *Agrobacterium* strain capable of transferring T-DNA re-localizes VirE2-Venus from the cellular periphery into the cytoplasm. Transgenic plants inducibly expressing the myosin VIII-B CBD and VirE2-Venus were treated with 5 μM β-estradiol for 24 hr, then inoculated with 10^8 cfu/ml of the *virE2* mutant strain *A. tumefaciens* At1872 without (left panel) or with (right panel) T-DNA. Z-stack images of cells in the root elongation zone were taken after 8 hr of infection using a Zesis LSM 880 Upright Confocal Plan-Apo microscope using a 20×/0.8 objective.

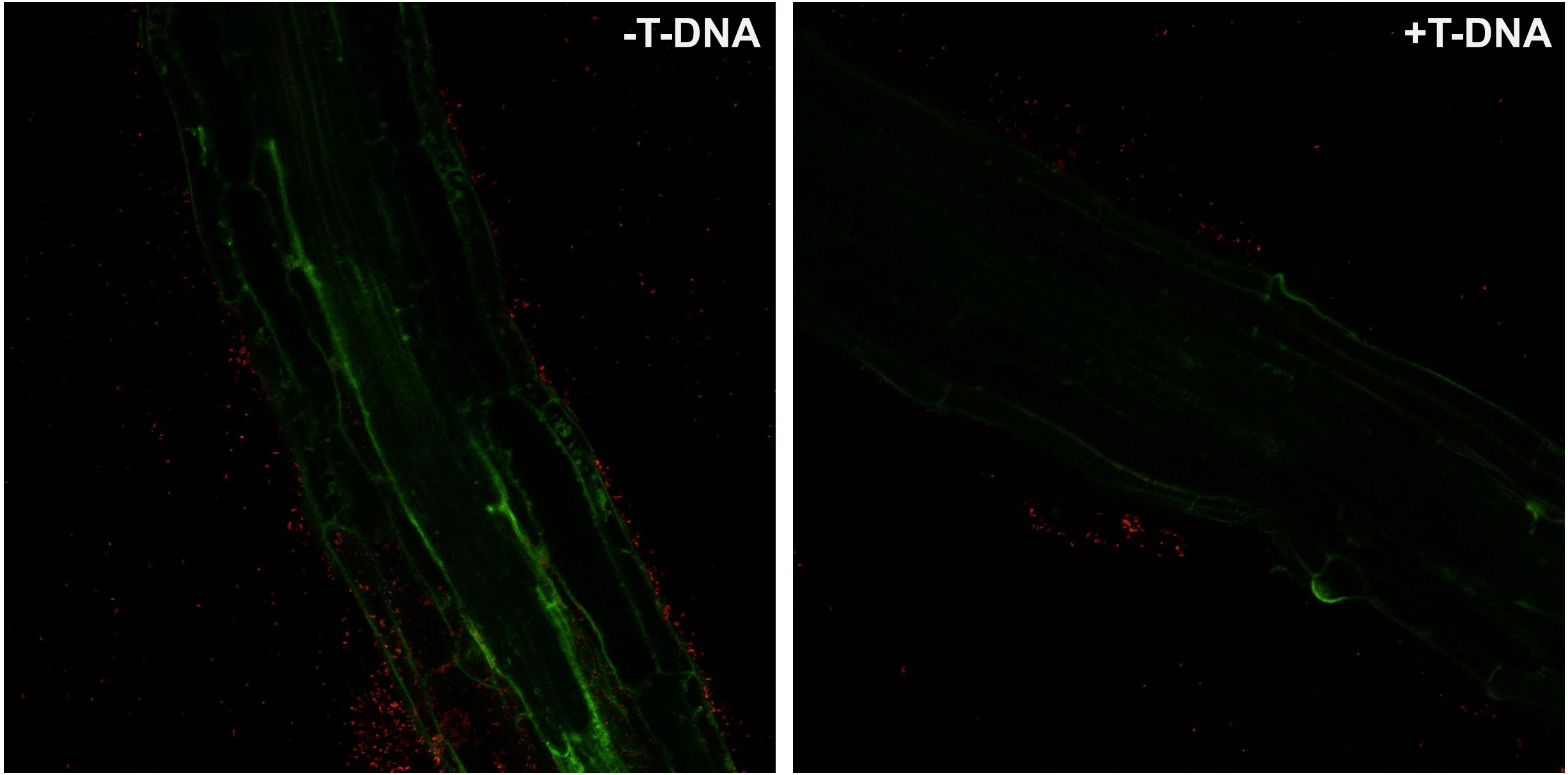

Supplemental Figure S16. Expression of the myosin XI-K CBD does not affect VirE2-Venus localization upon infection by *Agrobacterium*. Transgenic plants inducibly expressing the myosin XI-K CBD and VirE2-Venus were treated with 5 μM β-estradiol for 24 hr, then inoculated with 10^8 cfu/ml of the *virE2* mutant strain *A. tumefaciens* At1872 without (left panel) or with (right panel) T-DNA. Z-stack images of cells in the root elongation zone were taken after 8 hr of infection using a Zesis LSM 880 Upright Confocal Plan-Apo microscope using a 20×/0.8 objective.

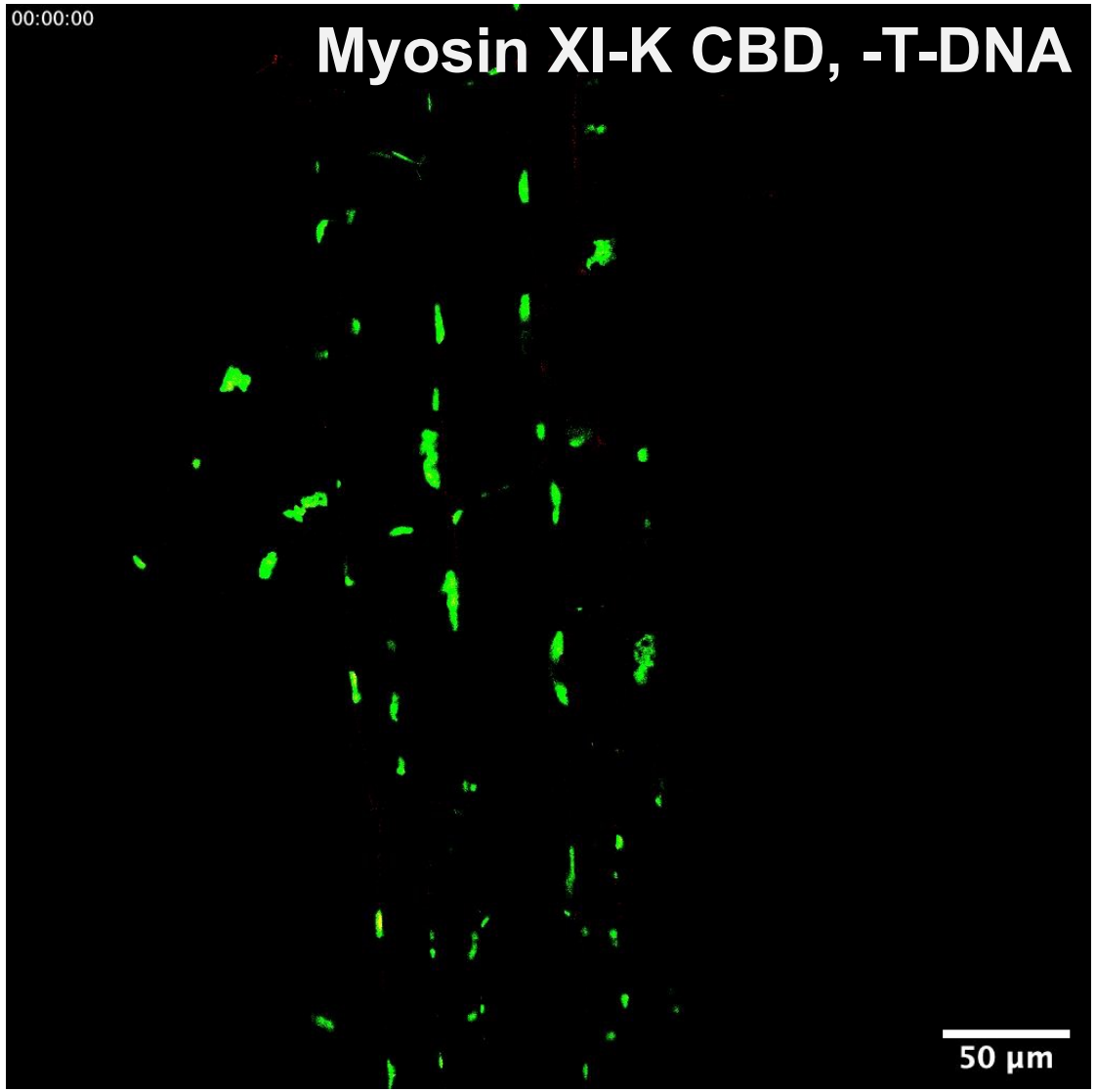

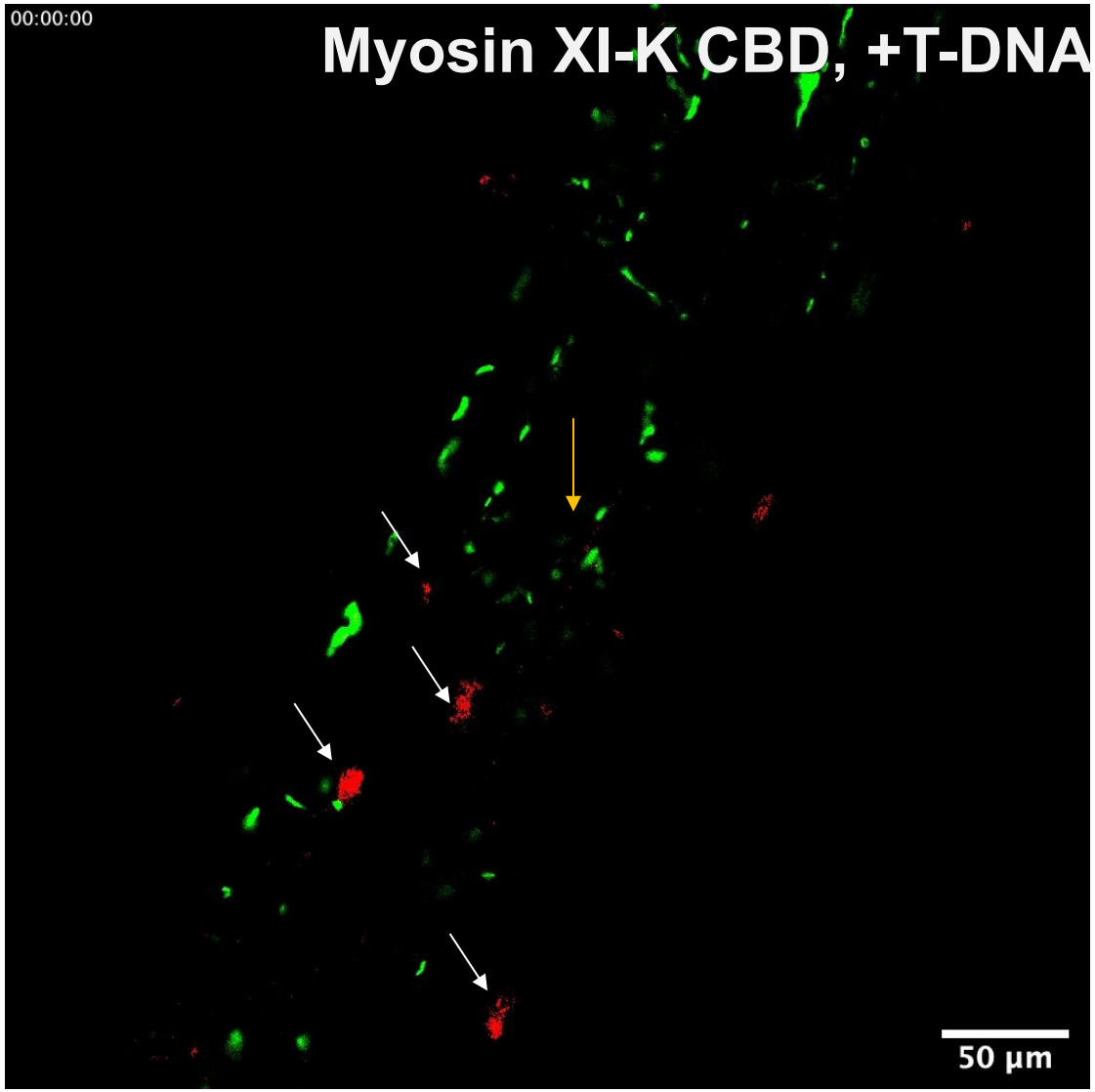

Supplemental Figure 17. Expression of the myosin XI-K CBD inhibits movement of VirE2-Venus. Transgenic plants inducibly expressing Myc-myosin XI-K CBD and VirE2-Venus were treated with 5 µM β-estradiol for 24 hr. Root segments were inoculated with 10^8 cfu/ml of the *virE2* mutant strain *A. tumefaciens* At2405 harboring a T-DNA which constitutively expressed mCherry-NLS (to mark nucleus of transformed cells) (right panel) or without T-DNA (left panel). Time lapse images were taken after 24 hr of infection using a Zesis LSM 880 Upright Confocal Plan-Apo microscope with a 20×/0.8 objective. White arrows indicate nuclei, yellow arrow indicates a non-transformed cell. Bars indicate 50 µm.

Parsed Citations

Amari K, Di Donato M, Dolja VV, Heinlein M. (2014) Myosins VIII and XI play distinct roles in reproduction and transport of tobacco mosaic virus. PLoS Pathog 10: e1004448
Google Scholar: Author Only Title Only Author and Title

Avisar D, Prokhnevsky AI, Dolja VV. (2008a) Class VIII myosins are required for plasmodesmatal localization of a closterovirus Hsp70 homolog. J Virol 82: 2836-2843
Google Scholar: Author Only Title Only Author and Title

Avisar D, Prokhnevsky AI, Makarova KS, Koonin EV, Dolja VV. (2008b) Myosin XI-K is required for rapid trafficking of Golgi stacks, peroxisomes, and mitochondria in leaf cells of Nicotiana benthamiana. Plant Physiol 146: 1098-1108
Google Scholar: Author Only Title Only Author and Title

Bar-Sinai S, Belausov E, Dwivedi V, Sadot,E. (2022) Collisions of cortical microtubules with membrane associated myosin VIII tail. Cells 11:145
Google Scholar: Author Only Title Only Author and Title

Bezanilla M, Horton AC, Sevener HC, Quatrano RS. (2003) Phylogenetic analysis of new plant myosin sequences. J Mol Evol 57: 229-239
Google Scholar: Author Only Title Only Author and Title

Bhattacharjee S, Lee L-Y, Oltmanns H, Cao H, Veena, Cuperus J, Gelvin SB. (2008) IMPa-4, an Arabidopsis importin alpha isoform, is preferentially involved in Agrobacterium-mediated plant transformation. Plant Cell 20: 2661-2680
Google Scholar: Author Only Title Only Author and Title

Bichet A, Desnos T, Turner S, Grandjean O, Hofte H. (2001) BOTERO1 is required for normal orientation of cortical microtubules and anisotropic cell expansion in Arabidopsis. Plant J 25: 137-148
Google Scholar: Author Only Title Only Author and Title

Bundock P, den Dulk-Ras A, Beijersbergen A, Hooykaas PJ. (1995) Trans-kingdom T-DNA transfer from Agrobacterium tumefaciens to Saccharomyces cerevisiae. EMBO J 14: 3206-3214
Google Scholar: Author Only Title Only Author and Title

Cascales E, Christie,PJ. (2004) Definition of a bacterial type IV secretion pathway for a DNA substrate. Science 304: 1170-1173
Google Scholar: Author Only Title Only Author and Title

Chang CW, Williams SJ, Counago RM, Kobe B. (2014) Structural basis of interaction of bipartite nuclear localization signal from Agrobacterium VirD2 with rice importin-alpha. Mol Plant 7: 1061-1064
Google Scholar: Author Only Title Only Author and Title

Chilton M-D, Drummond MH, Merio DJ, Sciaky D, Montoya AL, Gordon MP, Nester EW. (1977) Stable incorporation of plasmid DNA into higher plant cells: The molecular basis of crown gall tumorigenesis. Cell 11: 263-271
Google Scholar: Author Only Title Only Author and Title

Christie PJ, Atmakuri K, Krishnamoorthy V, Jakubowski S, Cascales E. (2005) Biogenesis, architecture, and function of bacterial type IV secretion systems. Annu Rev Microbiol 59: 451-485
Google Scholar: Author Only Title Only Author and Title

Citovsky V, Liu B. (2017) Myosin-driven transport network in plants is functionally robust and distinctive. Proc Natl Acad Sci USA 114: 1756-1758
Google Scholar: Author Only Title Only Author and Title

Citovsky V, Wong ML, Zambryski P. (1989) Cooperative interaction of Agrobacterium VirE2 protein with single-stranded DNA: Implications for the T-DNA transfer process. Proc Natl Acad Sci USA 86: 1193-1197
Google Scholar: Author Only Title Only Author and Title

Citovsky V, Zupan J, Warnick D, Zambryski P. (1992) Nuclear localization of Agrobacterium VirE2 protein in plant cells. Science 256: 1802-1805
Google Scholar: Author Only Title Only Author and Title

Clough SJ, Bent AF. (1998) Floral dip: A simplified method for Agrobacterium-mediated

transformation of Arabidopsis thaliana. Plant J 16: 735-743

de Groot MJ, Bundock P, Hooykaas PJ, Beijersbergen AG. (1998) Agrobacterium tumefaciens-mediated transformation of filamentous fungi. Nat Biotechnol 16: 839-842
Google Scholar: Author Only Title Only Author and Title

Djamei A, Pitzschke A, Nakagami H, Rajh I, Hirt H. (2007) Trojan horse strategy in Agrobacterium transformation: abusing MAPK

defense signaling. Science 318: 453-456
Google Scholar: Author Only Title Only Author and Title

Duan Z, Tominaga M. (2018) Actin-myosin XI: An intracellular control network in plants. Biochem Biophys Res Commun 506: 403-408
Google Scholar: Author Only Title Only Author and Title

Duckely M, Oomen C, Axthelm F, Van Gelder P, Waksman G, Engel A. (2005) The VirE1VirE2 complex of Agrobacterium tumefaciens interacts with single-stranded DNA and forms channels. Mol Microbiol 58: 1130-1142
Google Scholar: Author Only Title Only Author and Title

Dumas F, Duckely M, Pelczar P, Van Gelder P, Hohn B. (2001) An Agrobacterium VirE2 channel for transferred-DNA transport into plant cells. Proc Natl Acad Sci USA 98: 485-490
Google Scholar: Author Only Title Only Author and Title

Dym O, Albeck S, Unger T, Jacobovitch J, Branzburg A, Michael Y, Frenkiel-Krispin D, Wolf S., Elbaum M. (2008) Crystal structure of the Agrobacterium virulence complex VirE1-VirE2 reveals a flexible protein that can accommodate different partners. Proc Natl Acad Sci USA 105: 11170-11175
Google Scholar: Author Only Title Only Author and Title

Embley TM, Martin W. (2006) Eukaryotic evolution, changes and challenges. Nature 440: 623-630
Google Scholar: Author Only Title Only Author and Title

Engstrom P, Zambryski P, Van Montagu M, Stachel S. (1987) Characterization of Agrobacterium tumefaciens virulence proteins induced by the plant factor acetosyringone. J Mol Biol 197: 635-645
Google Scholar: Author Only Title Only Author and Title

Foth BJ, Goedecke MC, Soldati D. (2006) New insights into myosin evolution and classification. Proc Natl Acad Sci USA 103: 3681-3686
Google Scholar: Author Only Title Only Author and Title

Geeves MA. (2016) Review: The ATPase mechanism of myosin and actomyosin. Biopolymers 105: 483-491
Google Scholar: Author Only Title Only Author and Title

Gelvin SB. (1998) Agrobacterium VirE2 proteins can form a complex with T strands in the plant cytoplasm. J Bacteriol 180: 4300-4302
Google Scholar: Author Only Title Only Author and Title

Gelvin SB. (2000) Agrobacterium and plant genes involved in T-DNA transfer and integration. Annu Rev Plant Physiol Plant Mol Biol 51: 223-256
Google Scholar: Author Only Title Only Author and Title

Gelvin SB. (2003) Agrobacterium and plant transformation: The biology behind the "gene-jockeying" tool. Microbiol Mol Biol Rev 67: 16-37
Google Scholar: Author Only Title Only Author and Title

Gelvin, SB. (2006) Agrobacterium transformation of Arabidopsis thaliana roots: A quantitative assay. Methods Mol Biol 343: 105-113
Google Scholar: Author Only Title Only Author and Title

Gelvin SB. (2010) Finding a way to the nucleus. Curr Opin Microbiol 13: 53-58
Google Scholar: Author Only Title Only Author and Title

Gelvin SB. (2017) Integration of Agrobacterium T-DNA into the plant genome. Annual review of genetics 51: 22
Google Scholar: Author Only Title Only Author and Title

Golomb L, Abu-Abied M, Belausov E, Sadot E. (2008) Different subcellular localizations and functions of Arabidopsis myosin VIII. BMC Plant Biol 8: 3
Google Scholar: Author Only Title Only Author and Title

Grange W, Duckely M, Husale S, Jacob S, Engel A, Hegner M. (2008) VirE2: A unique ssDNA-compacting molecular machine. PLoS Biol 6: e44
Google Scholar: Author Only Title Only Author and Title

Haraguchi T, Tominaga M, Matsumoto R, Sato K, Nakano A, Yamamoto K, Ito K. (2014) Molecular characterization and subcellular localization of Arabidopsis class VIII myosin, ATM1. J Biol Chem 289: 12343-12355
Google Scholar: Author Only Title Only Author and Title

Hodges L, Cuperus J, Ream W. (2004) Agrobacterium rhizogenes GALLS protein

substitutes for Agobacterium tumefaciens single-stranded DNA-binding protein VirE2. J Bacteriol 186: 3065-3077

Hodges LD, Vergunst AC, Neal-McKinney J, den Dulk-Ras A, Moyer DM,

Hooykaas PJJ, Ream W. (2006) Agrobacterium rhizogenes GALLS protein contains domains for ATP binding, nuclear localization, and type IV secretion. J Bacteriol 188: 8222-8230
Google Scholar: Author Only Title Only Author and Title

Howard E, Citovsky V. (1990) The emerging structure of the Agrobacterium T-DNA transfer complex. Bioessays 12: 103-108
Google Scholar: Author Only Title Only Author and Title

Huang S, An YQ, McDowell JM, McKinney EC, Meagher RB. (1996) The Arabidopsis thaliana ACT4/ACT12 actin gene subclass is strongly expressed throughout pollen development. Plant J 10: 189-202
Google Scholar: Author Only Title Only Author and Title

Hussey,PJ, Ketelaar T, Deeks MJ. (2006) Control of the actin cytoskeleton in plant cell growth. Annu Rev Plant Biol 57: 109-125
Google Scholar: Author Only Title Only Author and Title

Hwang H-H, Gelvin SB. (2004) Plant proteins that interact with VirB2, the Agrobacterium tumefaciens pilin protein, mediate plant transformation. Plant Cell 16: 3148-3167
Google Scholar: Author Only Title Only Author and Title

Koncz C, Schell J. (1986) The promoter of TL-DNA gene 5 controls the tissue-specific

expression of chimaeric genes carried by a novel type of Agrobacterium binary vector. Mol Gen Genet 204: 383-396

Krendel M, Osterweil EK, Mooseker MS. (2007) Myosin 1E interacts with synaptojanin-1 and

dynamin and is involved in endocytosis. FEBS Lett 581: 644-650

Lacroix B, Citovsky V. (2013) The roles of bacterial and host plant factors in Agrobacterium-mediated genetic transformation. Int J Dev Biol 57: 467-481
Google Scholar: Author Only Title Only Author and Title

Lacroix B, Vaidya M, Tzfira T, Citovsky V. (2005) The VirE3 protein of Agrobacterium mimics a host cell function required for plant genetic transformation. EMBO J 24: 428-437
Google Scholar: Author Only Title Only Author and Title

Lapham RA, Lee L-Y, Xhako E, Gomez EG, Nivya VM., and Gelvin, S.B. (2021). Agrobacterium VirE2 protein modulates plant gene expression and mediates transformation from its location outside the nucleus. Front Plant Sci 12, 684192
Google Scholar: Author Only Title Only Author and Title

Lee L-Y, Wu F-H, Hsu C-T, She, S-C, Yeh,HY, Liao D-C, Fang M-J, Liu N-T, Yen Y-C, Dokládal L, Sýkorová E, Gelvin SB, Lin C-S (2012) Screening a cDNA library for protein-protein interactions directly in planta. Plant Cell. 24: 1746-1759
Google Scholar: Author Only Title Only Author and Title

Lee YR, Liu B. (2004) Cytoskeletal motors in Arabidopsis. Sixty-one kinesins and seventeen myosins. Plant Physiol 136: 3877-3883
Google Scholar: Author Only Title Only Author and Title

Li X, Pan SQ. (2017) Agrobacterium delivers VirE2 protein into host cells via clathrin-mediated endocytosis. Sci Adv 3: e1601528
Google Scholar: Author Only Title Only Author and Title

Li X, Tu H, Pan SQ. (2018) Agrobacterium delivers anchorage protein VirE3 for companion VirE2 to aggregate at host entry sites for T-DNA protection. Cell Rep 25: 302-311 e306
Google Scholar: Author Only Title Only Author and Title

Li X, Yang Q, Peng L, Tu H, Lee L-Y, Gelvin SB, Pan SQ. (2020) Agrobacterium-delivered VirE2 interacts with host nucleoporin CG1 to facilitate the nuclear import of VirE2-coated T complex. Proc Natl Acad Sci USA 117: 26389-26397
Google Scholar: Author Only Title Only Author and Title

Li X, Zhu T, Tu H, Pan SQ. (2020) Agrobacterium VirE3 uses its two tandem

domains at the C-terminus to retain its companion VirE2 on the cytoplasmic side of the host plasma membrane. Front Plant Sci 11:464

Madison SL, Nebenfuhr A. (2013) Understanding myosin functions in plants: Are we there yet? Curr Opin Plant Biol 16: 710-717
Google Scholar: Author Only Title Only Author and Title

Madison SL, Buchanan ML, Glass JD, McClain TF, Park E, Nebenfuhr A. (2015) Class XI myosins move specific organelles in pollen tubes and are required for normal fertility and pollen tube growth in Arabidopsis. Plant Physiol 169: 1946-1960
Google Scholar: Author Only Title Only Author and Title

McCullen CA, Binns AN. (2006) Agrobacterium tumefaciens and plant cell interactions and activities required for interkingdom

macromolecular transfer. Annu Rev Cell Dev Biol 22: 101-127
Google Scholar: Author Only Title Only Author and Title

Meagher RB, McKinney EC, Kandasamy MK. (1999) Isovariant dynamics expand and buffer the responses of complex systems: The diverse plant actin gene family. Plant Cell 11: 995-1006
Google Scholar: Author Only Title Only Author and Title

Narasimhulu SB, Deng XB, Sarria R, Gelvin SB. (1996) Early transcription of Agrobacterium T-DNA genes in tobacco and maize. Plant Cell 8: 873-886
Google Scholar: Author Only Title Only Author and Title

Ojangu EL, Jarve K, Paves H, Truve E. (2007) Arabidopsis thaliana myosin XIK is involved in root hair as well as trichome morphogenesis on stems and leaves. Protoplasma 230: 193-202
Google Scholar: Author Only Title Only Author and Title

Otten L, DeGreve H, Leemans J, Hain R, Hooykaas P, Schell J. (1984) Restoration of

virulence of vir region mutants of Agrobacterium tumefaciens strain B6S3 by coinfection with normal and mutant Agrobacterium strains. Mol Gen Genet 195: 159-163

Peremyslov VV, Prokhnevsky AI, Dolja VV. (2010) Class XI myosins are required for development, cell expansion, and F-Actin organization in Arabidopsis. Plant Cell 22: 1883-1897
Google Scholar: Author Only Title Only Author and Title

Peremyslov VV, Prokhnevsky AI, Avisar D, Dolja VV. (2008) Two class XI myosins function in organelle trafficking and root hair development in Arabidopsis. Plant Physiol 146: 1109-1116
Google Scholar: Author Only Title Only Author and Title

Peremyslov,VV, Mockler TC, Filichkin S., Fox SE, Jaiswal P, Makarova K., Koonin .V, Dolja,VV. (2011) Expression, splicing, and evolution of the myosin gene family in plants. Plant Physiol 155: 1191-1204
Google Scholar: Author Only Title Only Author and Title

Piers KL, Heath JD, Liang X, Stephens KM, Nester EW. (1996) Agrobacterium tumefaciens-mediated transformation of yeast. Proc Natl Acad Sci USA 93: 1613-1618
Google Scholar: Author Only Title Only Author and Title

Prokhnevsky AI, Peremyslov,VV, Dolja VV. (2008) Overlapping functions of the four class XI myosins in Arabidopsis growth, root hair elongation, and organelle motility. Proc Natl Acad Sci USA 105: 19744-19749
Google Scholar: Author Only Title Only Author and Title

Radford JE, White RG. (1998) Localization of a myosin-like protein to plasmodesmata. Plant J 14: 743-750
Google Scholar: Author Only Title Only Author and Title

Ream W. (2009) Agrobacterium tumefaciens and A. rhizogenes use different proteins to transport bacterial DNA into the plant cell nucleus. Micro Biotechnol 2: 416-42.
Google Scholar: Author Only Title Only Author and Title

Reichelt S, Knight AE, Hodge TP, Baluska F, Samaj J, Volkmann D, Kendrick-Jones J. (1999) Characterization of the unconventional myosin VIII in plant cells and its localization at the post-cytokinetic cell wall. Plant J 19: 555-567
Google Scholar: Author Only Title Only Author and Title

Reisen D, Hanson MR. (2007) Association of six YFP-myosin XI-tail fusions with mobile plant cell organelles. BMC Plant Biol 7: 6
Google Scholar: Author Only Title Only Author and Title

Richards TA, Cavalier-Smith T. (2005) Myosin domain evolution and the primary divergence of eukaryotes. Nature 436: 1113-1118
Google Scholar: Author Only Title Only Author and Title

Rossi L, Hohn B, Tinland B. (1996) Integration of complete transferred DNA units is dependent on the activity of virulence E2 protein of Agrobacterium tumefaciens. Proc Natl Acad Sci USA 93: 126-130
Google Scholar: Author Only Title Only Author and Title

Roushan MR, deZeeuw MAM, Hooykaas PJJ, van Heusden GPH. (2018) Application

of phiLOV2.1 as a fluorescent marker for visualization of Agrobacterium effector protein translocation. Plant J 96: 685-699

Sakalis,PA, van Heusden GP, Hooykaas PJ. (2014) Visualization of VirE2 protein translocation by the Agrobacterium type IV secretion system into host cells. Microbiologyopen 3: 104-117
Google Scholar: Author Only Title Only Author and Title

Salman H, Abu-Arish A, Oliel S, Loyter A, Klafter J, Granek R, Elbaum M. (2005) Nuclear localization signal peptides induce molecular delivery along microtubules. Biophys J 89: 2134-2145

Google Scholar: Author Only Title Only Author and Title

Sato T, Hanada M, Bodrug S, Irie, S, Iwama N, Boise LH, Thompson CB, Golemis E, Fong L, Wang HG. (1994) Interactions among members of the Bcl-2 protein family analyzed with a yeast two-hybrid system. Proc Natl Acad Sci U S A 91: 9238-9242
Google Scholar: Author Only Title Only Author and Title

Sattarzadeh A, Franzen R, Schmelzer E. (2008) The Arabidopsis class VIII myosin ATM2 is involved in endocytosis. Cell Motil Cytoskeleton 65: 457-468
Google Scholar: Author Only Title Only Author and Title

Schrammeijer B, den Dulk-Ras A, Vergunst AC, Jurado Jacome E, Hooykaas PJ. (2003) Analysis of Vir protein translocation from Agrobacterium tumefaciens using Saccharomyces cerevisiae as a model: Evidence for transport of a novel effector protein VirE3. Nucleic Acids Res 31: 860-868
Google Scholar: Author Only Title Only Author and Title

Sen P, Pazour GJ, Anderson D, Das A. (1989) Cooperative binding of Agrobacterium tumefaciens VirE2 protein to single-stranded DNA. J Bacteriol 171: 2573-2580
Google Scholar: Author Only Title Only Author and Title

Shi Y, Lee L-Y, Gelvin SB. (2014) Is VIP1 important for Agrobacterium-mediated transformation? Plant J 79: 848-860
Google Scholar: Author Only Title Only Author and Title

Simone M, McCullen CA, Stahl LE, Binns AN. (2001) The carboxy-terminus of VirE2 from Agrobacterium tumefaciens is required for its transport to host cells by the virB-encoded type IV transport system. Mol Microbiol 41: 1283-1293
Google Scholar: Author Only Title Only Author and Title

Smith LG, Oppenheimer .G. (2005) Spatial control of cell expansion by the plant cytoskeleton. Annu Rev Cell Dev Biol 21: 271-295
Google Scholar: Author Only Title Only Author and Title

Sparkes I, Runions J, Hawes C, Griffing L. (2009) Movement and remodeling of the endoplasmic reticulum in nondividing cells of tobacco leaves. Plant Cell 21: 3937-3949
Google Scholar: Author Only Title Only Author and Title

Stachel SE, Nester EW. (1986) The genetic and transcriptional organization of the vir region of the A6 Ti plasmid of Agrobacterium tumefaciens. EMBO J 5: 1445-1454
Google Scholar: Author Only Title Only Author and Title

Staiger CJ, Sheahan MB, Khurana P, Wang X, McCurdy DW, Blanchoin L. (2009) Actin filament dynamics are dominated by rapid growth and severing activity in the Arabidopsis cortical array. J Cell Biol 184: 269-280
Google Scholar: Author Only Title Only Author and Title

Szymanski DB, Cosgrove DJ. (2009) Dynamic coordination of cytoskeletal and cell wall systems during plant cell morphogenesis. Curr Biol 19: R800-811
Google Scholar: Author Only Title Only Author and Title

Tenea GN, Spantzel J, Lee L-Y, Zhu Y, Lin K, Johnson SJ, Gelvin SB. (2009) Over-expression of several Arabidopsis histone genes increases Agrobacterium-mediated transformation and transgene expression in plant cells. Plant Cell 21: 3350–3367
Google Scholar: Author Only Title Only Author and Title

Trybus KM. (2008) Myosin V from head to tail. Cell Mol Life Sci 65: 1378-1389
Google Scholar: Author Only Title Only Author and Title

Tu H, Li X, Yang Q, Peng L, Pan SQ. (2018) Real-time trafficking of Agrobacterium virulence protein VirE2 inside host cells. Curr Top Microbiol Immunol 418: 261-286
Google Scholar: Author Only Title Only Author and Title

Tzfira T, Vaidya M, Citovsky V. (2001) VIP1, an Arabidopsis protein that interacts with Agrobacterium VirE2, is involved in VirE2 nuclear import and Agrobacterium infectivity. EMBO J 20: 3596-3607
Google Scholar: Author Only Title Only Author and Title

Tzfira T, Li J, Lacroix B, Citovsky V. (2004) Agrobacterium T-DNA integration: Molecules and models. Trends Genet 20: 375-383
Google Scholar: Author Only Title Only Author and Title

Ueda H, Tamura K, Hara-Nishimura I. (2015) Functions of plant-specific myosin XI: from intracellular motility to plant postures. Curr Opin Plant Biol 28: 30-38
Google Scholar: Author Only Title Only Author and Title

Ueda H, Yokota E, Kutsuna N, Shimada T, Tamura K, Shimmen T, Hasezawa S, Dolja VV., Hara-Nishimura I. (2010) Myosin-dependent endoplasmic reticulum motility and F-actin organization in plant cells. Proc Natl Acad Sci USA 107: 6894-6899
Google Scholar: Author Only Title Only Author and Title

Ueki S, Citovsky V. (2005) Identification of an interactor of cadmium ion-induced glycine-rich protein involved in regulation of callose levels in plant vasculature. Proc Natl Acad Sci USA 102: 12089-12094
Google Scholar: Author Only Title Only Author and Title

Vale RD. (2003) The molecular motor toolbox for intracellular transport. Cell 112: 467-480
Google Scholar: Author Only Title Only Author and Title

Vergunst AC, van Lier MC, den Dulk-Ras A, Stuve TA, Ouwehand A, Hooykaas PJ. (2005) Positive charge is an important feature of the C-terminal transport signal of the VirB/D4-translocated proteins of Agrobacterium. Proc Natl Acad Sci USA 102: 832-837
Google Scholar: Author Only Title Only Author and Title

Wang H, Han S, Siao W, Song C, Xiang Y, Wu X, Cheng P, Li H, Jasik J, Micieta K, Turna J, Voigt B, Baluska F, Liu J, Wang Y, Zhao H. (2015) Arabidopsis synaptotagmin 2 participates in pollen germination and tube growth and is delivered to plasma membrane via conventional secretion. Mol Plant 8: 1737-1750
Google Scholar: Author Only Title Only Author and Title

Wang P, Hawkins TJ, Richardson C, Cummins I, Deeks MJ, Sparkes I, Hawes C, Hussey PJ. (2014) The plant cytoskeleton, NET3C, and VAP27 mediate the link between the plasma membrane and endoplasmic reticulum. Curr Biol 24: 1397-1405
Google Scholar: Author Only Title Only Author and Title

Wojtaszek P, Anielska-Mazur A, Gabrys H, Baluska F, Volkmann D. (2005) Recruitment of myosin VIII towards plastid surfaces is root-cap specific and provides the evidence for actomyosin involvement in root osmosensing. Funct Plant Biol 32: 721-736
Google Scholar: Author Only Title Only Author and Title

Wu Z, Bezanilla M. (2014) Myosin VIII associates with microtubule ends and together with actin plays a role in guiding plant cell division. Elife 3:e03498
Google Scholar: Author Only Title Only Author and Title

Yang L, Qin L, Liu G, Peremyslov VV, Dolja VV, Wei Y. (2014) Myosins XI modulate host cellular responses and penetration resistance to fungal pathogens. Proc Natl Acad Sci USA 111: 13996-14001
Google Scholar: Author Only Title Only Author and Title

Yang Q, Li X, Tu H, Pan SQ. (2017) Agrobacterium-delivered virulence protein VirE2 is trafficked inside host cells via a myosin XI-K-powered ER/actin network. Proc Natl Acad Sci USA 114: 2982-2987
Google Scholar: Author Only Title Only Author and Title

Yusibov VM, Steck TR, Gupta V, Gelvin, SB. (1994) Association of single-stranded transferred DNA from Agrobacterium tumefaciens with tobacco cells. Proc Natl Acad Sci USA 91: 2994-2998
Google Scholar: Author Only Title Only Author and Title

Zuo J, Niu Q-W, Chua N-H. (2000) An estrogen receptor-based transactivator XVE mediates

highy inducible gene expression in transgenic plants. Plant J 24: 265-273

Zupan JR, Citovsky V, Zambryski P. (1996) Agrobacterium VirE2 protein mediates nuclear uptake of single-stranded DNA in plant cells. Proc Natl Acad Sci USA 93: 2392-2397
Google Scholar: Author Only Title Only Author and Title